SLAC-PUB-3189
AUGUST 1983

CALT-68-989

DOE RESEARCH AND

DEVELOPMENT REPORT

Physics with the Crystal Ball Detector

Elliott D. Bloom
Stanford Linear Accelerator Center
Stanford University
Stanford, California 94305
U.S.A.

and

Charles W. Peck
High Energy Physics
California Institute of Technology
Pasadena, California 91125
U.S.A.

CONTENTS

1. Introduction and Outline

2. Description of the Apparatus and its Performance

3. The Charmonium ^3P_J States

   3.1 Dominant Features in the Inclusive Photon Spectrum of the ψ'

   3.2 The Photon Cascade $\psi' \to \gamma\chi_J \to \gamma\gamma J/\psi$

   3.3 Results from the Full Analysis of the Inclusive Spectrum and Some Comparisons to Exclusive Results

4. Hadronic Transitions from the ψ' to the J/ψ

   4.1 The Transitions $\psi' \to \eta(\pi^0)\, J/\psi$

5. The Charmonium $^1S_0$ States

   5.1 Evidence for the 1^1S_0 in Inclusive γ Spectra of the ψ' and the J/ψ

   5.2 Hadronic Decays of the 1^1S_0

   5.3 Evidence for the 2^1S_0 State in the Inclusive γ Spectrum of the ψ'

   5.4 Discussion

6. Radiative Transitions from the J/ψ

   6.1 The Fundamental Character of the Gluonic Mesons in QCD

   6.2 The "Endpoint" of the Inclusive γ Spectrum at the J/ψ

   6.3 Gamma Transitions to Well-Known Particles Using Exclusive Decays

   6.4 The Gluonium Candidates, $\iota(1440)$ and $\vartheta(1640)$

   6.5 Other Radiative Transitions

7. Searches for the F-Mesons, the Axion, and the $^1P_1$ State

7.1 The Inclusive η Cross Section

7.2 The Search for $J/\psi \to \gamma$ Axion

7.3 The Search for the Decays $\psi' \to \pi^0\, ^1P_1$

8. Measurements of R_h in the E_{CM} Range of 5.0 to 7.4 GeV

9. Two-Photon Physics

9.1 Measurement of $\Gamma(f \to \gamma\gamma)$ from $\sigma(\gamma\gamma \to f \to \pi^0\pi^0)$

9.2 Measurement of $\Gamma(A_2 \to \gamma\gamma)$ from $\sigma(\gamma\gamma \to A_2 \to \pi^0 eta)$

9.3 Other States

10. Measurements in the Region from Charm Threshold to 4.5 GeV

11. Summary and Future Prospects

1. INTRODUCTION AND OUTLINE

At the 1974 PEP Summer Study (1), one of the projects was to explore the possibilities and limitations of detectors optimized to measure photons produced in high energy e^+e^- collisions. It was realized that a device which had high detection efficiency over a large solid angle and which could measure the energy of photons in the region above a few tens of MeV with high precision (in the range of a few percent) would provide a unique capability offered by no existing apparatus. Thus it could possibly yield important and otherwise unattainable information about these fundamental interactions. Furthermore, if it also measured the directions of both photons and charged particles well enough, even a non-magnetic version of such a device would be able to compete with the large general-purpose magnetic spectrometers then in existence in the reconstruction of certain simple, few-particle final states. And finally, a device designed to absorb all the electromagnetic energy in an event would in fact quickly and directly measure a large fraction of its total energy. This prompt information could form the basis for an admirable trigger having very different biases from those used by the magnetic spectrometers. Thus such a device would be an interesting complementary technique for the investigation of e^+e^- physics. In particular an efficient "all-neutral" trigger would be possible.

Although the thrust of the summer's work had been directed toward instrumentation for PEP (an e^+e^- storage ring at the Stanford Linear Accelerator Center allowing beam energies up to about 15 GeV), which was still in the planning stages at that time, a keen interest in the idea developed among a group of people[1] from Caltech, Harvard, Stanford-HEPL and SLAC and this led to serious work in the fall of 1974 toward producing a formal proposal for the existing lower

[1] A group from Princeton joined the collaboration in 1977.

energy storage ring, SPEAR. Discovery of the $J/\psi(3100)$ and $\psi'(3700)$ in Nov/Dec of that year spurred on these efforts, especially as people realized there was the likely possibility of a rich gamma ray spectroscopy in the few hundred MeV range. Eventually, this work led the group to submit a proposal for a non-magnetic, large solid angle detector whose principal component was a spherical shell of NaI(Tl) with a 10" inner radius and a 26" outer radius. The device was quickly dubbed the "Crystal Ball" and it has been universally called that ever since. The proposal was approved in spring 1975 and the construction of the detector was completed three years later in the spring of 1978. Section 2 describes the configuration and performance of the detector.

The Ball was installed at SPEAR in fall 1978 and took data there on e^+e^- collisions in the energy region from 3.1 GeV to 7.4 GeV during the 40 months of calendar time until December 1981. SPEAR actually supplied beam during about half of this time. We spent about five months collecting about $2\ 10^6$ hadronic events at each of the two $^3S_1$ states, the $J/\psi(3100)$ and the $\psi'(3700)$. Typical luminosities at these energies were $0.5\ 10^{30}\ cm^{-2}\ sec^{-1}$ and $1.8\ 10^{30}\ cm^{-2}\ sec^{-1}$ respectively. About one month was spent at the $\psi''(3770)$ collecting $4\ 10^4$ hadronic events and the rest of the time was spent at energies in the continuum, almost all of which were above charm threshold. We obtained a cumulative exposure of 24.0 pb^{-1} in this region. At the highest energy at which we took data, 7.4 GeV, SPEAR provided a peak luminosity of about $2.0\ 10^{31}\ cm^{-2}\ sec^{-1}$.

In the spring of 1982 the Ball was moved as an intact experiment to the Deutsches Elektronen Synchrotron (DESY), Hamburg, Germany to run on the DORIS II e^+e^- storage ring in order to make a parallel study of the Υ system. Data taking in the 10 GeV region, in which DORIS II is optimized, had just begun as this paper was being prepared.

This brief review consists of a survey of all the Crystal Ball physics results that had been completed as of December 1982. The available space does not permit any detailed discussion of either the experimental details or the theoretical framework which provides the proper setting for the experimental findings described here. However, the interested reader can find a discussion of many of the theoretical questions in references 2 and 3 and in the literature cited therein; appropriate experimental references and only limited theoretical references are given in this review. A general survey of the physics of psionic matter up to 1977 can be found in (3a). Finally, in Section 11 we briefly discuss some of the analysis projects currently in progress as well as our expectations for results from the just begun exposure of the Crystal Ball at DORIS II.

The principal accomplishments of the Crystal Ball experiment have resulted from the study of radiative and certain hadronic transitions involving the charmonium states. Figure 1 shows the energy level diagram of this system and it also indicates the several radiative and hadronic transitions that have been the focus of the Crystal Ball efforts. The refreshing simplicity of this first-known heavy quark spectrum compared to the corresponding situation among the light quarks (u,d,s) has played an important role in the recent development of particle physics. This positronium-like structure gives strong qualitative evidence for the fundamental $c\bar{c}$ interpretation of charmonium and quantitative details about the energies and transition rates can be compared with phenomenological models motivated by Quantum Chromodynamics (QCD).

When the Crystal Ball experiment began, however, there were several outstanding difficulties with the then-favored, and now, well-established $c\bar{c}$ model. A total of five states had been reported in two-photon cascade transitions between the ψ' and the J/ψ and one state had been reported below the J/ψ in the 3γ decay mode. Preferred quantum numbers for three of the

intermediate mass states were indirectly inferred (4,5,6) from their hadronic decay patterns and mass ordering and these caused them to be identified with the three ^3P_J states. However, the experimental situation concerning the candidate $^1S_0$ states seemed to present an insurmountable challenge to the beautiful $c\bar{c}$ interpretation (7-9).

In brief, the $^1S_0$ problem was as follows. In 1977, the DASP collaboration (10,11) observed a significant signal at 2.83 ± 0.03 GeV/c^2 in the distribution of the highest $\gamma\gamma$ mass from the decay $J/\psi \to \gamma\gamma\gamma$. This state, the X(2830), immediately became a candidate for the $1\,^1S_0$ state, the η_c. The measured product branching ratio, $B(J/\psi \to \gamma X(2830)) \cdot B(X(2830) \to \gamma\gamma)$, was $(1.2 \pm 0.5)\,10^{-4}$. However, no evidence for $J/\psi \to \gamma X(2830)$ was seen in the inclusive γ spectrum from the J/ψ by the SPEAR experiment SP-27 (12), which set an upper limit of 2% for $B(J/\psi \to \gamma X(2830))$. These results were incompatible with any reasonable $c\bar{c}$ model since this interpretation predicts $B(J/\psi \to \gamma X(2830))$ to be an order of magnitude larger than the limit set by SP-27. Furthermore, it predicts $B(X(2830) \to \gamma\gamma)$ to be about five times smaller than the lower limit inferred from the DASP and SP-27 results combined. Finally, a hyperfine splitting of 265 MeV is surprisingly large within the $c\bar{c}$ model.

The second serious problem concerned the $2\,^1S_0$ state, the η'_c. Initially, some evidence for an η'_c candidate was reported (13) at a mass of 3455 MeV/c^2 in the cascade process $\psi' \to \gamma\,^1S_0 \to \gamma\gamma J/\psi$ by the Mark I experiment at SPEAR. This observation was not confirmed by a subsequent experiment (14), the DESY-Heidelberg collaboration at DORIS, which independently investigated the radiative cascade process. On the other hand, the DESY-Heidelberg experiment presented evidence for an alternative intermediate state at 3591 MeV/c^2 as a possible η'_c candidate. However, their reported branching ratio for $\psi' \to \gamma\chi(3591) \to \gamma\gamma J/\psi$ was orders of magnitude greater than predicted by the

model, if this state were taken to be the η'_c.

One of the first processes measured with the newly commissioned Crystal Ball was $J/\psi \to 3\gamma$. These new observations provided both higher statistics and better resolution than the earlier ones, but they did not confirm the X(2830). A lower limit of 2.2 10^{-5} was initially (15) set for the product branching ratio (this limit was subsequently lowered to 1.6 10^{-5} (90% C.L.); see Section 6.3). Nor did later data confirm either the $\chi(3455)$ or the $\chi(3591)$ in the radiative cascades from the ψ' to the J/ψ. Thus the experimental status of the two expected $^1S_0$ states was again open.

The first evidence for the η_c in the Crystal Ball came from the inclusive γ spectra observed from the ψ' and, shortly thereafter, that from the J/ψ. Somewhat later, with a doubling of the ψ' data sample, evidence for the η'_c was also found in the ψ' inclusive γ spectrum. The current status of these two charmonium states is discussed in Section 5 below. With these two contributions from the Crystal Ball, there is only one qualitative feature of the expected $c\bar{c}$ spectrum for which no experimental evidence has yet been found, namely, the $^1P_1$ state. Section 7 summarizes our current limits on certain decay modes involving this state.

The radiative transitions involving the three ^3P states give rise to the several prominent peaks in the ψ' inclusive γ spectrum shown in Figure 3. So characteristic, in fact, is this spectrum that it has become the logo of the Crystal Ball experiment. The careful study of all the systematics (efficiencies and resolutions) necessary to obtain the branching ratios and natural widths of these states from the inclusive γ spectrum has been recently completed and is discussed in Section 3. The radiative cascade exclusive channels $\psi' \to \gamma\, ^3P \to \gamma\gamma e^+e^-$ or $\gamma\gamma\mu^+\mu^-$ were susceptible to more rapid analysis and Section 3 also summarizes our results on product branching ratios, masses, and

angular distributions (which strongly support the earlier spin assignments for these states). As a by-product of our study of these exclusive channels, we also made measurements on the three transitions $\psi' \to \pi^0\pi^0 J/\psi$, $\psi' \to \eta J/\psi$, and $\psi' \to \pi^0 J/\psi$. The first simply corroborated the much better results from $\psi' \to \pi^+\pi^- J/\psi$, but the other two yielded significant improvements over earlier work. These hadronic transitions are discussed in Section 4.

Radiative transitions from the J/ψ are especially interesting since their primary mechanism is expected (in the context of QCD) to be $J/\psi \to \gamma gg$ with the two gluons in a singlet state of both color and flavor. Thus any gg bound states which are even under charge conjugation and less massive than the J/ψ are likely to be excited in this decay. At least two candidates for such objects have been observed in the Crystal Ball data. One, with a mass of about 1440 MeV/c^2 was thought to be the 1^{++}, $E(1420)$ meson when it was first found in J/ψ decays by the Mark II experiment. The existence of the state was quickly confirmed by the Crystal Ball. However, only after the partial wave analysis of twice the initial data sample did the Crystal Ball collaboration find that the 0^{-+} assignment for the state was favored. This state was then named $\iota(1440)$. A second gluonium candidate, the $\vartheta(1640)$, was found by the Crystal Ball in the $\eta\eta$ decay mode and the preferred spin-parity assignment is 2^+. Finally, searching in the channel $J/\psi \to \gamma\eta\pi\pi$, we find no evidence that the 1440 MeV/c^2 state decays into $\eta\pi\pi$ but we do see both the expected signal of $\eta' \to \eta\pi\pi$ and an unexpected very broad enhancement at an $\eta\pi\pi$ mass of 1710 MeV/c^2. The present status of these several interesting possibilities as well as the Crystal Ball's observations on the modes $J/\psi \to \gamma X$ where $X = \pi^0, \eta, \eta', f$, and f', is discussed in Section 6.

In addition to the extensive search for the $^1P_1$ charmonium state mentioned earlier, two other searches with negative results have been carried out and are described in Section 7. The first was an attempt to corroborate a strong

enhancement in the inclusive η cross section reported by the DASP experiment. This had been interpreted as evidence for $e^+e^- \to F + \ldots \to \eta + \ldots$ where the F is the charmed-strange meson. However, no significant enhancement was observed by the Crystal Ball. The second search with negative results was for evidence of the axion. Since there are quite sharp theoretical predictions for radiative decays of the J/ψ and Υ into the axion, we made a detailed investigation of our J/ψ data looking for this decay; nothing was found.

Finally, in addition to the charmonium studies which comprise the bulk of the Crystal Ball results, this experiment has also collected a body of data in the energy region above charm threshold. To date, in addition to the inclusive η cross sections mentioned earlier, we have made total hadronic cross section measurements (R_h) up to the highest energies at SPEAR (Section 8), we have observed production of the f and A_2 by two photon collisions from which we obtain the decay rates $\Gamma(f \to \gamma\gamma)$ and $\Gamma(A_2 \to \gamma\gamma)$ (Section 9), and finally, we have made several measurements in the region from charm threshold to 4.5 GeV (Section 10).

2. DESCRIPTION OF THE APPARATUS AND ITS PERFORMANCE

Over the years, many methods have been developed and extensively used for measuring the energy of high energy photons. By the mid-seventies, however, the pioneering work of R. Hofstadter and his colleagues (16) had shown that the technique of total absorption shower counters made of thallium doped sodium iodide (NaI(Tl)) was unsurpassed in the combination of high detection efficiency and energy resolution. Consequently, in spite of the technical difficulties occasioned by the extremely hydroscopic nature of NaI(Tl), this technique, supplemented by fine segmentation of the material, was selected to form

the basis of a detector covering nearly the full 4π sr solid angle about the e^+e^- collision point, the Crystal Ball. The final result of the design was a detector consisting of four main parts. These were: a central charged particle detection system, two hemispherical shells of NaI(Tl), endcaps of tracking chambers followed by sodium iodide which covered the beam entry holes into the spherical shell, and a small-angle luminosity monitor. Figure 2 shows the geometric arrangement of the two major components of the detector. Details about the apparatus can be found in reference 17.

The central tracking system consisted of three concentric cylindrical ionization detectors covering 71%, 83%, and 94% of 4 π sr, respectively. The middle detector (18) was a proportional chamber with two gaps, and the other two detectors were magnetostrictive spark chambers. For particles which were detected in both spark chambers, both direction and origin along the beam line could be determined. Those which failed to be detected in both spark chambers were only "tagged", i.e., identified as being charged.

The heart of the detector, of course, was the 16 radiation length thick spherical shell of sodium iodide. This thickness is sufficient to contain essentially the entire longitudinal development of electromagnetic showers in our energy range. As shown in Figure 2, the shell is actually a dense packing of truncated triangular pyramids of NaI(Tl). These are optically isolated one from another, and each is viewed from the outside by a single photomultiplier tube. The only materials separating the individual crystals are thin layers of white paper and aluminum foil (except for the plane separating the two hemispheres). The shell consists of a total of 672 of these crystals and it covers 93% of 4π sr. The missing 7% is due to beam entry holes, but these are almost completely covered by the endcaps.

With this geometric arrangement, we not only measure the amount of energy deposited in the NaI with little loss, but we also obtain information about the transverse structure of this energy deposition. Being minimum ionizing and lacking strong interactions, high energy muons leave simple tracks, with a deposited energy of about 200 MeV distributed over no more than two or three crystals. Electrons and photons with energy greater than about 20 MeV produce electromagnetic showers and deposit all of their energy in a reasonably characteristic pattern covering about 13 crystals. Finally, most hadrons strongly interact in the Ball since it is about one absorption length thick. They thus give rise to somewhat more irregular patterns than electromagnetic showers and the total deposited energy bears little relation to the hadron's energy. This geometric arrangement provides no information about the longitudinal distribution of an energy deposition, but we have found that careful statistical analysis of a transverse pattern is a useful technique for resolving some particle identification ambiguities.

The parameter of particular interest in this detector is its energy resolution for electromagnetic showers. For the energy range of interest, the standard deviation σ_E of this resolution is well approximated by $(0.0255 \pm 0.0013)E^{\frac{3}{4}}$ where E and σ_E are in GeV. Thus, for example, we measure the energy of a 1.55 GeV Bhabha scattered electron to an accuracy of 36 MeV and that of a 100 MeV photon to an accuracy of 4.6 MeV. An example of the utility of this relatively high resolution is that we can extract the natural widths of the charmonium $^1S_0$ and $^3P_{0,2}$ from our inclusive γ distributions. More generally, the goodness of our photon energy resolution has proved invaluable in allowing us to reliably identify certain reactions by the technique of kinematically constrained statistical fitting, which in turn leads to some of the physics results to be discussed later. It should be noted, however, that because of the size of

electromagnetic showers and the edge effects of the beam holes, the good energy resolution is only available over 85% of 4π *sr*. A detailed description of tests made on a prototype of the detector and the signal processing methods used can be found in reference 19.

A second parameter of considerable interest is the resolution with which the direction of a photon can be determined. By examining the profile of its shower's energy deposition we can determine the direction of a photon to much better than the size of one module. The limitation on the accuracy of angles determined in this manner is caused by shower fluctuations. The Crystal Ball has achieved a resolution with $\sigma_{\vartheta_\gamma}$ = 1.5° to 2°, where ϑ_γ is the polar angle from the photon's true direction. There is a slight energy dependence in this angular resolution.

An important design goal in this apparatus was to cover as much as possible of the solid angle around the collision point with high efficiency particle detectors. This was achieved by covering the necessary beam holes in the ball with endcaps consisting of 20 radiation length thick, individually packaged NaI(Tl) hexagonal prisms covered by two gaps of spark chambers. These brought the total coverage to 98% of 4π *sr*. Primarily because of edge effects, the energy resolution for photons and electrons going outside the central 85% of 4π *sr* of the main ball was relatively poor and strongly direction dependent. Consequently, the endcaps were primarily used as veto counters. They allowed us to determine the topology of events with very high confidence, and this was of crucial importance for reducing backgrounds in some of the physics measurements given later.

Finally, for many of our measurements an absolute luminosity determination was necessary. This was provided by a small angle Bhabha scattering detector consisting of four counter elements, symmetrically disposed about the

beam and centered at a 4° angle to the beam line. Each of the four elements was identical, consisting of three scintillators followed by a shower counter, and covered a solid angle of $4.2\,10^{-4}$ sr. The system provided a counting rate of about 0.7 Hz at the ψ' with our typical luminosity. The accuracy of luminosity determination was better than 3% with this monitor, as checked by using large angle Bhabha events observed in the full Ball.

The apparatus was triggered and events written on tape when at least one of several overlapping conditions was satisfied. Each of these triggers was based on a coincidence between a beam crossing signal and the analog sum of signals from the Ball and each required that this sum, proportional to the total energy in the Ball, be greater than some threshold. Generally, a further requirement was also imposed and the more restrictive it was, the lower the total energy threshold. The simplest trigger involved no other requirements and its total energy threshold was normally about 1 GeV. More restrictive triggers involved such event features as charged particles being detected in the proportional chambers, or a requirement on the general pattern of energy deposition in the Ball. In general, the hardware trigger conditions were highly efficient for the classes of events that have been studied with the Crystal Ball, and the Monte Carlo simulations which have been done to determine detection efficiencies have included these hardware trigger conditions.

Data acquisition and general system monitoring were performed by a PDP11/t55 computer. Reference 20 discusses in detail both the hardware and the flexible complement of software which was developed for this experiment.

3. THE CHARMONIUM ^3P_J STATES

3.1 Dominant Features in the Inclusive Photon Spectrum of the ψ'

After the discoveries of the J/ψ (21,22) and ψ' (23) in 1974, four experiments measured the inclusive photon spectrum from the ψ' with increasing levels of sensitivity. The first experiment was a two-crystal NaI(Tl) detector (24); it could only place upper limits on radiative transitions to the ^3P_J (χ_J) states. A magnetic detector, measuring converted photons, was able to measure the photon transition to the χ_0 state (13), but was not able to inclusively observe the other transitions. A moderately segmented NaI(Tl) detector (12) finally measured the photon transitions to each of the χ_J states and also inclusively observed the cascade transitions from the χ_2 and χ_1 to the J/ψ. Finally, Figure 3 shows the inclusive spectrum at the ψ' from the Crystal Ball detector, the most sensitive experiment so far. The main spectrum in the figure is from the analysis of approximately 0.9×10^6 ψ' events (the last half of the full sample) obtained at SPEAR. Severe cuts have been made in this spectrum to enhance structure. First, all photons are required to have $|\cos\vartheta_\gamma| < 0.85$, where ϑ_γ is the angle between the photon and the beam direction. The cosine of the angle between each photon and any charged particle is required to be less than 0.9. Pairs of γ's with invariant mass consistent with the mass of the π^0 have been eliminated. Finally, the lateral shower energy deposition in the NaI(Tl) crystals is required to be consistent with a single electromagnetic shower. This "pattern cut" removes most of those minimum ionizing charged particles which were not identified by the tracking chamber system, many of the spurious energy deposits resulting from interacting charged particles, and some of the high energy π^0's in which the electromagnetic showers from the two photons from the π^0 decay overlap. The pattern cut used for the spectrum in Figure 3, one of many algorithms possible, was designed to optimize the efficiency for photons with energy, E_γ, less

than or about 100 MeV.

As is seen in the figure, the photon transitions from the ψ' to the χ_J states and the cascade transitions from the χ_J states to the J/ψ stand out clearly in this inclusive spectrum. Indeed, the strength of these transitions in our detector has allowed frequent checks of the NaI(Tl) energy calibration and resolution over the course of our stay at SPEAR. Typically, two days of reasonable data-taking at SPEAR, yielding approximately $2.5\ 10^4$ ψ' decays, allowed an accurate determination of the transition energies to the χ_J states.

3.2 The Photon Cascade, $\psi' \to \gamma\chi_J \to \gamma\gamma J/\psi$

A study of the radiative transitions from the ψ' to the χ_J states and the cascade radiative decays from the χ_J states by means of the sequence, $\psi' \to \gamma\chi_J$, $\chi_J \to \gamma J/\psi$, $J/\psi \to l^+l^-$, where l^+l^- is e^+e^- or $\mu^+\mu^-$, provides a method for identifying the χ_J states (17) which is almost free of background. Indeed, it was in this reaction sequence that the $\chi_{1,2}$ were first observed (4,25). Additionally, an analysis of the angular correlations in the cascade final state of Crystal Ball data (17) has permitted a direct measurement of the spin of the $\chi_{1,2}$ states and of the multipole coefficients describing the two individual radiative transitions for each of these states. The decays, $\psi' \to \eta(\pi^0)J/\psi \to \gamma\gamma l^+l^-$ exhibit the same topology as the cascade reactions; these processes have also been studied by the Crystal Ball collaboration (17) in order to separate them from χ_J events as well as for their own sake (cf. Section 4.1). Note that the decay, $\psi' \to \pi^0 J/\psi$, which is forbidden by isospin symmetry, has been observed by the Crystal Ball (17) and the Mark II (26) detectors at SPEAR.

The details of the Crystal Ball data analysis for cascade reactions are discussed in reference 17 and the references cited therein.

Figure 4a shows the Dalitz plot of the final event sample (from the first half of the full data set) containing 1206 $\gamma\gamma e^+e^-$ and 1280 $\gamma\gamma\mu^+\mu^-$ decays prior to kinematic fitting. These same events are also shown on the Dalitz plot in Figure 4b after they have been kinematically fit to the hypothesis that they arise from $\psi' \to \gamma\gamma J/\psi \to \gamma\gamma l^+l^-$, (5-C for e^+e^-, 3-C for $\mu^+\mu^-$). The fit kinematics restrict all of the surviving 2234 $\gamma\gamma l^+l^-$ events to fall within the outer envelope illustrated in Figures 4a,b; the cuts to the data restrict the events to fall within the inner envelope.

The decay, $\psi' \to \pi^\circ\pi^\circ J/\psi$, $\pi^\circ \to \gamma\gamma$, $J/\psi \to l^+l^-$, in which two photons go undetected or have energies less than 20 MeV is a background of ~ 5% to the events of Figure 4a. This background as well as all other backgrounds which have been considered (17) are totally negligible in the final fit event sample shown in Figure 4b.

In both Figures 4a and 4b the horizontal band at the top occurs at the η mass; that near the bottom occurs at the π° mass. Two strong signals for $\chi_1(3508)$ and $\chi_2(3554)$ appear as vertical bands to the right of the symmetry line shown, which has slope, $d(m^2_{\gamma\gamma})/d(M^2_{\gamma J/\psi}) = -2$.

The Doppler-shifted bands on the left of the symmetry line (each event is plotted twice, once for each $\gamma J/\psi$ mass combination) are tilted with a slope of -1. The mass resolution for the π°, η and the low solution $\gamma J/\psi$ mass is better in Figure 4b than in the unfitted plot (4a). This is due to the fact that the kinematic fit reduces the absolute energy error of the higher-energy photon to that of the lower-energy one.

After separating the η and π° bands, the populous states at $\gamma J/\psi$ masses of 3554 and 3508 MeV/c^2 contain 479 and 943 events, respectively. Three of the 20 events associated with $\chi_0(3413)$ are expected to arise from the reaction $\psi' \to \pi^\circ\pi^\circ J/\psi$. The cuts on the data restrict the $\gamma J/\psi$ mass to the range 3129 to

3644 MeV/c^2; in this region we find no evidence for a fourth χ state.

The branching ratio for a particular $\gamma\gamma l^+l^-$ decay channel is obtained by taking the number of events observed in the channel, correcting for detection efficiency (from 0.5 to 0.25 for various channels, and typically about 0.4), photon conversion and charge particle identification efficiencies (0.95 and 0.96, respectively), and dividing by the total number of ψ' produced and the branching ratio for the decay of the J/ψ into dileptons. The J/ψ dilepton branching ratio (27) is the dominant systematic error (13%) in this measurement. The branching ratios obtained by the Crystal Ball are shown in Table 1 in comparison with those obtained from other experiments. There is good agreement for the χ_2 and χ_1 measurements; however, only the Crystal Ball measures a significant χ_0 branching ratio. Only upper limits are given for $\chi(3455)$ and $\chi(3591)$.

Additional information obtained from the Crystal Ball measurements of the photon cascade decays was the spins of the $\chi_{1,2}$ states and the multipolarity of the γ transitions. The particles participating in the cascade sequence, $e^+e^- \to \psi'$, $\psi' \to \gamma'\chi_J$, $\chi_J \to \gamma J/\psi$, $J/\psi \to l^+l^-$ define the five angles, $\cos\vartheta' = \hat{e}^+ \cdot \hat{\gamma}'$, $\cos\vartheta_{\gamma\gamma} = \hat{\gamma}' \cdot \hat{\gamma}$, $\tan\varphi' = [\hat{e}^+ \cdot (\hat{\gamma}' \times \hat{\gamma})]/[\hat{e}^+ \cdot [(\hat{\gamma}' \times \hat{\gamma}) \times \hat{\gamma}']]$, $\cos\vartheta = \hat{l}^+ \cdot \hat{\gamma}$, $\tan\varphi = [\hat{l}^+ \cdot (\hat{\gamma}' \times \hat{\gamma})]/[\hat{l}^+ \cdot [(\hat{\gamma}' \times \hat{\gamma}) \times \hat{\gamma}]]$. The angular distribution function $w(\cos\vartheta', \varphi', \cos\vartheta_{\gamma\gamma}, \cos\vartheta, \varphi, \vec{p})$, detailed in reference 28, which describes the above cascade sequence is a function of the five angles, and of the multipole parameters $\vec{p} = (J, \alpha'_J, \alpha_J)$, where α'_J and α_J describe the multipole structure for the two radiative transitions. The multipole coefficients are α_J (α'_J) and they satisfy the relation, $\Gamma(\chi_J \to \gamma J/\psi) \propto \sum_{j=1}^{J+1} |\alpha_j|^2$, and similarly for α'_J. The explicit form of the multipole coefficients is given in reference 28. Given the standard charmonium model, one expects that the electric dipole amplitudes dominate the transitions. Thus, the coefficients α_3 and α'_3 which are possible in the spin-2

case can be expected to be very small and they were set to zero.

The data was analyzed by means of a histogram over the five angles. A maximum likelihood comparison was made to a binned Monte Carlo simulation which was acceptance corrected and constrained to have a total number of events equal to that in the experimental sample. Table 2 contains the results of the likelihood fit.

The multipolarities of the radiative transitions for the $\chi_{1,2}$ are thus found to be predominantly dipole. An earlier analysis (6) also found this to be the case for the χ_1, but only when its spin was assumed to be 1. The data from the Crystal Ball study yield high confidence levels for the spin and multipole values preferred in the standard charmonium models (2).

3.3 Results from the Full Analysis of the Inclusive Spectrum and Some Comparisons to Exclusive Results

In this section our focus will be on the results of a detailed study (29), using the Crystal Ball, of the radiative transitions from ψ' to the χ_J states. Measurements of the natural line widths of the χ_J states will also be discussed briefly. The results are derived from 1.8×10^6 ψ' hadronic decays selected using criteria designed to reject cosmic rays, beam gas and QED events. These criteria rejected all but a negligible part of the background while maintaining a 94% efficiency for the hadronic events.

The selection of tracks from the hadronic events for the inclusive photon analysis was done in four different ways. This was done to compare the effects of the different sets of cuts and the resulting different background shapes on the measured photon branching ratios and $\chi_{0,1,2}$ line widths. The following cumulative selection criteria were applied to the data to yield the four ψ' inclusive

photon spectra shown in Figure 5(a-d):

a) Removal of tracks with $|\cos\vartheta_j| > 0.85$ where ϑ_j is the angle of the track to the positron beam direction. This solid angle restriction ensures that each particle in the spectrum is in a fiducial volume of the NaI(Tl) which has a uniform energy resolution and scale. Since both charged and neutral tracks are accepted into this spectrum, an enormous peak at about 200 MeV is observed corresponding to minimum ionizing charged particles passing through the detector. The peak presents a very large background which dwarfs the χ_J lines. However, these lines are still highly significant and measurable.

b) Removal of charged tracks using tracking chamber information. Most charged particles are removed by this cut as is evidenced by the great reduction in the relative size of the peak at ~200 MeV; however, the persistence of a remnant bump at the minimum ionization energy indicates some small inefficiency in charge particle identification.

c) Removal of neutral tracks close to charged tracks, $\cos\vartheta_{ij} < 0.9$, and removal of neutral pairs which reconstruct to a π^0 mass. These last cuts improve the signal-to-noise by about a factor of two while reducing γ detection efficiency by about a factor of 0.7.

d) Removal of tracks identified as minimum ionizing charged particles by their lateral energy deposition in the NaI(Tl) crystals. These charged particles were not rejected in b) due to the charged particle identification inefficiency of the tracking chambers. In this heavily cut spectrum, the minimum ionizing signal is negligible. The signal-to-noise of the photon transitions has been maximized so that the $\psi' \to \gamma\eta_c$ transition is clearly visible at $E_\gamma \sim 640$ MeV (cf. Section 5.1). Note that because of the fine (1%) binning of the data in histograms 5(a-d), the signal at $E_\gamma \sim 92$ MeV arising

from the transitions $\psi' \to \gamma\eta'_c$ is not clearly visible (cf. Section 5.3).

The signals corresponding to the χ_J radiative transitions were obtained from fits to the spectra of Figures 5(a-d) (29). The results from the fits are summarized in Figure 6 after corrections for photon detection efficiency, photon conversion probability, and the photon angular distributions arising from the different spins of the χ_J states have been made.

By comparing the branching ratios $B(\psi' \to \gamma\chi_J)$ extracted from the four spectra, one is able to assess the magnitude of the systematic errors contributing to the measurement. As is seen in Figure 6, the variation among the four branching ratio values for each line is consistent within the statistical errors of the measurements. The fact that consistent results are obtained with such widely different looking spectra gives one confidence in the finally extracted branching ratios.

A second check is the comparison of the cascade branching ratios $B(\psi' \to \gamma\chi_{1,2}) \cdot B(\chi_{1,2} \to \gamma J/\psi)$ as measured using the Doppler-broadened secondary transition lines seen in the inclusive photon spectra of Figure 5(a-d) with the values obtained from the exclusive events discussed in Section 3.2. The results of the cascade measurement are shown as the points on the bottom part of Figure 6. The dashed bands show the exclusive measurement of the same transitions given in Table 1. As is seen in this figure, the inclusive measurement for the χ_2 is somewhat lower than the exclusive measurement, while for χ_1 it is somewhat higher. However, the sum of the χ_1 and χ_2 branching ratios yields good agreement between inclusive and exclusive measurements. This effect has also been reproduced in Monte Carlo calculations. It is due to the overlap of the two transitions in the inclusive spectra. That the sum of the inclusive lines is in good agreement with the sum of the exclusive measurements allows an

uncertainty in the absolute normalization of the inclusive result of less than 16%, the absolute error in the exclusive measurement (remember that this error is dominated by the uncertainty in $B(J/\psi \to l^+l^-)$).

The final results of the analysis, including branching ratios and the values for the natural line widths of the χ_J states, are shown in Table 3. For the branching ratios the first error is dominated by the statistical uncertainty and point-to-point errors in the photon detection efficiency. The second error is an estimate of the overall normalization error due mainly to a ±5% uncertainty in both the hadronic event selection efficiency and the overall photon detection efficiency.

Agreement between these Crystal Ball branching ratio measurements and those of the lower statistics experiment of reference 12 are within the experimental errors. However, our branching ratios to the χ_J states are consistently higher, and within the point-to-point errors of our measurements there is an indication for an increase in rate from χ_2 to χ_0 transitions. In non-relativistic models, $\Gamma(\psi' \to \chi_J) \propto (2J + 1)E_\gamma^3$, and thus we expect, $\Gamma'_0 : \Gamma'_1 : \Gamma'_2 = 1 : 1 : 1$ where $\Gamma'_J = \Gamma(\psi' \to \gamma\chi_J) / ((2J + 1)\, E_\gamma^3(\chi_J))$. As shown in Table 3, we obtain, $1 : 1.07 \pm 0.08 : 1.39 \pm 0.11$, in reasonable agreement with the simple theory. However, our absolute branching ratios are a factor of two to three lower than the predictions of the simple non-relativistic charmonium models (29). Models which include relativistic corrections, variations of the 2S and 3P wave function shapes resulting from higher order corrections, and coupled channels achieve better agreement with the data.

The measurement of the natural line widths of the χ_J states is a tricky one since the Crystal Ball's photon energy resolution is comparable to or greater than these widths. It does appear, however, that the χ_0 is much broader than

predicted by QCD, while the χ_1 and χ_2 widths are in good agreement with QCD within errors (29,30).

4. HADRONIC TRANSITIONS FROM THE ψ' TO THE J/ψ.

Figure 1b shows the hadronic transitions that have been observed between the ψ' and J/ψ. All of these transitions have been observed by at least two experiments, and the $\pi\pi$ and η transitions have been observed by many experiments. As the $\pi\pi$ transition can easily be observed in the charge mode ($B(\psi' \to \pi^+\pi^- J/\psi) = 33 \pm 2\%$ (27)), excellent measurements of this mode have been made by other detectors stressing charged particle detection. The Crystal Ball has measured the neutral $\pi^0\pi^0$ mode (31), as a check on measurements of the η and π^0 transitions. Comparison of the neutral $\pi^0\pi^0$ to the charged (32) $\pi^+\pi^-$ mass distributions show the shapes of the two distributions to be the same within error, as is expected from isospin symmetry.

4.1 The Transitions $\psi' \to \eta(\pi^0)J/\psi$

The study of these processes is related to that of the ^3P_J state cascades and so is detailed in reference 17 (cf. Section 3.2). The $m_{\gamma\gamma}$ distribution for all fitted events is shown in Figure 7a. Of the events in this figure, 412 candidates for the η events are separated from χ_J and π^0 events by using the cut $m_{\gamma\gamma} > 525$ MeV/c^2. This cut loses no η events, but does admit some χ_1 events into the η sample.

Monte Carlo calculations determined that 21 χ_1 events, as well as 5 $\pi^0\pi^0$ events are expected in the η sample. The resulting η mode branching ratio is compared in Table 1 with other measurements. The Crystal Ball and Mark II results (26) are in good agreement, while the other measurements shown are

larger than our measurement by about a factor of two.

Existence of the transition $\psi' \to \pi^0 J/\psi$ is apparent in the Dalitz plots of Figures 4a,b. A π^0 signal is observed in the diphoton mass plot by removing the dominant background from cascade photons using a cut on the $\gamma J/\psi$ masses. A subtraction of events from the $m_{\gamma\gamma}$ plot of Figure 7a with $(M_{\gamma J/\psi})_{\rm high}$ in the ranges 3410 ± 5 and 3530 ± 60 MeV/c^2, and $m_{\gamma\gamma} > 525$ MeV/c^2, results in the distribution shown in Figure 7b. These data have been fitted to a Gaussian peak with a quadratic background distribution. The fit yields 23 events above background having $m_{\gamma\gamma} < 200$ MeV/c^2. The resulting π^0 mode branching ratio is compared in Table 1 with another measurement from the Mark II (26). The two measurements are in good agreement. This decay violates isospin symmetry. A review of the theoretical literature relevant to our measurement can be found in reference 17.

5. THE CHARMONIUM $^1S_0$ STATES

It is likely that the discoveries of the Crystal Ball which created the most excitement were the lack of a signal in $J/\psi \to \gamma\gamma\gamma$ at $M_{\gamma\gamma} = M_{\chi(2830)}$ (15), which had been reported by the DASP collaboration (10,11) (cf. Section 6.4), and the discovery of an η_c candidate state at $M_{\eta_c} = 2984 \pm 4$ MeV/c^2 by means of the radiative transitions from the ψ' (33) and J/ψ (34). Since the original observations were made, the Crystal Ball has doubled both the ψ' and J/ψ data sets to about 2×10^6 hadronic decays each. This increase in data has allowed a more precise determination of the η_c parameters (29). Furthermore, it has also resulted in the discovery of an η'_c candidate at $M_{\eta'_c} = 3592 \pm 5$ MeV/c^2 via a radiative transition from the ψ'.

The two Crystal Ball states at 2984 and 3592 MeV/c^2 can be naturally associated with the 1^1S_0 and 2^1S_0 charmonium states the η_c and η'_c. As we shall see in this section their properties fall well within the range of theoretical expectations. Thus, with the work described in previous sections we have come from a state of relative confusion and uncertainty concerning the validity of charmonium as a model of the J/ψ system to one of good agreement between theory and experiment in most cases.

5.1 Evidence for the 1^1S_0 in Inclusive γ Spectra of the ψ' and the J/ψ

The analysis of the inclusive photon spectra from the 1.8×10^6 ψ' and 2.2×10^6 J/ψ decays when studying the $\eta_c(2984)$ is very similar to that described in Section 3.3 and is detailed in reference 29. However, not only were the four spectra from the ψ' shown in Figure 5(a-d) and the corresponding four from the J/ψ (not shown) used, but a fifth spectrum from both the J/ψ and the ψ' was included in the analysis. The pattern cuts for this fifth spectrum were designed to improve the efficiency for detection of low energy photons, at the expense of reduced efficiency for removing minimum ionizing charged particles. It is shown for the J/ψ in Figure 8. The inserts on the upper left of Figures 3 and 8 show the result of one of the simultaneous fits made to correspondingly cut J/ψ and ψ' inclusive photon spectra. For the radiative transition to the η_c, the η_c mass and width are constrained to be the same for both spectra. The results of the fits to each of the five pairs of spectra were compared as a consistency check. An additional check was made by measuring the mass and width in the γ spectrum coming from events containing exactly two observed charged particles.

The results of this analysis are (29), $M_{\eta_c} = 2984 \pm 5$ MeV/c^2, $\Gamma_{\eta_c} = 11.5^{+4.5}_{-4.0}$ MeV, $B(J/\psi \to \gamma\eta_c) = (1.27 \pm 0.35)\%$, and $B(\psi' \to \gamma\eta_c) = (0.28 \pm 0.06)\%$. The

errors are dominated by the statistical uncertainties, except for the mass error which is mainly due to the uncertainty in our absolute energy calibration. These values are in good agreement, within errors, with previously reported Crystal Ball values (34).

5.2 Hadronic Decays of the 1^1S_0

Confirmation of the $\eta_c(2984)$ came soon after its discovery in the ψ' and J/ψ inclusive γ spectra with the first reports of the observation of its hadronic decays by the Mark II collaboration at SPEAR (35). A number of decay modes were seen, as is shown in Table 4.

We also have looked for exclusive decays of the $\eta_c(2984)$ into hadrons by performing kinematic fits to exclusive final states with multiple photons and two charged hadrons (34,36). Remember that the Crystal Ball measures both the energy and angle of electromagnetically showering particles but for charged hadrons (π,K) it measures only the angles well. Secondary interactions of the charged hadrons in the sodium iodide complicate the fitting of some events, but special pattern recognition algorithms have been developed to deal with this effect.

Events with a 3-photon, 2-charged particle topology were selected from the sample of J/ψ hadronic decays and subjected to a 3C kinematic fit to the hypotheses, $J/\psi \to \gamma\eta\pi^+\pi^-$ and $\gamma\eta K^+K^-$, $\eta \to \gamma\gamma$. The energy spectrum for the low energy radiated photon, arising from events which have a χ^2 probability greater than 0.1 for the $\eta\pi^+\pi^-$ hypothesis, showed a clear signal above background at the $\eta_c(2984)$ mass, within errors. No comparable signal was seen for the ηK^+K^- hypothesis.

The $\gamma\eta\pi^+\pi^-$ data in principle containes additional information on the width of the $\eta_c(2984)$. However, given the limited statistics of this measurement,

which comes from only half the presently available J/ψ data, we believe the inclusive measurement of the width to be more reliable at this time. From the signal of (18±6) events, we obtain the product branching ratio, $B(J/\psi \to \gamma\eta_c) \cdot B(\eta_c \to \eta\pi\pi)$, and branching ratio, $B(\eta_c \to \eta\pi\pi)$ given in Table 4. In addition, to compare directly with the Mark II observation of the $K^{\pm}K^{0}_{s}\pi^{\mp}$ final state of the $\eta_c(2984)$ our upper limit for the $K^+K^-\pi^0$ final state is also given. Note that the Crystal Ball value must be doubled before comparing with the Mark II result due to isospin; we assume $I = 0$ for $\eta_c(2984)$. Also, for completeness, the $\gamma\gamma$ final state branching ratio is given here (cf. Section 6.4).

5.3 Evidence for the 2^1S_0 State in the Inclusive γ Spectrum of the ψ'

As mentioned in Section 5, a candidate for the 2^1S_0 state or η'_c has been found by the Crystal Ball using inclusive photon decays of the ψ'. In this section we briefly describe our evidence for the state. A more complete description can be found in reference 37.

The event selection for the analysis as well as the photon selection criteria used are the same as those described in Section 3.3 with two minor changes. First, events with more than 10 charged or more than 10 neutral observed tracks are not considered. Secondly, a somewhat different lateral shower energy deposition pattern in the NaI(Tl) crystals is used to define photons than in the analysis described in Sections 3.3 and 5.1. In this case, an extra premium was placed on good efficiency for $E_\gamma < 100$ MeV. The main spectrum of Figure 3 results from about half the 1.8×10^6 ψ' decays, cut as described in Section 3.1. A signal at 3592 ± 5 MeV is evident in this spectrum. The insert on the upper left of Figure 3 shows the result of performing a fit to the region containing the structure at $E_\gamma \sim 90$ MeV; this insert contains a spectrum obtained from all 1.8×10^6 ψ' decays. A clear signal is obtained with 4.4σ to 6σ significance,

depending on how the fit is performed. The properties obtained from the fit for the η'_c candidate state are: $M_{\eta'_c} = 3592 \pm 5$ MeV/c^2, $\Gamma_{\eta'_c} < 8$ MeV (95% C.L.), and $B(\psi' \to \gamma\eta'_c)$, in the range 0.2% to 1.3% with a confidence level of 95%. The confidence interval for the uncertainty in the branching ratio includes the correlation with $\Gamma_{\eta'_c}$.

It should be noted that the DESY-Heidelberg group reported evidence (14) for a state at a mass of 3592 ± 7 MeV/c^2 in the exclusive channel $\psi' \to \gamma\gamma J/\psi$, $J/\psi \to \mu^+\mu^-$. However, as reviewed in Section 3.2, we have looked for evidence of such a state in the cascade decays and find none. If we assume that the object we observe in the inclusive spectrum is the η'_c, then it is expected (37) that $B(\psi' \to \gamma\eta'_c) \cdot B(\eta'_c \to \gamma J/\psi) < 10^{-6}$. This estimate is based on our measured value of $B(\psi' \to \gamma\eta'_c)$ and on theoretical calculations (5) for the η'_c total width and radiative transition rate. The estimate for the hindered magnetic dipole transition $\eta'_c \to \gamma J/\psi$ was based upon our measurement of the similar transition $\psi' \to \gamma\eta_c$, which reduces the estimate's sensitivity to the details of the wave functions. Such a small product of branching ratios has not been accessible to any experiment.

5.4 Discussion

Clear signals have been seen for states at $M = 2984 \pm 5$ MeV/c^2, and $M = 3592 \pm 5$ MeV/c^2 by the Crystal Ball detector; the Mark II has confirmed the state at 2984. These states are obvious candidates for the $1^1S_0(\eta_c)$ and $2^1S_0(\eta'_c)$ states of charmonium. What evidence makes these tentative assignments plausible?

First, the η_c is seen to decay into three pseudoscalars and not two. This allows only 0^-, 1^+,... assignments for the J^P of the state. As discussed in reference 3, the measured radiative transition branching ratio $B(J/\psi \to \gamma\eta_c)$ is in

good agreement with both the non-relativistic and QCD sum rule calculations, which assume $J^{PC} = 0^{\mp}$ for the observed state. In addition, the branching ratio $B(\psi' \to \gamma\eta_c)$ was also predicted by theory (38) and these predictions are in agreement with the observation. The mass splitting $1^3S_1 - 1^0S_1$ is predicted by a number of theories, including non-relativistic models and QCD sum rule calculations (38,39) and these are again in good agreement with the data. Finally, the width of the η_c is predicted to be 8.3 ± 0.5 MeV using QCD with higher order corrections (40) and the experimental value of $\Gamma_{\eta_c} = 11.5^{+4.5}_{-4.0}$ MeV agrees within the error. The important partial width $\Gamma(\eta_c \to \gamma\gamma)$, which has been predicted to be 4.2 ± 0.4 keV using the QCD sum rules (41) is well below the Crystal Ball upper limit of $\Gamma(\eta_c \to \gamma\gamma) < 20$ keV (90% CL) (c.f. Section 6.4). One can thus conclude with some certainty, given the above evidence, that the Crystal Ball state at 2984 ± 4 MeV/c^2 is truly the 1^1S_0 of charmonium.

Unfortunately, the case is not so clear for the η'_c candidate at M = 3592 ± 5 MeV/c^2. Relatively little is known about this state. No exclusive decays have been seen, and only an upper limit exists on its width. Within the limits of uncertainty concerning $2^3S_1 - 3^3D_1$ mixing (42), the agreement between theory and experiment is reasonable for the $\psi' - \eta'_c$ mass splitting. Also, the observed value for $B(\psi' \to \gamma\eta_c)$ agrees with non-relativistic model calculations within the large range allowed by observations. However, confirmation and more information is needed on this state before a firm connection to the 2^1S_0 state of charmonium can be made.

6. RADIATIVE TRANSITIONS FROM THE J/ψ

Other than for $J/\psi \to \gamma\eta_c$, $\eta_c \to$ hadrons, interest in radiative decays of the J/ψ first centered on 3γ decays, e.g., $\gamma\eta(\gamma\gamma)$ or $\gamma\eta'(\gamma\gamma)$, and particularly on searches for $\gamma\eta_c(\gamma\gamma)$. However, in recent years the possibility of observing gluonic meson states, particles made up entirely of gluons, has also stimulated much interest in J/ψ radiative decays.

6.1 The Fundamental Character of Gluonic Mesons in QCD

The existence of an extensive spectrum of colorless, flavorless bound states of two or more gluons has been firmly predicted by QCD (3). These gluonic bound states have been given the name "gluonic mesons" by their inventors, H. Fritzsch and M. Gell-Mann (43). It is expected that the lower mass gluonic meson states are bound states of mostly two gluons; in analogy to quarkonium, a bound state of a quark and antiquark, these systems are called gluonium. It is also expected that gluonium states should be by far easier to observe than the higher mass gluonic mesons due to their relatively lower masses. These are predicted to lie in the range of 1 to 2 GeV. Although the existence of gluonium has not yet been experimentally established, the interest in this new form of matter has increased considerably since the observation of two new mesons, the $\iota(1440)$ (44,45) and the $\vartheta(1640)$ (46). These are seen in a reaction thought to be a copious source of gluonic meson states (47), namely, $J/\psi \to \gamma\varkappa$. The mechanism is shown diagramatically in Figure 9. According to lowest order QCD calculations, the hadronic decays of quarkonium $^3S_1$ states, such as the J/ψ, proceed mainly via annihilation of the $q\bar{q}$ system into three gluons. Although this process might seem well suited to the production of gluonium states, it is not since each pair of the three final state gluons must be in a color-octet state. This follows from the fact that the overall state must be a color singlet and each pair

recoils against a single color-octet gluon. However, if a photon is radiated with two gluons in the decay, as shown in Figure 9, the recoiling gluon pair must form a color singlet state which is even under charge conjugation.

Perturbative QCD indicates (48,49) a partial width for the process $J/\psi \to \gamma gg$ of about 8 keV, which is relatively large. Various authors (47) have used duality principles, and other ideas, together with the perturbative result to show that gluonium states should be copiously produced in this process. However, the experimental search for such states has proven to be a difficult and confusing one with a number of guiding theoretical principles losing credibility as the field has matured (3).

6.2 The "Endpoint" of the Inclusive γ Spectrum at the J/ψ

One can qualitatively appreciate the major features of the radiative decays of the J/ψ by viewing the "endpoint" of the inclusive γ spectrum as measured by the Crystal Ball detector (42), and shown in Figure 10.

Relatively narrow peaks at the $\iota(1440)$ and $\eta'(958)$ are evident, and there is also a broad structure centered at a recoil mass of about 1700 MeV/c^2 (the ϑ has a mass close to 1700 MeV/c^2 but it is not as broad as the structure seen in the inclusive spectrum). The tails of the $\iota(1440)$ structure include the regions where radiative transitions to the $f(1270)$, $D(1285)$, and $f'(1515)$ would appear.

Transitions to the $\eta(549)$ should also be seen, but these are suppressed in this spectrum due to event selection cuts (42). Likewise, even if the $J/\psi \to \gamma\pi^0$ rate were large, no signal would be seen due to these cuts. Up to the time of this writing, very little quantitative analysis of the spectrum in Figure 10 has been done, and so only the above qualitative information can be drawn from it. A strong analysis effort has started recently in the Crystal Ball collaboration which will hopefully remedy this situation in the near future.

6.3 Gamma Transitions to Well-Known Particles Using Exclusive Decays

Experimental measurements have been reported by the Crystal Ball collaboration for the processes $J/\psi \to \gamma\pi^0$, $\gamma\eta$, $\gamma\eta'$, γf, and an estimate for $\gamma f'$, $f' \to \eta\eta$. Crystal Ball measurements for the η and η' have been published (15); however, new measurements by the Crystal Ball collaboration (50) derived from the full data sample of 2 10^6 J/ψ decays, about twice the data of the previously published results, disagree somewhat with the older measurements. The new measurements are in agreement within errors with three measurements from other experiments (10,50,51).

Table 5 shows the most recent Crystal Ball results for the various decays. Note that the new results on the η' use the $\eta\pi^+\pi^-$, $\eta\pi^0\pi^0$ and $\gamma\rho^0$ decay modes as well as the $\gamma\gamma$ decay mode which was the only one used in the old result. The Dalitz plot for $J/\psi \to 3\gamma$ from all our data is shown in Figure 11. Prominent signals are seen for the η and η'. No signal is seen at M_X = 2830 MeV/c^2, and M_{η_c} = 2984 MeV/c^2. Upper limits for these processes are given in Table 5. The direct decay $J/\psi \to 3\gamma$ as well as the QED process $e^+e^- \to 3\gamma$ also contribute to the Dalitz plot.

As an example of the analysis of an hadronic final state of the η', Figure 12 shows the signal for $J/\psi \to \gamma\eta'$, $\eta' \to \gamma\rho$, $\rho \to \pi^+\pi^-$. These events satisfy a 2C fit to the hypothesis $\gamma\gamma\pi^+\pi^-$. They also were subjected to several more constraints:

i) the high energy neutral track was required to satisfy a lateral energy deposition in the NaI(Tl) crystals expected of a high energy photon, rather than two photons from a high energy π^0;

ii) photon pairs forming a π^0 or an η were excluded;

iii) the energy of the charged particles had to be less than 1360 MeV;

iv) the $\pi\pi$ mass was cut about the ρ mass.

These requirements removed the strong $J/\psi \to \pi\rho$, and $J/\psi \to \gamma\eta'$, $\eta' \to \eta\pi^+\pi^-$ backgrounds. A Monte Carlo calculation gives an efficiency of 24% for the 666 events found and displayed in Figure 12. The ratio, $B(J/\psi \to \gamma\eta')/B(J/\psi \to \gamma\eta)$ has been of theoretical interest with the QCD sum rules (52), and other models (52), yielding values in the range from 3.7 to 4.0. In order to further compare data to theory we calculate from our data, $B(J/\psi \to \gamma\eta')/B(J/\psi \to \gamma\eta) = 4.7 \pm 0.6$.

Table 5 also shows a new Crystal Ball result for $J/\psi \to \gamma\pi^0$ (50). This result is in good agreement with the only other measurement of this quantity by DASP (10).

Although the process $J/\psi \to \gamma f$ (1270) has been well studied in other experiments (53), the analysis of this process in the Crystal Ball (54) provides a useful check on the analysis techniques employed in the ι and ϑ studies (cf. Section 6.4). It also provides a check that the Crystal Ball efficiencies are well understood in this complex $\gamma\pi^0\pi^0$ (5γ) final state. In addition, our measurement provides confirmation of previous results, and has also yielded the most precise determination of the helicity amplitudes for the process $J/\psi \to \gamma f$ available. Figure 13 shows the $\pi^0\pi^0$ invariant mass distribution; a prominent f (1270) signal is seen with 178 ± 30 event. The solid curve represents a fit to the f plus background. The dashed curve represents the background contribution. Figure 14 shows contours of equal probability as a function of x and y, $x = A_1/A_0$ and $y = \overline{A_2}/A_0$, where A_0, A_1 and A_2 are the f helicity amplitudes (55). The errors on our measurement are small enough that a quantitative comparison with theory can be made. Theoretical predictions for pure $M2$ and $E3$ transitions (El

is offscale), QCD (56), and tensor meson dominance (TMD) (57) are also shown in Figure 14. All of these predictions are inconsistent with the experimental measurement. In particular, the QCD calculation based on two-gluon exchange (56) is more than three standard deviations from the experimental point.

As discussed in the next section, a by-product of the $\vartheta(1640)$ study has been a rough measurement of $B(J/\psi \to \gamma f') \cdot B(f' \to \eta\eta)$. This result is listed in Table 5, along with the Mark II measurement of $B(J/\psi \to \gamma f') \cdot B(f' \to K\bar{K})$.

6.4 The Gluonium Candidates, $\iota(1440)$ and $\vartheta(1640)$

A state at 1440 MeV/c^2 was first seen in the reaction, $J/\psi \to \gamma K^{\pm} K^0_s \pi^{\mp}$, by the Mark II collaboration at SPEAR (44). They tentatively identified it as $E(1420)$, a state with $J^{PC} = 1^{++}$, but their experiment was not able to determine the J^P value. The existence of this state was soon confirmed by the Crystal Ball collaboration at SPEAR (36) using the reaction, $J/\psi \to \gamma K^+ K^- \pi^0$. However, much more J/ψ data was needed (2.2×10^6 decays in total) before the Crystal Ball collaboration was able to measure the J^P of the state as 0^- (45).

This 0^{-+} state may have been previously observed in $p\bar{p}$ annihilations (58). The state seen in the $p\bar{p}$ case was named $E(1420)$. However, the 0^{-+} assignment from that experiment was not considered conclusive (59) and so the name "$E(1420)$" was subsequently assigned to the $J^{PC} = 1^{++}$ state seen in $\pi^- p$ interactions (60). Thus, the Crystal Ball and Mark II experimenters (in collaboration) have named the 0^{-+} state seen in J/ψ radiative decays the $\iota(1440)$ (44).

Figure 15a shows the $K^+K^-\pi^0$ invariant mass distribution for events which satisfy 3C fits to the process $J/\psi \to \gamma K^+ K^- \pi^0$. This analysis is based on 2.2×10^6 produced J/ψ events. The shaded region corresponds to events with $M_{KK} < 1125$ MeV.

The $K\bar{K}\pi$ Dalitz plot from the Crystal Ball is shown in Figure 15b. A low $K\bar{K}$ mass enhancement (in the upper right corner of the plot) is evident. This enhancement has been associated with the $\delta(980)\pi$ decay of the resonance. No evidence for K^* bands, which would indicate a $K^*\bar{K}$ + c.c. decay, is observed, although the situation is potentially confusing because of the limited phase space available for the decay and the fact that the K^* bands overlap in the region of the δ. The Mark II results are consistent with this. They find the ι to decay primarily into $\delta\pi$.

Before discussing the Crystal Ball spin analysis of the $\iota(1440)$, we will review the status of the $E(1420)$. The best estimate of the mass (27) is M_E = 1418 ± 10 MeV/c^2. This is somewhat lower than, but not inconsistent with, the average of the Mark II and Crystal Ball measurements of the ι mass, M_ι = 1440 ± 10 MeV/c^2. The widths of the E(Γ_E = 50 ± 10 MeV) and the ι (Γ_ι = 55 ± 20 MeV) are also consistent. Thus the mass and width measurements of the ι do not clearly identify it as a different state than the E.

As mentioned previously, the spin of the E was established in an experiment which analyzed the reaction $\pi^-p \rightarrow K_s K^\pm\pi^\mp n$ at 3.95 GeV/c (60). The results of a partial-wave analysis of the $K\bar{K}\pi$ system determined $J^{PC} = 1^{++}$ for the E, thus making it the SU(3) nonet partner of the $D(1285)$ and the A_1. An additional result of the partial-wave analysis of Dionisi et al (60), is that the E decays primarily into $K^*\bar{K}$ + c.c. with $B(E \rightarrow K^*\bar{K} + \text{c.c.})/B(E \rightarrow (K^*\bar{K} + \text{c.c.})\ or\ \delta\pi) = 0.86 \pm 0.12$.

The spin of the $\iota(1440)$ was determined from a partial-wave analysis of the Crystal Ball data (45). Contributions from five partial waves were included: 1. $K\bar{K}\pi$ flat (phase space); 2. $\delta^\circ\pi^\circ - 0^-$; 3. $\delta^\circ\pi^\circ - 1^+$; 4. $K^*\bar{K}$ + c.c. $- 0^-$; 5. $K^*\bar{K}$ + c.c. $- 1^+$. Note that $J^P = 0^+$ is not allowed for a state decaying into three pseudoscalars. $J^P = 1^-$, although allowed for $K^*\bar{K}$ + c.c., would require the

Dalitz plot to vanish at the boundaries, which is inconsistent with the data of Figure 15b. Amplitudes with $J \geq 2$ were not considered. Contributions from all partial waves except the $K\bar{K}\pi$ phase space contribution were allowed to interfere with arbitrary phase. The $K\bar{K}\pi$ contribution due to phase space was assumed to be incoherent. The full angular decay distributions in each case were included in the amplitudes. The ι and K^* helicities were allowed to vary in the fits. The δ and K^* parameters were taken to be the standard values (27). In other words, a standard isobar analysis (61) was done here.

The analysis was done for events with $K\bar{K}\pi$ masses between 1300 and 1800 MeV/c^2. The data were divided into five bins of 100 MeV/c^2 each. The standard procedure of eliminating those partial waves which do not contribute significantly to the likelihood was utilized (i.e., the number of events contributed by a given partial wave was required to be larger than the error on that number). The only significant contributions were from $K\bar{K}\pi$ flat, $\delta^0\pi^0 - 0^-$, and $K^*\bar{K} + c.c. - 1^+$. These contributions, corrected for detection efficiency, are shown as a function of $K\bar{K}\pi$ mass in Figure 16. The $K^*\bar{K} + c.c. - 1^+$ contribution is relatively small and independent of mass. On the other hand, the $\delta\pi - 0^-$ contribution shows clear evidence for resonant structure in the ι signal region ($1400 \leq M_{K\bar{K}\pi} < 1500$ MeV/c^2). This establishes the spin-parity of the ι as 0^-. (The C-parity is required to be even because of the production mechanism.) In addition, contrary to the case of the $E(1420)$, the principal decay of the ι is into $\delta\pi$ and $B(\iota \to K^*\bar{K} + c.c.)/B(\iota \to (K^*\bar{K} + c.c.) \text{ or } \delta\pi) < 0.25$ (90% C.L.).

Since a number of assumptions went into the partial-wave analysis, and, in particular, only a limited number of partial waves were considered, checks were made to show that the results of the analysis were valid. First, maximum likelihood fits were made to the restricted hypothesis that in each mass interval, only one partial-wave contribution in addition to the flat contribution was allowed.

The relative probabilities resulting from fits to the data in the signal region ($1400 \leq M_{K\bar{K}\pi} < 1500$ MeV/c^2) are given in Table 6. Note that compared to the $\delta\pi - 0^-$ hypothesis, the next best hypothesis ($K^*\bar{K}$ + c.c. $- 1^+$) has a relative probability of only 1%. This establishes that there is not a strong correlation between the $\delta\pi$ and $K^*\bar{K}$ + c.c. amplitudes. The properties of the ι as measured by the Mark II and Crystal Ball collaboration are shown in Table 7. Also shown is the Crystal Ball upper limit (cf. Section 6.5) for $B(J/\psi \to \gamma\iota) \cdot B(\iota \to \eta\pi\pi)$. This upper limit is in mild conflict with the hypothesis that the $K\bar{K}\pi$ decay of the ι is dominated by $\delta\pi$ as hypothesized above (see Table 7), although some theoretical interpretations can avoid this conflict (62). Note that $\delta\pi$ dominance of the ι decay is an important element in our spin parity analysis of the ι.

The $\vartheta(1640)$ was first observed in the process, $J/\psi \to \gamma\eta\eta$, $\eta \to \gamma\gamma$ by the Crystal Ball collaboration (46). The analysis was based on the full data sample. Figure 17a shows the $\eta\eta$ invariant mass distribution for events consistent with $J/\psi \to \gamma\eta\eta$ after a 5C fit has been performed. Only events with $\chi^2 < 20$ are shown. The solid curve represents a fit to one Breit-Wigner resonance plus a flat background. The dashed curve represents a fit to two Breit-Wigner resonances, one with mass and width fixed at the f' and variable amplitude, the other with all three parameters variable; a flat background is also included. Because of the limited statistics, it is not possible to establish whether the ϑ peak is one or two peaks (the ϑ and f'). However, it is probably most reasonable to assume that the f' is present and fit for its amplitude. This was not done in reference 46; however, it was done in reference 63 and we will also use the results from the fit including two resonances. The spin of the ϑ was determined from a maximum likelihood fit to the angular distribution $W(\vartheta_\gamma, \vartheta_\eta, \varphi_\eta)$ for the process $J/\psi \to \gamma\vartheta$, $\vartheta \to \eta\eta$. The parameter ϑ_γ is the polar angle of the γ with respect to the beam axis, and $(\vartheta_\eta, \varphi_\eta)$ are the polar and azimuthal angles of one

of the η's with respect to the γ direction in the ϑ rest frame. ($\varphi_\eta = 0$ is defined by the electron beam direction.) The probability for the spin 0 hypothesis relative to the spin 2 hypothesis is 0.045. Spins greater than 2 were not considered. Note that the $\eta\eta$ decay mode establishes the parity of the state as even. Figures 17b and 17c show the $|\cos\vartheta_\gamma|$ and $|\cos\vartheta_\eta|$ distributions, respectively. Although the spin determination depends on information which cannot be displayed in these projections, it is clear that the $|\cos\vartheta_\eta|$ distribution plays the major role in the preference for spin 2. (The solid curves in the figures show the best fit distributions for spin 2; the dashed curves are the expected distributions for spin 0.) This is primarily due to the excess of events with $|\cos\vartheta_\eta| > 0.9$. The inset in Figure 17c shows these events on an expanded scale. There is no evidence that these events are anomalous.

The Crystal Ball and the Mark II (64) have searched for $J/\psi \to \gamma\vartheta$, $\vartheta \to \pi\pi$. Figure 13 shows the Crystal Ball results for the π^0's from 2.2 10^6 J/ψ decays. The binning in $M_{\pi\pi}$ is 50 (MeV/c^2)/bin. As summarized in Table 8, only upper limits were obtained from both the Crystal Ball and Mark II experiments.

The Mark II collaboration has obtained confirming evidence for the ϑ in the process $J/\psi \to \gamma\vartheta$, $\vartheta \to K^+K^-$ (64). They find the spin-parity assignment 2^+ to be favored at the 78% C.L. A summary of the Mark II results on the ϑ is also given in Table 7.

6.5 Other Radiative Transitions

The Mark II (65) reports a signal in the process $J/\psi \to \gamma\rho^0\rho^0$, $\rho^0 \to \pi^+\pi^-$. They interpret their $\rho^0\rho^0$ spectrum in this process as a combination of $\gamma\rho^0\rho^0$ phase space and a Breit-Wigner resonance. A maximum likelihood fit to this hypothesis yields, $M_{res} = 1650 \pm 50$ MeV/c^2, $\Gamma_{res} = 200 \pm 100$ MeV. These values are comparable to the mass and width of the ϑ shown in Table 7.

Also, they obtain, $B(J/\psi \to \gamma\rho^0\rho^0,\ M_{\rho^0\rho^0} < 2\ \text{GeV}) = (1.25 \pm 0.35 \pm 0.4) \times 10^{-3}$. Assuming that the $\rho\rho$ is in the decay in an $I = 0$ state, we have $B(J/\psi \to \gamma\rho\rho,\ M_{\rho\rho} < 2\ \text{GeV}) = (3.75 \pm 1.05 \pm 1.3) \times 10^{-3}$. This branching ratio is approximately equal to the $\iota(1440)$ and η' branching ratios. As a strong note of caution, the Mark II collaboration states that much more data is needed to establish the connection, if any, between the $\rho\rho$ structure and the ϑ meson.

The Crystal Ball collaboration (66) has also found additional structure in the region of the ϑ by examining the process, $J/\psi \to \gamma\eta\pi^+\pi^-,\ \eta \to \gamma\gamma$. Figure 18 shows the $M_{\eta\pi^+\pi^-}$ and $M_{\eta\pi^0\pi^0}$ distributions obtained from the analysis of 2.2×10^6 J/ψ decays. A large signal at $M_{\eta\pi\pi} = M_{\eta'}$ is evident, and in addition, there is a broad enhancement centered at about 1700 MeV/c^2.

Examination of the Dalitz plots for the $\eta\pi^+\pi^-$ events (66) with $1600 < M_{\eta\pi\pi} < 1850$ MeV/c^2 shows no structure. Thus the broad enhancement is not strongly associated with a δ, or any other resonance in either $\eta\pi^\pm$ or $\pi^+\pi^-$. Three possible interpretations are suggested for this new enhancement.

First, the $\eta\pi\pi$ mass distribution for events with a prompt γ may be quite different from Lorentz invariant phase space. Then the enhancement could arise from the (non-resonant) decay of the J/ψ to a photon plus two gluons. Secondly, the enhancement could be a group of resonances. A third possibility is that it is a single resonance. The data may be fit with a single Breit-Wigner line shape. For the fit, the $\eta\pi^+\pi^-$ and $\eta\pi^0\pi^0$ mass spectra are fit simultaneously with the mass and width parameters constrained to be the same for both channels. A constant background was assumed for the $\eta\pi^0\pi^0$ channel. For $\eta\pi^+\pi^-$, the background was determined by fitting the $\gamma\gamma\pi^+\pi^-$ mass spectrum for events with a $\gamma\gamma$ mass combination in the η sidebands ($320 < M_{\gamma\gamma} \leq 470$ MeV/c^2 or $610 < M_{\gamma\gamma} < 760$ MeV/c^2). The fit has a χ^2 of 66 for 69 d.o.f. and yields, $M = 1710 \pm 45$ MeV/c^2, $\Gamma = 530 \pm 110$ MeV, where the errors include estimates of

the systematic uncertainty.

Using the number of events in the peak, as determined by the fit and an efficiency obtained from Monte Carlo calculations of 18% (6.6%) for $J/\psi \to \gamma\eta\pi^+\pi^-$ ($\gamma\eta\pi^0\pi^0$), one obtains the branching ratios, $B(J/\psi \to \gamma\eta\pi^+\pi^-) = (3.5 \pm 0.3 \pm 0.7) \times 10^{-3}$, $B(J/\psi \to \gamma\eta\pi^0\pi^0) = (2.3 \pm 0.3 \pm 0.7) \times 10^{-3}$, where the first error is statistical and the second is systematic. These branching ratios, when added, are comparable to or larger than those for the ι and η'.

The fit shown in Figure 18 also includes a term for the ι, from which the upper limit in Table 7 was obtained. The implications of this low value for $\iota \to \eta\pi\pi$ are discussed in Section 6.4.

It is of interest to note that if the presently known contributions to radiative decays of the J/ψ in the ϑ region are added together, one obtains, $B(J/\psi \to \gamma\vartheta(\text{region})) \geq B(J/\psi \to \gamma\vartheta + \gamma\rho\rho + \gamma\eta\pi\pi) = (1.1 \pm 0.2) \times 10^{-2}$. This is the second largest branching ratio seen in the J/ψ radiative decays being about equal to that of the $\eta_c(2984)$.

The interpretation of the character of the ι and ϑ and the other new states seen for the first time in radiative transitions from the J/ψ is complex (3). In particular, the discussion of whether some of these states are gluonic mesons is beyond the scope of this review.

7. SEARCHES FOR THE F MESON, THE AXION, AND THE $^1P_1$ STATE

7.1 The Inclusive η Cross Section

In 1977, the DASP collaboration reported (67) a strong increase in the inclusive η production in e^+e^- collisions at $E_{CM} \cong 4.4$ GeV (and possibly at 4.17 GeV) relative to the production at 4.03 GeV. They interpreted this as evidence

for production of the charmed-strange F-meson which is expected to have a strong branching fraction into η's (68). Correlations with electrons and low energy γ's (expected from $F^* \to \gamma F$) strengthened this interpretation. Furthermore, they observed a cluster of events at E_{CM} = 4.42 GeV fitting the hypothesis $e^+e^- \to FF^* \to \gamma F\eta\pi$. Based on all of this, they reported that $R(e^+e^- \to F\bar{F}X) \cdot B(F \to \eta\pi) = 0.46 \pm 0.10$ in the E_{CM} range from 4.36 to 4.49 GeV, where $R(e^+e^- \to F\bar{F}X) = \sigma(e^+e^- \to F\bar{F}X)/\sigma(e^+e^- \to \mu^+\mu^-)$. The final state is written "$F\bar{F}X$" to take into account the possibility that F-meson pairs may occur via production of excited F-mesons, e.g., $e^+e^- \to F^*\bar{F} \to \gamma F\bar{F}$.

In order to study this interesting phenomenon, the Crystal Ball data was analyzed for inclusive η production. The data sample consisted of hadronic events from six fixed c.m. energies and seven c.m. energy bands. The fixed points consisted of the J/ψ, ψ', ψ'', a point at 3.670 GeV in the continuum just below the J/ψ to act as a control from below charm threshold, and two energies above charm threshold (4.028 and 5.200 GeV). The seven energy bands cover a range in E_{CM} from 3.878 to 4.500 GeV. These data were taken in fine scans with steps in E_{CM} of between 2 and 12 MeV. For purposes of measuring $R_\eta = \sigma(e^+e^- \to \eta\pi)/\sigma(e^+e^- \to \mu^+\mu^-)$, the seven energy bins were chosen to correlate with observed structure in $R(e^+e^- \to \text{hadrons})$ (69).

The method for obtaining the number of produced η mesons at each energy was to study the inclusive $\gamma\gamma$ mass distribution in the vicinity of the η mass. In all cases, a clear enhancement at the η mass was visible to the naked eye. The number of observed η's was obtained by standard statistical fitting of the observed distribution to a smooth background function plus a resolution function of adjustable size centered on the η mass. The observed number was then corrected for the branching ratio for $\eta \to \gamma\gamma$ and the η detection efficiency which ranged from 38% at the J/ψ to 27% at 5.2 GeV. Uncertainties in the detection

efficiencies due to our uncertain knowledge of the details of e^+e^- annihilation physics are included in the limits which are finally obtained.

Figure 19 shows our results for R_η. The off-scale values at the J/ψ and ψ' are excluded[2] and the other points have been corrected for the radiative tails of these two resonances. Although there may be some correlation with the total hadronic cross section, we see that there is no dramatic difference in R_η below and above charm threshold. If we assume that the contribution to R_η due to non-charm physics is constant and that all excess in R_η is due to F-decays, we can set limits on $R(e^+e^- \to F\bar{F}X) \cdot B(F \to \eta\pi)$ by comparing the values for R_η above charm threshold with that below it at 3.67 GeV. The 90% confidence level limits are all below 0.32 and for the energy band from 4.365 to 4.500 GeV, it is 0.19. This disagrees with the DASP result (67). Most of the disagreement is due to the fact that the earlier experiment saw essentially no η-signal at 4.03 GeV whereas the Crystal Ball observed almost the same strength at 4.03 GeV as at other energies, even below charm threshold. At energies above about 4.1 GeV, the cross sections reported by the two experiments are on the average compatible. Up to the time of this writing, the Crystal Ball has found no firm evidence for the elusive charmed-strange F-meson.

7.2 Search for $J/\psi \to \gamma$ Axion

Because of its exceptionally large solid angle coverage by charged particle and photon detectors with essentially 100% detection efficiency and its moderately good time resolution (about 3 ns), the Crystal Ball is well-adapted to

[2] When the results are expressed in terms of f_η, the average number of η's per hadronic event, the two resonances are not special; f_η has a value of about 0.13 and shows little variation over this energy range.

search for certain exotic phenomena, especially those of the class $e^+e^- \rightarrow \gamma X$ where X escapes detection for some fundamental reason. An example of such a reaction involving known particles is that in which X is $\nu\bar{\nu}$ resulting from either direct production, or the decay of a light, neutral spin-1 gauge boson as suggested by some supersymmetric theories (70), or, at higher energies, the decay of the Z^0. Another possibility, which has been searched for in the Crystal Ball and is reported in reference 71, is the radiative decay of the J/ψ into an axion. The axion (a) is the Goldstone boson appearing from the breaking of a chiral U(1) symmetry which has been postulated to avoid large P- and CP-invariance violations in QCD (72). If the number of quark generations is assumed known, then this theory has only one free parameter, the ratio, x, of the vacuum expectation values of the two Higgs fields present in the theory. However, it does endow the axion with a sufficiently long life and weak enough interactions that it would escape detection in the Ball. The theory reliably predicts that $B(J/\psi \rightarrow \gamma a) = (5.7 \pm 1.4) \times 10^{-5} x^2$. Positive evidence for an axion or axion-like particle was reported by Faissner et al (73) with a mass $m_a = 250 \pm 25$ keV/c^2 and $x = 3.0 \pm 0.3$ (but these values seem inconsistent with other experiments (74)). They imply that there should be about 800 events in the Ball with $|\cos\vartheta| < 0.8$ and these events would have the distinctive signature of a single photon with beam energy. No significant numbers of such events are seen.

The dominant background in this search comes from cosmic rays and most of these can be eliminated by restricting attention to the bottom hemisphere of the Ball, which simply reduces the overall detection efficiency to 30%. After making a cosmic ray background subtraction using events out of time with the beam, we obtain a 90% confidence level upper limit of 6.2 events in an energy range from 1.3 GeV to two energy resolution standard deviations above the beam energy. This implies an upper limit of $1.4\ 10^{-5}$ (90% C.L.) on the branching

fraction. The corresponding upper limit on x is 0.6, in disagreement with the result in reference 73.

A definitive test of the standard axion model, which eliminates any dependence on x, has been proposed (75) by setting limits on both $J/\psi \to \gamma a$ and $\Upsilon \to \gamma a$. Recent results from the LENA collaboration at DORIS (76) and the CUSB collaboration at CESR (76a) have established that $B(\Upsilon \to \gamma a)$ is less than $9.1\ 10^{-4}$ (90% C.L.) and $3.5\ 10^{-4}$ (90% C.L.), respectively. These results together with the above Crystal Ball limit on $\psi \to \gamma a$ violate the results of the standard axion model and it now seems necessary to retreat to an even more elusive axion (such as has been proposed in grand unified theories (77)).

7.3 The Search for Decays $\psi' \to \pi^0\ ^1P_1$

The only predicted $c\bar{c}$ bound state for which no evidence exists is the $^1P_1$ with $J^{PC} = 1^{+-}$. Its mass is expected to be approximately equal to the center of gravity of the ^3P states, or about 3520 MeV (78). Experimental determination of its mass is important since any significant deviation from the above value would suggest a long range spin-spin term in the quarkonium potential. We have searched extensively in our large ψ' data sample for evidence of this state and have not found it (79).

Single photon transitions between the ψ' and $^1P_1$ states are forbidden by C conservation and so one must investigate double photon transitions. Four possibilities are indicated in Figure 20. Estimates based on related measured rates indicate that only the $\psi' \to \pi^0\ ^1P_1$ process can be reasonably expected to have a branching ratio in the percent range. This process would lead to a monochromatic π^0 in ψ' decay having an energy which is expected to be below about 200 MeV; 165 MeV is favored. Figure 21a shows the inclusive π^0 distribution observed in ψ' decays. The evident structures at about 200 MeV and just above

400 MeV are expected backgrounds. They are due to fake π^0's generated with the monochromatic photons from $\psi' \to {}^3P_J$ transitions, and the reactions $\psi' \to \pi^0\pi^0 J/\psi$ and $\psi' \to \pi^0 J/\psi$. No other structure is evident and 95% confidence level limits of less than 1.09% have been set for $B(\psi' \to \pi^0\, {}^1P_1)$ for any ${}^1P_1$ mass between 3440 MeV/c^2 and 3535 MeV/c^2. In particular, at the favored mass of 3520 MeV/c^2, the limit is 0.42%.

In an effort to reduce backgrounds and so increase sensitivity at the expense of a less general result, we have also searched for evidence of the cascade decay $\psi' \to \pi^0\, {}^1P_1 \to \gamma\gamma\gamma\, \eta_c$ where the η_c is constrained in mass, but not decay mode. Study of this particular configuration is motivated by a reasonable expectation that $B({}^1P_1 \to \gamma\, \eta_c)$ is in the vicinity of 50%. Figure 21b shows the γ(prompt)η_c mass distribution for events fitting the hypothesis $\psi' \to \pi^0\, \gamma\, \eta_c$ and again there is no evidence for the ${}^1P_1$ state. We have set 95% confidence limits of less than 0.35% for $B(\psi' \to \gamma\, {}^1P_1) \cdot B({}^1P_1 \to \gamma\, \eta_c)$ for ${}^1P_1$ masses in the same range as above. At the preferred mass, the limit is 0.14%. Although the ${}^1P_1$ state has not been found, the limits which have been set are sufficiently low to be theoretically interesting.

8. MEASUREMENTS OF R_h IN THE E_{CM} RANGE OF 5.0 TO 7.4 GeV

One of the most fundamental and difficult measurements that can be done at an e^+e^- storage ring is that of the total hadronic cross section, $\sigma_h = \sigma(e^+e^- \to \text{hadrons})$. In order to remove the straightforward effects of QED and so reveal the strong interaction effects more clearly, it is customary to normalize the hadronic cross section to the theoretical, lowest-order, purely QED cross section $\sigma_{\mu\mu}$ for $e^+e^- \to \mu^+\mu^-$, which, in the energy range of interest here, is $(4\pi/3)(\hbar c)^2\alpha^2/E_{CM}^2 = 86.8/E_{CM}^2$ (nb, GeV). In the energy range well above

charm threshold and below bottom threshold, the prediction of QCD for the normalized cross section, $R_h = \sigma_h / \sigma_{\mu\mu}$, is, to first order, $R_{QCD} = 3 \sum_i Q_i^2 (1 + \alpha_s(s)/\pi + \ldots)$, where $s = E_{CM}^2$, $i = (u, d, s, c)$ is the quark flavor index, Q_i is the charge of the i'th quark, and $\alpha_s(s)$ is the QCD running coupling constant (80). The sum over Q_i^2 yields a value of 10/3 and, at E_{CM} = 6 GeV, the first

order[3] QCD result increases this by about 6% for $\Lambda_{\overline{MS}}$ = 100 MeV.

In 1980, Barnett et al (80) made a careful comparison of all available measurements of R_h (81) to the predictions of QCD. They concluded that above 5.5 GeV, a potentially serious discrepancy, in the range of 15% to 17%, existed. This was just outside the quoted systematic uncertainties of 10% and there was the exciting possibility that it represented new phenomena or difficulties with QCD. This prompted the Crystal Ball collaboration to undertake a series of new R_h measurements from 5.0 GeV to the top of the SPEAR range, 7.4 GeV (81a). To do this, a total exposure of 12.7 pb^{-1} was distributed over eleven energies in this range.

The two ingredients in the experimental determination of R_h are the integrated luminosity of the exposure and the number of hadronic events produced (and corrected for QED radiative effects). The luminosity was obtained both by the small angle Bhabha scattering monitor and by observation of large-angle QED events in the Ball itself. These independent determinations of the integrated luminosity agreed to about 2% and their average was used.

The determination of the radiatively-corrected number of hadronic events produced by annihilations involved three steps. First, criteria were developed and applied to efficiently distinguish individual annihilation hadronic events from five classes of backgrounds: cosmic rays, beam-gas collision, QED events, two-photon collisions, and $\tau\bar{\tau}$ events. Next, properly normalized statistical subtractions were made to eliminate the residual backgrounds that slipped through the first step. And finally, the resulting count was corrected for the detection

[3] The next higher order in the QCD calculation using the modified minimal subtraction renormalization scheme is known (80). It contributes only 0.7% to the prediction, well below present experimental precision.

efficiency of both the triggering hardware and the event selection software of the first step. The purely QED radiative effects were also included in this step. Pure samples from each of the five event classes, were obtained either experimentally (cosmic rays and beam-gas events) or by Monte Carlo simulation. These were examined and efficient criteria for event selection developed. These criteria were then applied to both the data and the five pure samples. The residuals from the backgrounds were then subtracted from the data, and the result was then corrected by the detection efficiency determined from the Monte Carlo simulation of the annihilation events. The Monte Carlo calculation incorporated all radiative correction effects in the event generation algorithms and so this last step automatically includes these corrections.

The most important backgrounds were those due to cosmic ray events, beam-gas collisions, and τ decays. Criteria to identify the first two of these were based on the spatial distribution of energy in the Ball and were developed by studying events out of time with the beam and those obtained in runs with the beams separated. The cosmic ray background was reduced to negligible levels by these criteria and the residual beam gas background which had to be removed by a statistical subtraction was typically at the 10% to 12% level. No attempt was made to identify $\tau\bar{\tau}$ events or those arising from $\gamma\gamma$ collisions and so these backgrounds were removed by subtraction only. The pure samples of these two background classes were obtained by Monte Carlo simulation. Together, these two background sources gave a subtraction of about 12%. Finally, the QED contamination was easily reduced to negligible levels by criteria involving leading particle energy and number of observed particles.

The important questions of detection efficiency and radiative corrections were answered by subjecting simulated annihilation events generated by the LUND81 (82) Monte Carlo program (including radiative corrections) to the same

criteria as the data. The result of this was the product of detection efficiency and the radiative correction factor. This product had a typical value of 1.06.

Table 9 gives the results of the experiment. The point-to-point systematic errors are given in the table and include the effects of uncertainty in the normalization of the several background subtractions and the statistical errors in the several Monte Carlo simulations. In addition, there is an overall systematic scale uncertainty of 5.3% (for the 1981 data) arising from various effects: 3.0% from radiative corrections, 3.0% from the detection efficiency, 2.5% from the luminosity, 1.4% from tau-tau bar events, 1.3% from beam-gas interactions, and 0.6% from two-photon collisions. Figure 22 compares these results with those of other of the data is completely consistent with that of QCD. The absolute value of the measurements is about 6% lower than the QCD predictions for reasonable values of the QCD parameter $\Lambda_{\overline{MS}}$. This disagreement, of course, is easily accommodated by the systematic scale uncertainty of the data. We conclude that these results rule out the possibility of any new phenomena in this energy range, at least, at the level suggested by the Mark I data.

9. TWO-PHOTON PHYSICS

In addition to studying the physics of e^+e^- annihilations, the Crystal Ball experiment has been able to investigate certain two-photon reactions. More precisely, we can investigate the reaction $e^+e^- \rightarrow e^+e^- +$ hadrons in the configuration that each of the two leptons scatters through a very small angle. Because of the small scattering angle, the outgoing electrons are not detected. To lowest order in QED, then, the hadrons result from the collision of two photons, which, though virtual, are very nearly on their mass shell. The Crystal Ball is particularly adapted to study the case that the hadrons decay into only

photons and, to date, the work on the four-photon final state has been completed (83). The data for this analysis came from an integrated luminosity of 21 pb^{-1} distributed over an E_{CM} range from 3.9 GeV to 7.0 GeV.

9.1 Measurement of $\Gamma(f \rightarrow \gamma\gamma)$ from $\sigma(\gamma\gamma \rightarrow f \rightarrow \pi^0\pi^0)$

All neutral events with exactly four energy clusters inside $|\cos\vartheta| < 0.9$, each with more than 20 MeV and with energy deposition patterns consistent with photons, were selected. Furthermore, it was required that the endcaps contain less than 40 MeV, and that the total invariant mass of the event be in the range from 720 MeV to E_{CM}. The resulting sample of events shows a strong peak at zero in the square of the total transverse momentum as expected for 2γ events. Only those in this peak (the cut was at 0.03 $(GeV/c)^2$) were subsequently used.

In essentially all of the final sample, photon pairings could be made which were consistent with either $\pi^0\pi^0$ or $\pi^0\eta$ being the primary hadrons. The top part of Figure 23 gives the invariant mass distribution of the $\pi^0\pi^0$ sample which clearly shows a strong signal near the f mass and no other significant structure. Of special note here is the smallness of the background. This is in contrast to earlier experiments which detect the charged pion decay mode of the f and tend to be troubled with large non-resonant $\pi^+\pi^-$ and QED $\mu^+\mu^-$ backgrounds (84-87).

To obtain the cross section for $\gamma\gamma \rightarrow \pi^0\pi^0$, the $\pi^0\pi^0$ mass spectrum was corrected for the variation in the $\gamma\gamma$ flux over it (88) and detection efficiency. The bottom part of Figure 23 gives the resulting cross section with the added restriction that $|\cos\vartheta^*| < 0.7$ where ϑ^* is the angle between the beam and the outgoing π^0 direction in the $\pi^0\pi^0$ rest frame. The solid curve shows a fit with three contributions: a relativistic Breit-Wigner function (including slight spreading due to the experimental mass resolution) with mass and width parameters

taken from the Particle Data Group compilation (27) for the f, the same for a possible $S^*(980)$, and a straight line to describe $\pi^0\pi^0$ non-resonant background. As is clear, the curve does not give a good fit since the data's mass peak is lower than that of the curve by about 40 MeV. The broken curve is the fit obtained when the f mass and width are allowed to be free, the best fit values being 1238 $\pm$ 14 MeV/c^2 and 248 $\pm$ 38 MeV, respectively. This mass shift could, in fact, be accommodated within the estimated systematic error of about 2% and the statistical error, but other $\gamma\gamma$ experiments have observed a very similar effect (85,86), which suggests that the effect is due to some underlying physical mechanism rather than an instrumental artifact. Possible sources of this effect are interference with non-resonant background (89) or the $\varepsilon(1300)$. Finally, there is the interesting possibility that the f may be mixed with a predicted gluonic meson almost degenerate with it (90). In this last case, different production and/or decay channels would yield different resonance shapes, and so f production in the $\gamma\gamma$ channel could possibly give different phenomenological resonance parameters than those found in other hadronic interactions.

Previous determinations of $\Gamma(f \to \gamma\gamma)$ from two-photon collisions have assumed the theoretical prediction that the f is produced predominantly with helicity 2 (91,92). Because of the negligible backgrounds in this experiment, it is possible to verify this theoretical expectation by observing the ϑ^* angular distribution. This is shown in Figure 24. It is clear that the spin 2 assumption with helicity 2 domination gives a good fit; the other helicity contributions are consistent with zero. If we assume that the mass peak is due to the f and that the decay is purely helicity 2, then we obtain $\Gamma_{f \to \gamma\gamma} = 2.7 \pm 0.2 \pm 0.6$ keV, the first error being statistical and the second, systematic. This agrees well with the results from other experiments (84-87).

9.2 Measurement of $\Gamma(A_2 \to \gamma\gamma)$ from $\sigma(\gamma\gamma \to A_2 \to \pi^0\eta)$

After the $\pi^0\pi^0$ events were removed from the 4γ sample, the resulting events were essentially all $\pi^0\eta$ and their invariant mass peaks at around 1300 MeV/c^2. Identifying this peak with the $A_2(1320)$ and assuming pure helicity 2, we can extract the $\gamma\gamma$ partial width of the A_2. We obtain $\Gamma(A_2 \to \gamma\gamma) = 0.77 \pm 0.18 \pm 0.27$ keV. The naive quark model with ideal mixing predicts a ratio of 9/25 for $\Gamma(A_2 \to \gamma\gamma)/\Gamma(f \to \gamma\gamma)$ which is in agreement with the Crystal Ball observations of $0.29 \pm 0.07 \pm 0.07$ for this ratio.

9.3 Other States

In addition to the two measurements discussed above, we can also set several limits based on the absence of signals. First, as is seen in Figure 23b, there is no evidence for $\gamma\gamma \to S^*(980) \to \pi^0\pi^0$. From this, we can set the limit $\Gamma(S^* \to \gamma\gamma)B(S^* \to \pi\pi) < 0.8$ keV. This limit is considerably smaller than the value of about 20 keV expected by most theoretical estimates (92), but consistent with a single-quark-exchange calculation (93) which predicts less than 0.4 keV for mesons in the 0^{++} nonet. Finally, no signal for $\gamma\gamma \to \eta\eta$ was observed. This allows two 95% C.L. limits to be set. First a limit of 0.05 can be put on $\Gamma(f \to \eta\eta)/\Gamma(f \to \pi\pi)$. This is consistent with the limit of 0.016 obtained in earlier work (94). And secondly, this absence implies that $\Gamma(\vartheta(1640) \to \gamma\gamma)B(\vartheta(1640) \to \eta\eta)$ is less than 5 keV.

10. MEASUREMENTS IN THE REGION FROM CHARM THRESHOLD TO 4.5 GeV

It has been known for a long time that the energy region above charm threshold, from the ψ'' at 3.77 GeV to about 4.5 GeV is rich in charmed physics phenomena. The ψ'' itself is known to be a D-factory, 4.03 GeV is a D^*-factory, F and F^* mesons are expected, and, more generally, there should be a rich spectrum of excited D and F mesons produced in e^+e^- collisions in this energy range (95). The strong structure in R_h in this region (81) is ample evidence for this but so far no details have been fully resolved above 4.03 GeV. In order to investigate this potentially interesting area of physics, the Crystal Ball accumulated an exposure at the $\psi''(3770)$ yielding about 1.3 10^4 produced ψ'', and an exposure of 11.3 pb^{-1} distributed over the range 3.8 GeV to 4.5 GeV. Although a great deal of effort has gone into analyzing this data, only the results on R_η discussed above are considered complete. Preliminary reports on some of the other work have been given, however, and we give a short review of them here.

The global structure of the physics in this region is shown by the energy dependence of the normalized hadronic cross section itself, charged and neutral multiplicities, and charged and neutral energy fraction. Preliminary results on some of these from the Crystal Ball data are given in reference 96. The R_h measurements confirm the structure seen in other experiments (81): clear peaks at 3.77, 4.03, and 4.4 GeV, a broad peak with possibly some substructure around 4.16 GeV followed by a broad "valley" in the 4.2 to 4.3 GeV region. The statistical precision of this set of measurements is very high but much work remains to be done to reduce the point-to-point systematic uncertainties to fully exploit it. Analysis of R_h over the ψ'' excitation curve gives resonance parameters (97) in reasonable agreement with earlier work (98).

The observed neutral energy fraction is quite smooth through the whole region and so seems to be insensitive to the underlying physics However, the

observed neutral multiplicity does show large changes. Together, these two facts suggest that *low-energy* γ's, π^0's and η's could be useful indicators and these have been stressed in the data analysis. The resonance at E_{CM} = 4.03 GeV serves as a source of almost monochromatic low-energy π^0's and photons. This results from the combination of a large D^* cross section at this energy and low Q values for both the production channels, $D^*\bar{D}^*$ and $D^*\bar{D} + \bar{D}^*D$, and the decay channels $D^* \to \pi^0 D$ and γD. These circumstances give rise to an inclusive photon spectrum at this energy which is quite complex since there are significant contributions from all eight sources (π^0 and γ from both charged and neutral D^* decays arising from both $D^*\bar{D}^*$ and $D^*\bar{D}$ + c.c.). Qualitatively, the π^0 and γ contributions are resolvable since the former is peaked around 70 MeV and the latter, around 135 MeV (the Doppler broadening gives rise to only a slight overlap). Further information is provided by the π^0 energy spectrum which shows strong peaking at small kinetic energies. By contrast to the strong structure in these spectra at E_{CM} = 4.03 GeV, the corresponding ones below D^* threshold at the $\psi''(3770)$ are smooth and featureless. We have used these as background functions in quantifying the effects due to the D^* mesons. The spectra allow a new determination of the $D^{*0} - D^0$ mass difference of 142.2 ± 0.5 ± 1.5 MeV/c^2 in agreement with earlier Mark I results (99). However, because of the relatively large number of cross sections (those for $e^+e^- \to D^{*0}\bar{D}^{*0}$, $D^{*+}D^{*-}$, $D^{*0}\bar{D}^0$ + c.c., $D^{*+}D^-$ + c.c.) and branching ratios (those for $\bar{D}^{*0} \to \pi^0 D^0$ and γD^0, $\bar{D}^{*+} \to \pi^0 D^+$ and γD^+) which are involved, the finite resolution of the apparatus, and the limited statistics, it is only possible to directly measure certain combinations of the physically interesting quantities. Guided by theoretical calculations (99) and Mark I measurements (100), we can make reasonable assumptions about some of these quantities and so obtain $\sigma(D^{*0}\bar{D}^0 + c.c.)/\sigma(D^{*0}\bar{D}^{*0}) \cong 1.6$ and $B(D^{*0} \to \gamma D^0) \cong 0.37$. These results are

consistent with those of Mark I (99).

11. SUMMARY AND FUTURE PROSPECTS

Although the people who studied photon detectors for e^+e^- storage rings at the 1974 PEP Summer Study did not yet know about the soon-to-be-discovered charmed quarks, subsequent events have shown that the practical realization of their ideas has borne rich rewards in understanding this sector of nature. The Crystal Ball detector grew out of that work and, as this brief review has shown, it has proved to be an especially versatile instrument in spite of features (or lack of them) which at first sight would make it seem to be very specialized and restricted in application. Of course, the dominant strength of this detector has been, and always will be, the measurement of monochromatic photons, and it was this capability that allowed the Ball to resolve the old problems with the charmonium interpretation of psionic matter. However, the measurements of R_h, for example, demonstrate the instrument's capability to determine global properties of e^+e^- annihilations, and, at the other extreme, kinematically constrained fitting to very specific final states which include just two charged particles but are rich in photons has been successfully exploited.

Work is currently in progress on several projects involving our large SPEAR data sample. These include searches for the F meson by means of specific exclusive channels, study of D decays, further work on D^* physics, completion of the work on R_h just above charm threshold, measurement of certain interesting exclusive hadronic final states in J/ψ and ψ' decays, and further work on radiative decays of the J/ψ and ψ' and in two-photon physics. However, an increasingly large fraction of the group's efforts is going into new ventures in Υ physics. Within the next few years, we expect to have sufficiently large data samples at

the T, T', T'', and other energies to be able to make contributions toward understanding upsilonic matter comparable to what we have done in the psionic sector. The difficulties are formidable since the rate of data accumulation at the higher energies is considerably smaller than in the J/ψ-region, but the work has begun. Finally, we expect to utilize the higher $\gamma\gamma$ flux in the 10 GeV energy range to explore further questions in two-photon physics.

ACKNOWLEDGMENTS

The work reported here would not have been possible without the dedicated, innovative, and, at times, brilliant efforts of the many members of the Crystal Ball collaboration and their supporting engineers and technicians, the staffs of the accelerators at SLAC, Harshaw Chemical Co., and other people who played important roles in building the detector. The members of the Crystal Ball collaboration were: C. Edwards, R. Partridge, C. Peck, F. Porter (Caltech); D. Antreasyan, Y. Gu, W. Kollmann, M. Richardson, K. Strauch, K. Wacker, A. Weinstein (Harvard); D. Aschman, T. Burnett, M. Cavalli-Sforza, D. Coyne, C. Newman, H. Sadrozinski (Princeton); D. Gelphman, R. Hofstadter, R. Horisberger, I. Kirkbride, H. Kolanoski, K. Königsmann, R. Lee, A. Liberman, J. O'Reilly, A. Osterheld, B. Pollock, J. Tompkins (Stanford-HEPL); E. Bloom, F. Bulos, R. Chestnut, J. Gaiser, G. Godfrey, C. Keisling, W. Lockman, M. Oreglia, D. Scharre (SLAC). The work of the collaboration was supported in part by the Department of Energy under contracts DE-AC03-76SF00515 (SLAC), DE-AC02-76ER03064 (Harvard), DE-AC03-81ER40050 (Caltech), and DE-AC02-76ER03072 (Princeton); by the National Science Foundation contracts PHY81-07396 (HEPL), PHY79-16461 (Princeton), and PHY75-22980 (Caltech); and by fellowships from the NATO Fellowship, the Chaim Weizmann Fellowship, and the Sloan Foundation, which provided partial

support to members of the collaboration.

Literature Cited

1. Bloom, E. D. et al 1974. *1974 PEP Summer Study Report, PEP Note 155;* Mast, T., Nelson, J. 1974. *1974 PEP Summer Study Report, PEP Note 153*

2. Bloom, E. D. 1981. *SLAC Summer Institute* 1981:1, and references therein.

3. Bloom, E. D. 1982. *21st Int. Conf. on High Energy Physics*, Paris, France, July 26-31, 1982, C3:407. This reference has an extensive review of gluonic mesons and contains references to the relevant theoretical literature.

3a. Chinowsky, W. 1977. *Ann. Rev. Nucl. Sci.* 27:393

4. Feldman, G. J. et al 1975. *Phys. Rev. Lett.* 35:821

5. Chanowitz, M. S., Gilman, F. J. 1976. *Phys. Lett. B* 63:178

6. Tanenbaum, W. et al 1978. *Phys Rev. D* 17:1731

7. Appelquist, T., Barnett, R. M., Lane, K. 1978. *Ann. Rev. Nucl. Sci.* 28:387

8. Shifman, M. A. 1978. *Phys. Lett. B* 77:80

9. Vainshtein, A. et al 1978. *Yad. Fiz.* 28:465

10. Braunschweig, W. et al 1977. *Phys. Lett. B* 67:243

11. Wiik, B. H., Wolf, G. 1978. DESY 78/23

12. Biddick, et al 1977. *Phys. Rev. Lett.* 38:1324

13. Whitaker, J. S. et al 1976. *Phys. Rev. Lett* 37:1596

14. Bartel, W. et al 1978. *Phys. Lett. B* 79:492

15. Partridge, R. et al 1980. *Phys. Rev. Lett.* 44:712

16. Hughes, E. B. et al 1972. *IEEE Trans. Nucl. Sci.* 19:126

17. Oreglia, M. et al 1982. *Phys. Rev. D* 25:2259

18. Gaiser, J. E. et al 1979. *IEEE Trans. Nucl. Sci.* 26:173

19. Chan, Y. et al 1978. *IEEE Trans. Nucl. Sci.* 25:333

20. Chestnut, R. et al 1979. *IEEE Trans. Nucl. Sci.* 26:4395

21. Aubert, J. J. et al 1974. *Phys. Rev. Lett.* 33:1404

22. Augustin, J. E. 1974. *Phys. Rev. Lett.* 33:1406

23. Abrams, G. S. et al 1974. *Phys. Rev. Lett.* 33:1453

24. Simpson, J. W. et al 1975. *Phys. Rev. Lett.* 35:699

25. Braunschweig, W. et al 1975. *Phys. Lett. B* 57:407

26. Himel, T. M. et al 1980. *Phys. Rev. Lett.* 44:920

27. Aguilar-Benitez, M. et al 1982. *Particle Data Tables*, Particle Data Group, CERN and U. C. Berkeley, April 1982; *Phys. Lett. B* 111:1

28. Karl, G. Meshkov, S., Rosner, J. 1976. *Phys. Rev.* D13:1203

29. Gaiser, J. et al 1983. *SLAC-PUB-2899*, to be submitted to *Phys. Rev. Lett.*; a complete discussion of the analysis can be found in: Gaiser, J. 1982. Ph.D. Thesis, Stanford University, SLAC-255 (unpublished)

30. Bloom, E. D. 1982. *Proc. 2nd Int. Conf. on Physics in Collision: High Energy ee / ep / pp Interactions* Stockholm, Sweden, June 2-4, 1982.

31. Oreglia, M. et al 1980. *Phys. Rev. Lett.* 45:959

32. Himel, T. M. 1979. Ph.D. Thesis, Stanford University, SLAC-223 (unpublished)

33. Bloom, E. D. 1979. *Proc. 1979 Int. Symp. on Lepton and Photon Interactions at High Energy*, Batavia, Illinois, August 23-29, 1979:92, Fermi National Accelerator Laboratory, Batavia, Illinois

34. Partridge, R. et al 1980. *Phys. Rev. Lett.* 45:1150

35. Himel, T. M. et al 1980. *Phys. Rev. Lett.* 45:1146

36. Aschman, D. 1980. *Proc. XV Rencontre de Moriond*, Les Arcs, France, March 15-21, 1980, Vol. 2, p. 83

37. Edwards, C. et al 1982. *Phys. Rev. Lett.* 48:70

38. Eichten, E. et al 1980. *Phys. Rev.* D21:203

39. Novikov, V. A. et al 1977. *Phys. Lett.* B67:409; Schifman, M. et al 1979. *Nucl. Phys. B* 147:448

40. Barbieri, R. et al 1976. *Phys. Lett. B* 61:465; Barbieri, R. et al 1980. *Phys. Lett. B* 95:93; Barbieri, R. et al 1981. *Phys. Lett. B* 106:497

41. Reinder, J. L. et al 1982. *Rutherford Lab. Preprint RL-82-017*

42. Porter, F. C. 1981., *SLAC-PUB-2796*

43. Fritzsch, H., Gell-Mann, M. 1972. *Proc. 16th Int. Conf. on High Energy Physics*, Chicago, Illinois, 2:135, Fermi National Accelerator Laboratory, Batavia, Illinois; and personal communication.

44. Scharre, D. L. et al 1980. *Phys. Lett. B* 97:329

45. Edwards, C. et al 1982. *Phys. Rev. Lett.* 49:259

46. Edwards, C. et al 1982. *Phys. Rev. Lett.* 48:458

47. Brodsky, S. et al 1978. *Phys. Lett. B* 73:203; Koller, K., Walsh, T. 1978. *Nucl. Phys. B* 140:449; Bjorken, J. D. 1980. *Proc. Summer Inst. on Particle Physics* SLAC Report No. 224

48. Appelquist, T. et al 1975. *Phys. Rev. Lett.* 34:365

49. Chanowitz, M. S. 1975. *Phys. Rev.* D12:918; Okun, L. G., Voloshin, M. B. 1976. *ITEP Preprint No. ITEP-95-1976*

50. Königsmann, K. C. 1982. *XVIIth Rencontre de Moriond; Workshop on New Spectroscopy*, Les Arcs, France, March 20-26, 1982; also SLAC-PUB-2910 (1980)

51. Bartel, W. et al 1977. *Phys. Lett. B* 64:483 and *Phys. Lett. B* 66:489

52. Novikov, V. A. et al 1979. *Phys. Lett. B* 86:347; Novikov, V. A. et al 1980. *Nucl. Phys. B* 165:55; Karl, G. 1977. *Il Nuovo Cimento* 38:315; Fritzsch, H., Jackson, J. D. 1977. *Phys. Lett. B* 66:365; Pham, T. N. 1979. *Phys. Lett. B* 87:267

53. Alexander, G. et al 1978. *Phys. Lett. B* 72:493; Brandelik, R. et al 1978. *Phys. Lett. B* 74:292; Alexander, G. et al 1978. *Phys. Lett. B* 76:652

54. Edwards, C. et al 1982. *Phys. Rev.* D25:3065

55. Kabir, P. K., Hey, A. J. G. 1976. *Phys. Rev. D* 13:3161. Note that the first occurrence of $\sin^2\vartheta_W$ in Eq. (6) of this reference should be replaced by $\sin 2\vartheta_W$.

56. Krammer, M. 1978. *Phys. Lett. B* 74:361

57. Gampp, W., Genz, H. 1978. *Phys. Lett. B* 76:319

58. Baillon, P. et al 1967. *Nuovo Cimento A* 50:393

59. Montanet, L. 1980. *Proc. XX Conf. on High Energy Physics*, Madison, Wisconsin, 17-23 July 1980

60. Dionisi, C. et al 1980. *Nucl. Phys.* B169:1

61. Herndon, D. J., Söding, P., Cashmore, R. J. 1975. *Phys. Rev. D* 11:3165

62. Palmer, W. F., Pinsky, S. S. 1982. DOE/ER/01545-328, Ohio State University Preprint

62a. Stanton, R. N. et al 1979. *Phys. Rev. Lett.* 42:346

63. Scharre, D. L. 1982. To be published in the *Proc. Orbis Scientiae*, Coral Gables, Florida; also SLAC-PUB-2880

64. Franklin, M. E. B. 1982. Ph.D. Thesis, Stanford University, SLAC-254 (unpublished)

65. Burke, D. L. et al 1982. *Phys. Rev. Lett.* 49:632

66. Newman-Holmes, C. 1982. *SLAC-PUB-2971*

67. Brandelik, R. et al 1977. *Phys. Lett. B* 70:132; Brandelik, R. et al 1979. *Phys. Lett B* 80:412; Brandelik et al 1979. *Z. Physik C* 1:233

68. Einhorn, M. B., Quigg, C. 1975. *Phys. Rev. D* 12:2015;Ellis, J., Gaillard, M. K., Nanopoulos, D. V. 1975. *Nucl. Phys. B* 100:313; Quigg, C. Rosner, J. L. 1978. *Phys. Rev. D* 17:239; Fakirov, D., Stech, B. 1978. *Nucl. Phys. B* 133:315

69. Porter, F. C. 1980. *AIP Conf. Proc.* 68:380

70. Fayet, P., Mezard, M. 1981. *Phys. Lett. B* 104:226

71. Edwards, C. et al 1982. *Phys. Rev. Lett.* 48:903

72. Pecci, R. D., Quinn, H. R. 1977. *Phys. Rev. Lett.* 38:1440 and *Phys. Rev. D* 16:1791; Weinberg, S. 1978. *Phys. Rev. Lett.* 40:223; Wilczek, F. 1978. *Phys. Rev. Lett.* 40:279

73. Faissner, H. et al 1981. *Phys. Lett. B* 103:234

74. Goldman, T., Hoffman, C. M. 1978. *Phys. Rev. Lett.* 40:220; Bechis, D. J. et al 1979. *Phys. Rev. Lett.* 42:1511; Zehnder, A. 1981. *Phys. Lett. B* 104:494

75. Porter, F. C., Königsmann, K. C. 1982. *Phys. Rev. D* 25:1993 and *Phys. Rev. D* 26:716

76. Niczyporuk, B. et al 1982. *DESY 82-068*

76a. Sivertz, M. et al 1982. *Phys. Rev. D* 26:717

77. Dine, M., Fischler, W., Srednicki, M. 1978. *Phys. Lett. B* 104:199; Kim, J. 1979. *Phys. Rev. Lett* 43:193;Wise, M. B., Georgi, H., Glashow, S. I. 1981. *Phys. Rev. Lett.* 47:402; Wilczek, F. 1982. *Phys. Rev. Lett.* 49:1549

78. Eichten, E. et al 1975. *Phys. Rev. Lett.* 34:369

79. Porter, F. C. et al 1982. *17th Rencontre de Moriond Workshop on New Flavors*, Les Arc, France, Jan. 24-30, 1982:27

80. Barnett, R. M., Dine, M., McLerran, L. 1980. *Phys. Rev. D* 22:594

81. Siegrist, J. 1979. *SLAC Report No. SLAC-225*, Ph.D. Thesis

81a. Lockman, W. et al 1983. *SLAC-PUB-3030*

82. Sjostrand, T. 1982. *LU-TP-82-3*

82a. Siegrist, J. L. et al 1982. *Phys. Rev. D* 26:991 (Mark I);Rice, E. et al 1982. *Phys. Rev. Lett.* 48:906 (CUSB);Berger, C. et al 1979. *Phys. Lett. B* 81:410 (PLUTO);Bock, P. et al 1980.*Z. Phys. C* 6:125 (DESY-Heidelberg);Albrecht, H. et al 1982. *Phys. Lett. B* 116:383 (DASP II);Niczyporuk, B. et al 1982.*Z. Phys. C* 15:229 (LENA)

83. Edwards, C. et al 1982. *Phys. Lett. B* 110:82

84. Berger, C. et al 1980.*Phys. Lett. B* 94:254

85. Roussarie, A. et al 1981. *Phys. Lett. B* 105:304

86. Brandelik, R. et al 1981. *Zeit. Phys. C* 10:117

87. Biddick, C. J. et al 1980. *Phys. Lett. B* 97:320

88. Bonneau, G., Gourdin, M., Martin, F. 1973. *Nucl. Phys. B* 54:573

89. Brodsky, S. L., Lepage, G. P. 1981. *Phys. Rev. D* 24:1808

90. Rosner, J. L. 1981. *Phys. Rev. D* 23:2625; Donoghue, J. F., Johnson, K., Li, B. A. 1981. *Phys. Lett. B* 99:416

91. Gilman, F. J. 1979. *Int. Conf. on Two Photon Interactions* 1979:215

92. Greco, M. 1980. *Proc. Int. Workshop on* $\gamma\gamma$ Collisions, Amiens, France, 1980:311; *Lecture Notes in Physics*, Vol. 134, Springer-Verlag, Berlin

93. Babcock, J. Rosner, J. 1976. *Phys. Rev. D* 14:1286

94. Emms, M. J. et al 1975. *Nucl. Phys. B* 96:155

95. De Rújula, A., Georgi, H., Glashow, S. L. 1976. *Phys. Rev. Lett.* 37:785.

96. Tompkins, J. C. 1980. *Quantum Chromodynamics*, ed. A. Mosher, p. 556 (SLAC)

97. Sadrozinski, H. F. W. 1980. *Proc. 20th Int. Conf. on High Energy Physics* Madison, Wisconsin, July 17-23, 1980

98. Rapidis, P. et al 1977. *Phys. Rev. Lett.* 39:5261; Bacino, W. et al 1978. *Phys. Rev. Lett.* 40:671

99. Goldhaber, G. et al 1977. *Phys. Lett. B* 69:503

100. Ono, S. 1976. *Phys. Rev. Lett.* 37:655

Figure Captions

Figure 1. (a) The current status of the charmonium spectrum below charm threshold. All the observed photon transitions between these states are shown, solid lines indicating electric dipole transitions, broken lines, allowed magnetic dipole transitions (between states with the same radial wavefunction) and broken-dotted lines, "hindered" magnetic dipole transitions (between states with different radial wavefunctions). (b) The observed hadronic transitions between the ψ' and the J/ψ. The $\pi\pi$ transitions are allowed, the η transition is $SU3_F$ forbidden, and the π° transition is $SU2_F$ forbidden.

Figure 2. The two principal elements of the Crystal Ball detector, the charged particle tracking chambers in the 25 cm diameter cavity of the shell, and the NaI(Tl) shell itself. The middle chamber is a continuously sensitive wire proportional chamber and the other two are magnetostrictive spark chambers. The shell itself is segmented into optically separated triangular pyramids in a solidly packed geometry based on an icosohedron. Each pyramid is viewed from the outside by a single photomultiplier. [From "Quarkonium", by E. D. Bloom and G. J. Feldman. Copyright (c) 1982 by Scientific American, Inc. All rights reserved.]

Figure 3. Inclusive γ spectrum at the ψ'.Note that the spectrum is $\Delta N/\Delta(\log E) \cong EdN/dE$. The upper inserts show the background subtracted signals for the η_c and η'_c candidate states. The numbers over the spectrum key the observed spectral features with the expected radiative transitions in the charmonium spectrum inset.

Figure 4. (a) Dalitz plot showing events from the two exclusive decays $\psi' \to \gamma\gamma e^+e^-$ and $\psi' \to \gamma\gamma\mu^+\mu^-$. The kinematic boundary is the outer one shown and inscribed within it are the boundaries imposed by the event selection cuts. Each event appears twice in this plot, once to the right of the almost vertical central dividing line, once to the left. The combination with the lower energy photon is on the right and the clear verticality of the bands shows that the lower energy photon is the first emitted. Horizontal bands corresponding to the η and π^0 are also evident. (b) The same as (a) but after kinematic fitting. The $\psi' \to \gamma\gamma e^+e^-$ events are subjected to five constraints and $\psi' \to \gamma\gamma\mu^+\mu^-$ to three. The main effect of fitting is to remove background and to improve the energy resolution of the higher energy photon. The latter significantly sharpens the bands on the left and those for the η and the π^0.

Figure 5. Inclusive γ spectra at the ψ' used in the measurement of $\psi' \to \gamma\chi_J$ and $\psi' \to \gamma\eta_c(2984)$. (a) All tracks neutral and charged with $|\cos\vartheta| < 0.85$. (b) Same as (a), except that tracks tagged as charged by the tracking chambers are removed. (c) Same as (b), except that photons resulting from reconstructed π^0 decays, and those near interacting charged particles are removed. (d) Same as (c), except that each track is required to have a lateral energy deposition pattern consistent with that of an electromagnetically showering particle.

Figure 6. The upper part of the figure shows the observed values of $B(\psi' \to \gamma\chi_J)$ as obtained from independent analysis of each of the four spectra shown in Figure 5. The lower part compares the cascade product branching ratios $B(\psi' \to \gamma\chi_{1,2})\, B(\chi_{1,2} \to \gamma J/\psi)$ from the four spectra (dots) with the direct measurements of these products from our analysis of the exclusive events $\psi' \to \gamma\gamma l^+ l^-$ (dashed bands). Since separation of the overlapping lines from the two photons $\chi_1 \to \gamma J/\psi$ and $\chi_2 \to \gamma J/\psi$ in the inclusive spectra is difficult, the comparison with the sum is also shown.

Figure 7. Diphoton masses of fitted events for $\psi' \to \gamma\gamma J/\psi \to \gamma\gamma l^+ l^-$. (a) The peak due to the η; the smooth line is a ten times magnified calculated curve for the expected contamination from $\psi' \to \pi^0\pi^0 J/\psi$. (b) The same as (a) except that events consistent with $\psi' \to \eta J/\psi$, and $\psi' \to \gamma\chi_J$ have been removed. These cuts allow the π^0 peak to show clearly.

Figure 8. Inclusive γ spectrum at the J/ψ. $\Delta N/\Delta(\log E) \cong E dN/dE$. The strong peak at 200 MeV is due to charged particles which were not tagged by the tracking system. The inset shows the background subtracted signal from the η_c candidate state. The two prominent peaks near the high energy end point of the spectrum are from the monochromatic photons in the reactions $\psi \to \gamma\eta'$ and $\psi \to \gamma\iota(1440)$. The photons from $\psi \to \gamma\eta$ (π^0) were eliminated from this spectrum by a hard QED cut.

Figure 9. Lowest order QCD diagram for the radiative decay of the J/ψ into a gluonic meson.

Figure 10. The same as Figure 8 showing details near the high energy end point of the spectrum.

Figure 11. Dalitz plot for $J/\psi \to \gamma\gamma\gamma$. The two sets of dashed lines indicate where events from $J/\psi \to \gamma\eta$ and $J/\psi \to \gamma\eta'$ should be clustered. Except for a QED background, no other signals are seen.

Figure 12. Distribution of the $\gamma_1\pi^+\pi^-$ mass from events satisfying the hypothesis $J/\psi \to \gamma_2\gamma_1\pi^+\pi^-$ where $E_{\gamma_1} < E_{\gamma_2}$, and $m_{\pi\pi}$ has been cut about the ρ^0 mass. The solid curve shows a fit to an η' peak plus a smooth background (dotted).

Figure 13. Distribution of the $\pi^0\pi^0$ mass from events which satisfy the 4C fits to the hypothesis $J/\psi \to \gamma\pi^0\pi^0$. The solid curve shows a fit to an f peak plus a smooth background (dashed).

Figure 14. Contours of equal probability as a function of x and y, the ratios of helicity amplitudes in the decay of the f in $J/\psi \to \gamma f \to \gamma\pi^0\pi^0$. The data point with error bars represents the measurement and the others are theoretical predictions (see text). Number next to the curves are in units of standard deviations.

Figure 15. (a) Distribution of the $K^+K^-\pi^0$ mass from events consistent with the hypothesis $J/\psi \to \gamma K^+K^-\pi^0$. The events in the shaded region satisfy the further requirement $M_{K^+K^-} < 1125$ MeV/c^2. (b) Dalitz plot for $K^+K^-\pi^0$ events from $J/\psi \to \gamma K^+K^-\pi^0$ with $1400 < M_{K\bar{K}\pi} < 1500$ MeV/c^2. The solid curve shows the boundary for $M_{K\bar{K}\pi} = 1450$ MeV/c^2 and the dashed line shows $M_{K\bar{K}} = 1125$ MeV/c^2.

Figure 16. Partial-wave contributions to $J/\psi \to K^+K^-\pi^0$ as a function of $K\bar{K}\pi$ mass for (a) $K\bar{K}\pi$ flat, (b) $K^*\bar{K}$ + c.c. with $J^P = 1^+$, and (c) $\delta\pi$ with $J^P = 0^-$.

Figure 17. (a) The $\eta\eta$ mass distribution from the process $J/\psi \to \gamma\eta\eta$ for $M_{\eta\eta} < 2.5$ GeV/c^2. The solid curve is a fit to a flat background plus one Breit-Wigner resonance. The dashed curve is a fit to a flat background plus two Breit-Wigner resonances, one with the mass and width of the f' but fitted amplitude and the other with all three parameters fitted. (b) $|\cos\vartheta_\gamma|$ and (c) $|\cos\vartheta_\eta|$ distributions for $J/\psi \to \gamma\vartheta$, $\vartheta \to \eta\eta$. Solid curves are best fit distributions for a ϑ spin of 2 and the dashed curves are expected distributions for spin 0. The inset shows the $|\cos\vartheta_\eta|$ distribution on an expanded scale.

Figure 18. $\eta\pi\pi$ mass spectrum from (a) $J/\psi \to \gamma\eta\pi^+\pi^-$ and (b) $J/\psi \to \gamma\eta\pi^0\pi^0$. The curves are fits including contributions for the $\iota(1440)$ as described in the text.

Figure 19. R_η as a function of E_{CM}. The first two points are for E_{CM} = 3.67 GeV and the ψ''. The ψ' point is off-scale. The error bars include the point-to-point systematic uncertainty, but not the estimated 20% overall systematic uncertainty.

Figure 20. Possible mechanisms contributing to the decay $\psi' \to \gamma\gamma^1P_1$.

Figure 21. (a) The inclusive π^0 energy spectrum from ψ' decays. (b) Distribution of the $\gamma\eta_c$ mass for events satisfying the hypothesis $\psi' \to \pi^0\gamma\eta_c$

Figure 22. (a) Crystal Ball measurements of R_h compared to theoretical prediction. The solid points are from data taken in 1980 and the open squares are from a much larger data sample taken in 1981. The dotted curve is the simple quark-parton model prediction and

the others are QCD predictions with $\Lambda_{\overline{MS}}$ = 100 MeV (solid), 200 MeV (dashed), and 300 MeV (dash-dot).The error bars do not include the 5.3% (1981 data) or 7.0% (1980 data) overall systematic error. (b) Comparison Crystal Ball results (solid circles and open squares) with other measurements (82a) (Mark I, open circles; PLUTO, open triangles; LENA, crossed dot; DASP II, solid triangle; CUSB, plus sign; DESY-Heidelberg, cross). The curves are as in (a).

Figure 23. The top part of the figure shows the $\pi^0\pi^0$ mass distribution for 4γ events consistent with $e^+e^- \to e^+e^-\gamma\gamma \to e^+e^-\pi^0\pi^0$ The shaded histogram shows the non-$\pi^0\pi^0$ background. The bottom part of the figure gives $\sigma(\gamma\gamma \to \pi^0\pi^0)$ for $|\cos\vartheta^*| < 0.7$. The curves are described in the text.

Figure 24. Acceptance corrected distribution for $|\cos\vartheta^*|$ for $\pi^0\pi^0$ events in the f mass region (1040-1480 MeV/c^2). The solid curve is the best fit spin 2 distribution and the dashed curves show the contributions from each of the three helicity amplitudes.

TABLE 1. Comparison of Crystal Ball results for $\psi' \to \gamma\gamma J/\psi$ with those from other experiments. Limits are at 90% confidence level. Masses as measured by the Crystal Ball are denoted by an asterisk, and those measured by Mark II, by a double asterisk. There is an additional 4 MeV/c^2 systematic uncertainty on all the masses.

State (MeV/c^2)	Crystal Ball	Mark II (26)	Mark I (13)	DESY-Heidelberg (14)
		$B(\psi' \to \gamma\gamma J/\psi)(\%)$		
$\chi(3553.9\pm0.5)^*$	1.26±0.22	1.1±0.3	1.0±0.6	1.0±0.2
$\chi(3508.4\pm0.4)^*$	2.38±0.40	2.4±0.6	2.4±0.8	2.5±0.4
$\chi(3412.9\pm0.6)^{**}$	0.06±0.02	<0.56	0.2±0.2	0.14±0.09
$\chi(3455)$	<0.02	<0.13	0.8±0.4	<0.25
$\chi(3591)$	<0.04	---	---	0.18±0.06
		$B(\psi' \to \pi J/\psi)(\%)$		
η	2.18±0.38	2.5±0.6	4.3±0.8	3.6±0.5
π^0	0.09±0.03	0.15±0.06	---	---

TABLE 2. Results of likelihood fit of data for $\psi' \to \gamma\gamma J/\psi \to \gamma\gamma l^+ l^-$ to correlated angular distributions for various χ spin values. The multipole amplitudes have been normalized so that $\sum_{j=1}^{J+1} |a_j|^2 = 1$, and for spin 2, a_3 has been set to zero.

Hypothesis	$-2\ln(L/L_{max})$	a'_2	a_2
$\chi(3508)$ data:			
$J_\chi = 1$	0	$+(0.077^{+0.050}_{-0.046})$	$-(0.002^{+0.020}_{-0.008})$
$J_\chi = 2$	16		
$J_\chi = 0$	162		
$\chi(3554)$ data:			
$J_\chi = 2$	0	$+(0.132^{+0.096}_{-0.075})$	$-(0.333^{+0.292}_{-0.116})$
$J_\chi = 1$	20		
$J_\chi = 0$	40		

TABLE 3. Results from the $\psi' \to \gamma\chi_J$. When two errors are given, the first error is statistical and the second is systematic. Ranges and upper limits are 90% confidence levels.

Datum	χ_0	χ_1	χ_2
E_γ (MeV)	258.4 ± 0.4 ± 4	169.6 ± .3 ± 4	126.0 ± 0.2 ± 4
$\Gamma(\chi_J)$ (MeV)	(13.5 - 20.4)	< 3.8	(0.85 - 4.9)
$B(\psi' \to \gamma\chi_J)$ (%)	9.9 ± 0.5 ± 0.8	9.0 ± 0.5 ± 0.7	8.0 ± 0.5 ± 0.7
Ratio $\left\{\frac{B(\psi' \to \gamma\chi_J)}{E_\gamma^3(2J+1)}\right\}$	1 :	1.07 ± .08 :	1.39 ± .11
$B(\chi_J \to \gamma J/\psi)$ (%)	0.60 ± 0.17	28.4 ± 2.1	12.4 ± 1.5

TABLE 4. η_c Branching Ratio Measurements

Mark II (35)

Decay Mode	$B(\psi' \to \gamma\eta_c) \cdot B(\eta_c \to X)$	$B(\eta_c \to X)$[a]
$p\bar{p}$	$(8^{+5}_{-4})\times10^{-6}$	$(2.9^{+3.0}_{-1.6})\times10^{-3}$
$\pi^+\pi^-\pi^+\pi^-$	$(5.7^{+3.9}_{-2.4})\times10^{-5}$	$(2.0^{+1.5}_{-0.9})\times10^{-2}$
$\pi^+\pi^-K^+K^-$	$(4.0^{+3.0}_{-2.5})\times10^{-5}$	$(1.4^{+2.1}_{-0.9})\times10^{-2}$
$\pi^+\pi^-p\bar{p}$	$<5\times10^{-5}$ (90% C.L.)	$<2.3\times10^{-2}$ (~90% C.L.)
$K^\pm\pi^\mp K^0_s$	$(1.5^{+0.8}_{-0.6})\times10^{-4}$	$(5.4^{+3.3}_{-2.4})\times10^{-2}$

Crystal Ball

Decay Mode	$B(J/\psi \to \gamma\eta_c) \cdot B(\eta_c \to X)$	$B(\eta_c \to X)$[b]
$\eta\pi^+\pi^-$	$(3.1\pm1.9)\times10^{-4}$	$(2.6^{+1.8}_{-1.7})\times10^{-2}$
$\gamma\gamma$[c]	$<1.6\times10^{-5}$ (90% C.L.)	$<1.8\times10^{-3}$ (~90 % C.L.)
$K^+K^-\pi^0$	$<1.5\times10^{-4}$ (90% C.L.)	$<1.7\times10^{-2}$ (~90% C.L.)

a) uses Crystal Ball value for $B(\psi' \to \gamma\eta_c)$.

b) uses Crystal Ball value for $B(J/\psi \to \gamma\eta_c)$.

c) see Section 6.4.

TABLE 5. Crystal Ball measurements (except as noted) of $J/\psi \to \gamma\pi^0$, $\gamma\eta$, $\gamma\eta'$, γf, $\gamma f'$. Where two errors are given, the first is statistical and the second, systematic.

$B(J/\psi \to \gamma\pi^0) = (3.6 \pm 1.1 \pm 0.7) \times 10^{-6}$

$B(J/\psi \to \gamma\eta) = (0.88 \pm 0.08 \pm 0.11) \times 10^{-3}$

η' Decay Mode	$B(J/\psi \to \gamma\eta') \times 10^{-3}$
$\eta' \to \eta\pi^+\pi^-$	$3.9 \pm 1.0 \pm 1.1$
$\eta' \to \eta\pi^0\pi^0$	$4.2 \pm 0.6 \pm 0.6$
$\eta' \to \gamma\rho^0$	$4.1 \pm 0.4 \pm 0.6$
$\eta' \to \gamma\gamma$	$4.4 \pm 0.9 \pm 0.5$
Average	$4.1 \pm 0.3 \pm 0.6$

$B(J/\psi \to \gamma f) = (1.46 \pm 0.25 \pm 0.30) \times 10^{-3}$

$B(J/\psi \to \gamma f') \times B(f' \to \eta\eta) = (0.9 \pm 0.9) \times 10^{-4}$

$B(J/\psi \to \gamma f') \times B(f' \to K\bar{K})^{a)} = (1.8 \pm 0.6 \pm 1.0) \times 10^{-4}$

$B(J/\psi \to \gamma X)B(X \to 2\gamma) < 1.6 \times 10^{-5}$ (90% C.L.)

for, $2600 < M_X < 3000$ MeV/c^2, and, $\Gamma_X \lesssim 25$ MeV

$B(J/\psi \to 3\gamma \text{ (direct)}) < 5.5 \times 10^{-5}$ (90% C.L.)

a) Mark II, reference 63

TABLE 6. Relative partial-wave probabilities for various hypotheses for the structure of the $K\bar{K}\pi$ system in $J/\psi \to \gamma K^+K^-\pi^0$, $(1400 \leq M_{K\bar{K}\pi} < 1500\ \mathrm{MeV/c^2})$.

Partial-wave contribution	Relative probability
flat + $\delta\pi$ - 0^-	1.0
flat + $\delta\pi$ - 1^+	0.006
flat + $K^*\bar{K}$ + c.c. - 0^-	10^{-7}
flat + $K^*\bar{K}$ + c.c. - 1^+	0.01

TABLE 7. Parameters for the $\iota(1440)$. Where two errors are given, the first is statistical and the second, systematic.

$\iota(1440)$

Parameter	Crystal Ball	Mark II (44)
M (MeV/c^2)	1440^{+20}_{-15}	1440^{+10}_{-15}
Γ (MeV)	55^{+20}_{-30}	50^{+30}_{-20}
$B(J/\psi \to \gamma\iota)B(\iota \to K\bar{K}\pi)$[a]	$(4.0 \pm 0.7 \pm 1.0) \times 10^{-3}$	$(4.3 \pm 1.7) \times 10^{-3}$[b]
$B(J/\psi \to \gamma\iota)B(\iota \to \eta\pi\pi)$[c]	$< 2 \times 10^{-3}$ (90% C.L.)	—
C	+	+
J^P	0^-	—

a) $I = 0$ is assumed in the isospin correction.

b) This product branching ratio has been increased by 19% as compared to the value published in reference 44. This accounts for the differential efficiency correction from the spin 1 to spin 0 case as discussed in the reference.

c) Note that one experiment gives $B(\delta \to \eta\pi\pi)/B(\delta \to K\bar{K}) = 1.4 \pm 0.6$ (62a), while $\iota \to \delta\pi$ has been measured as the dominant decay for the $K\bar{K}\pi$ final state.

TABLE 8. Parameters for the $\vartheta(1640)$. Where two errors are given, the first is statistical and the second, systematic.

$\vartheta(1640)$

Parameter	Crystal Ball	Mark II (64)
M (MeV/c^2)	1670 ± 50	1700 ± 30
Γ (MeV)	160 ± 80	156 ± 20
$B(J/\psi \to \gamma\vartheta)B(\vartheta \to \eta\eta)$	$(3.8 \pm 1.6) \times 10^{-4}$	---
$B(J/\psi \to \gamma\vartheta)B(\vartheta \to K\bar{K})$[a]	---	$(12.0 \pm 1.8 \pm 5.0) \times 10^{-4}$
$B(J/\psi \to \gamma\vartheta)B(\vartheta \to \pi\pi)$[a]	$<6 \times 10^{-4}$ (90% C.L.)	$<3.2 \times 10^{-4}$ (90% C.L.)
C	+	+
J^P	2^+ (95% C.L.)	2^+ (78% C.L.)

a) $I = 0$ is assumed in the isospin correction.

TABLE 9. Measured values of $R_h = \sigma(e^+e^- \to \text{hadrons})/\sigma(e^+e^- \to \mu^+\mu^-)$. The error on R_h consists of 3 parts, a statistical error $(\delta R_h / R_h)_{\text{stat}}$, a systematic error which depends upon E_{CM}, $(\delta R_h / R_h)_{\text{point sys.}}$, and a systematic error which is uniformly applicable to all the 1981 data of 5.3% and to all of the 1980 data of 7.0%.

1981 *data*

E_{CM} (GeV)	R_h	$(\delta R_h / R_h)_{\text{stat}}$ (%)	$(\delta R_h / R_h)_{\text{point sys.}}$ (%)
5.00	3.46	3.3	3.4
5.25	3.60	2.8	1.2
5.50	3.33	2.9	2.4
5.75	3.40	3.1	1.4
6.00	3.25	2.8	2.3
6.25	3.31	2.8	1.4
6.50	3.33	2.8	2.2
6.75	3.38	2.3	1.5
7.00	3.34	2.9	1.5
7.25	3.56	3.0	2.2
7.40	3.32	4.0	2.9

1980 *data*

5.20	3.51	3.5	3.5
6.00	3.43	3.5	3.5
6.75	3.38	3.8	3.5
7.40	3.67	3.5	3.5

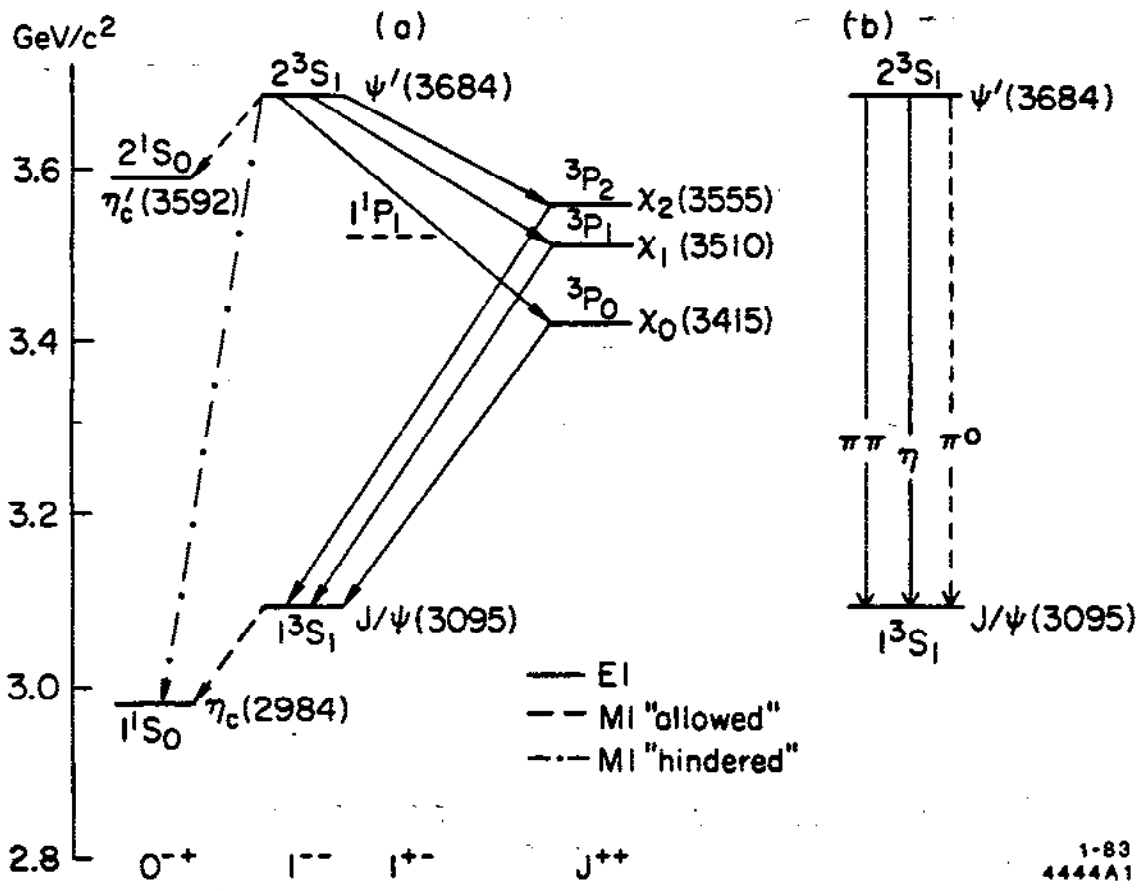
GeV/c²
(a)
(b)
2³S₁ ψ'(3684)
2¹S₀ η_c'(3592)
1¹P₁
³P₂ χ₂(3555)
³P₁ χ₁(3510)
³P₀ χ₀(3415)
1³S₁ J/ψ(3095)
1¹S₀ η_c(2984)
3.6
3.4
3.2
3.0
2.8
0⁻⁺
1⁻⁻
1⁺⁻
J⁺⁺
E1
M1 "allowed"
M1 "hindered"
ππ
η
π⁰
1-83
4444A1

Figure 1

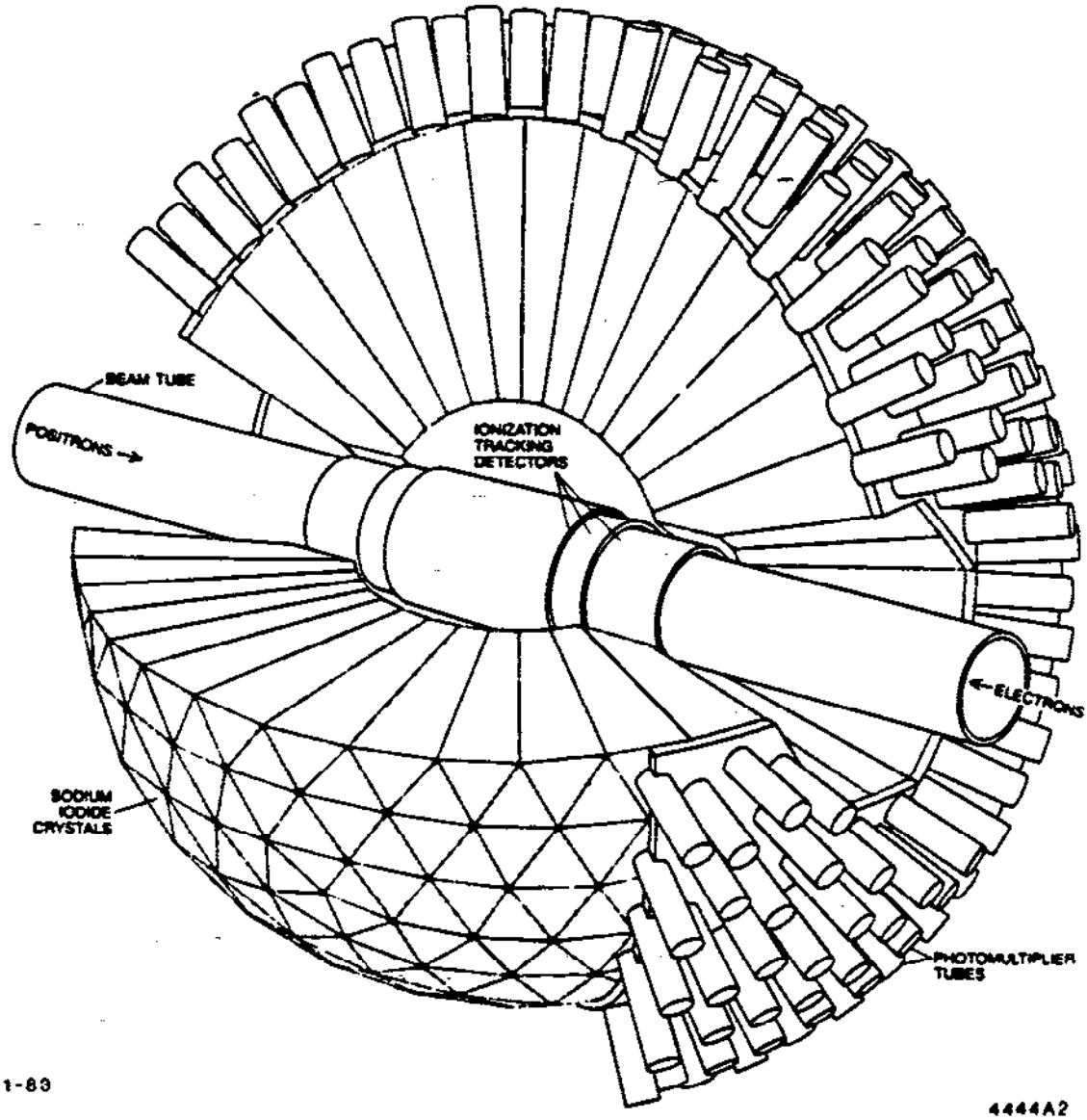
BEAM TUBE
POSITRONS
IONIZATION TRACKING DETECTORS
ELECTRONS
SODIUM IODIDE CRYSTALS
PHOTOMULTIPLIER TUBES
1-83
4444A2

Figure 2

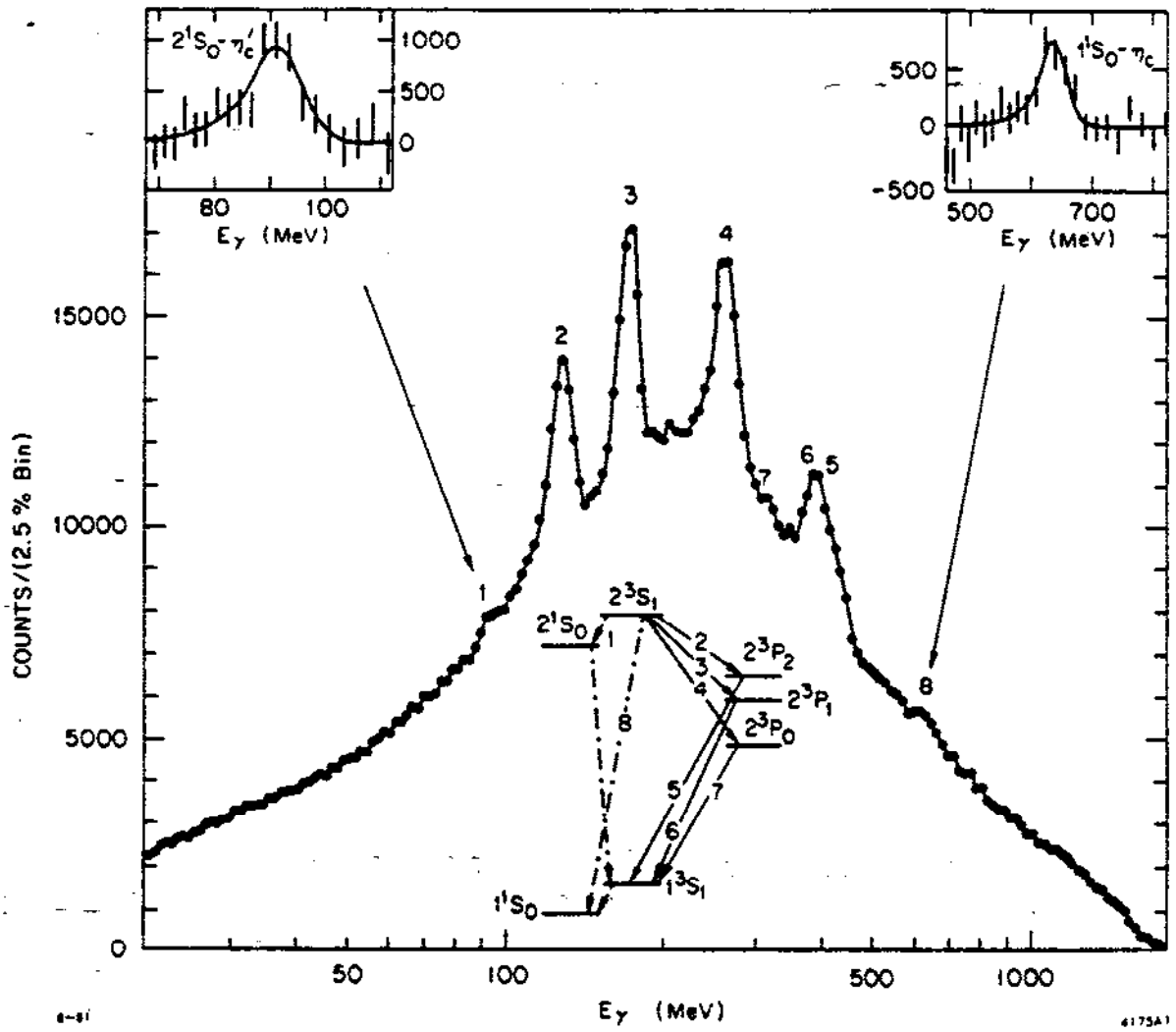
$2^1S_0 - \eta_c'$
1000
500
0
80
100
E_γ (MeV)
$1^1S_0 - \eta_c$
500
0
-500
500
700
E_γ (MeV)
15000
10000
5000
0
COUNTS/(2.5 % Bin)
1
2
3
4
5
6
7
8
2^3S_1
2^1S_0
2^3P_2
2^3P_1
2^3P_0
1^1S_0
1^3S_1
50
100
500
1000
E_γ (MeV)

Figure 3

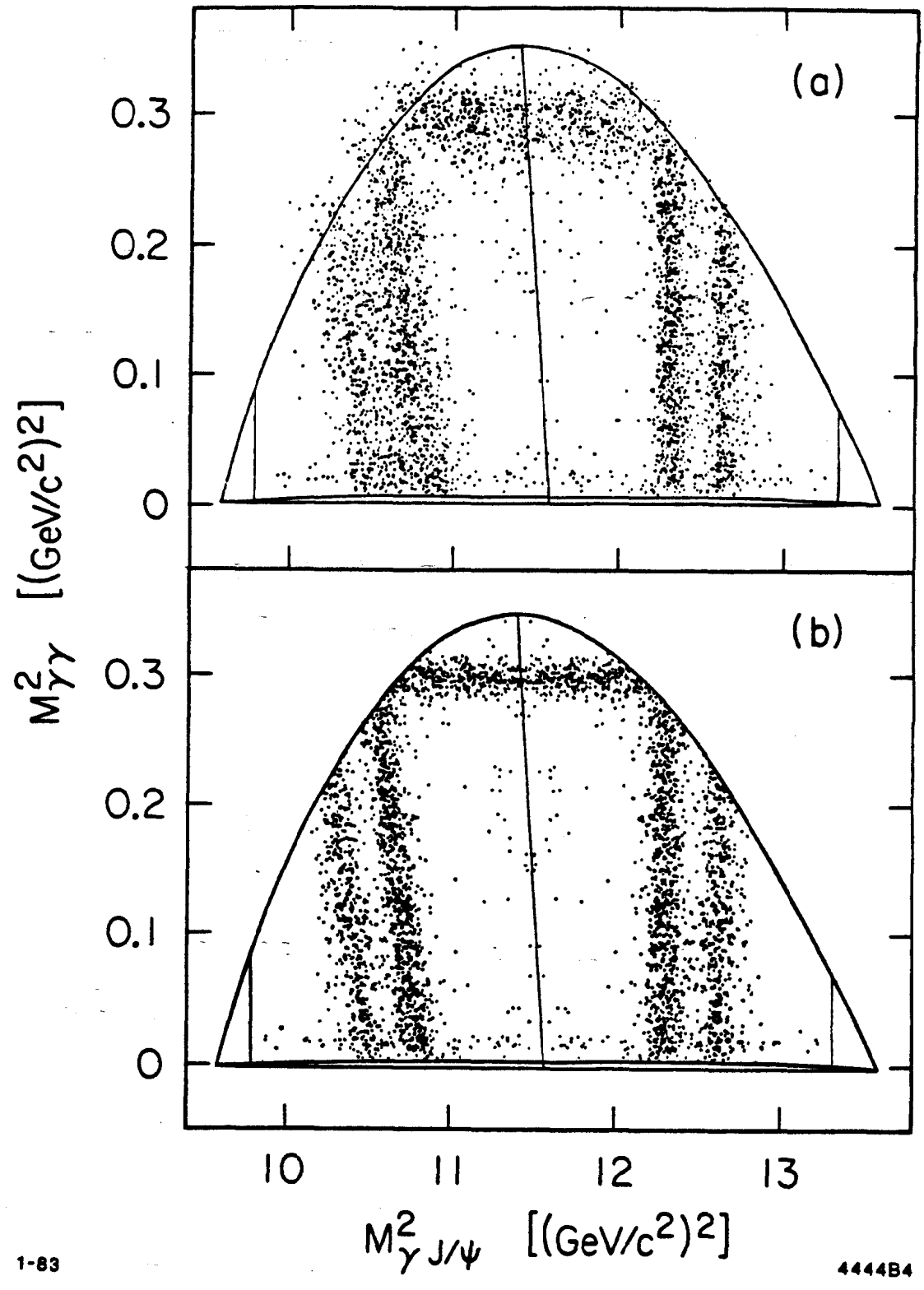
(a)
(b)
0.3
0.2
0.1
0
10
11
12
13
$M^2_{\gamma\gamma}$ [(GeV/c^2)^2]
$M^2_{\gamma J/\psi}$ [(GeV/c^2)^2]
1-83
4444B4

Figure 4

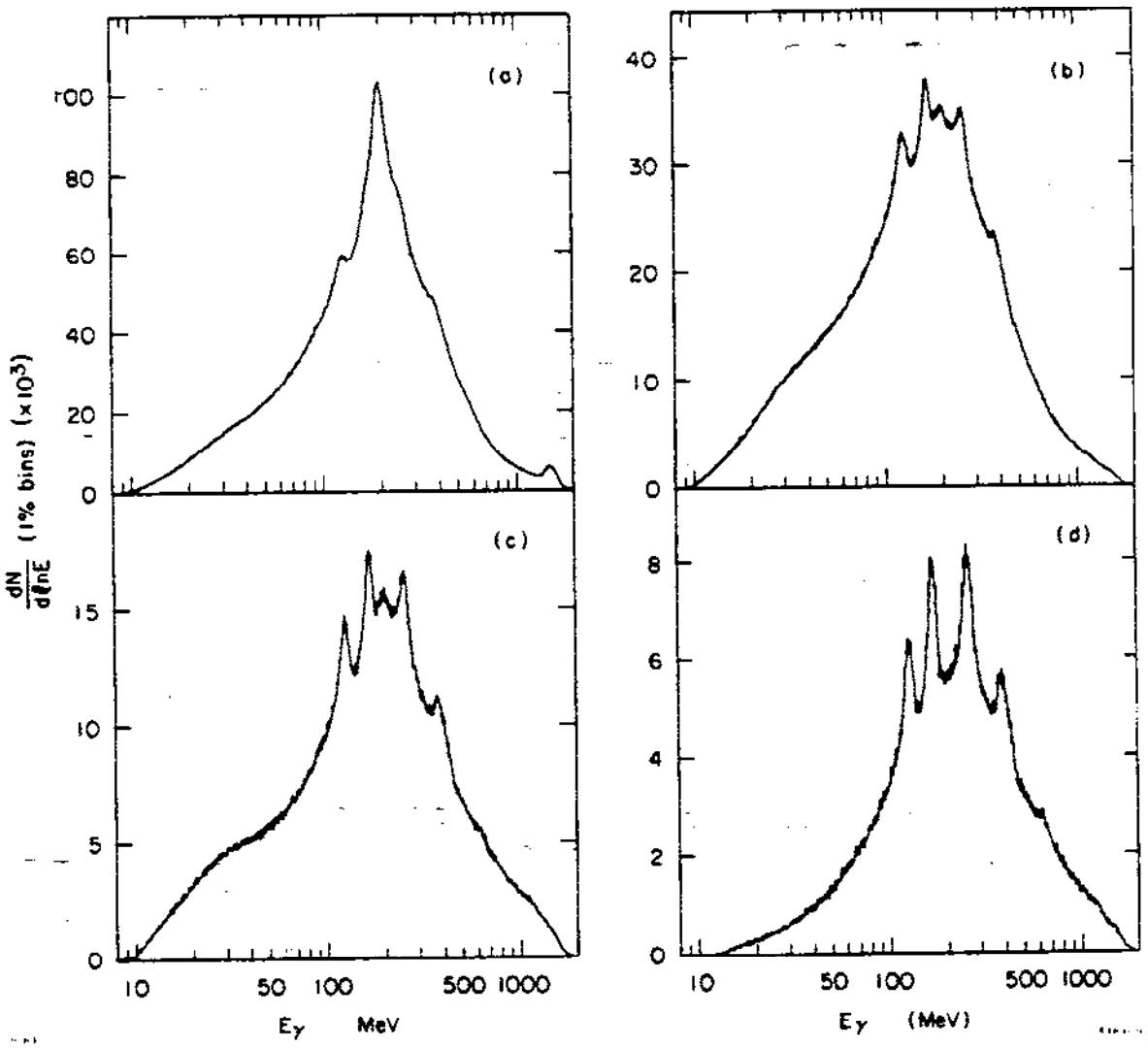
(a)
(b)
(c)
(d)
$\frac{dN}{d(\ln E}$ (1% bins) ($\times 10^3$)
E_γ MeV
E_γ (MeV)
10
50
100
500
1000

Figure 5

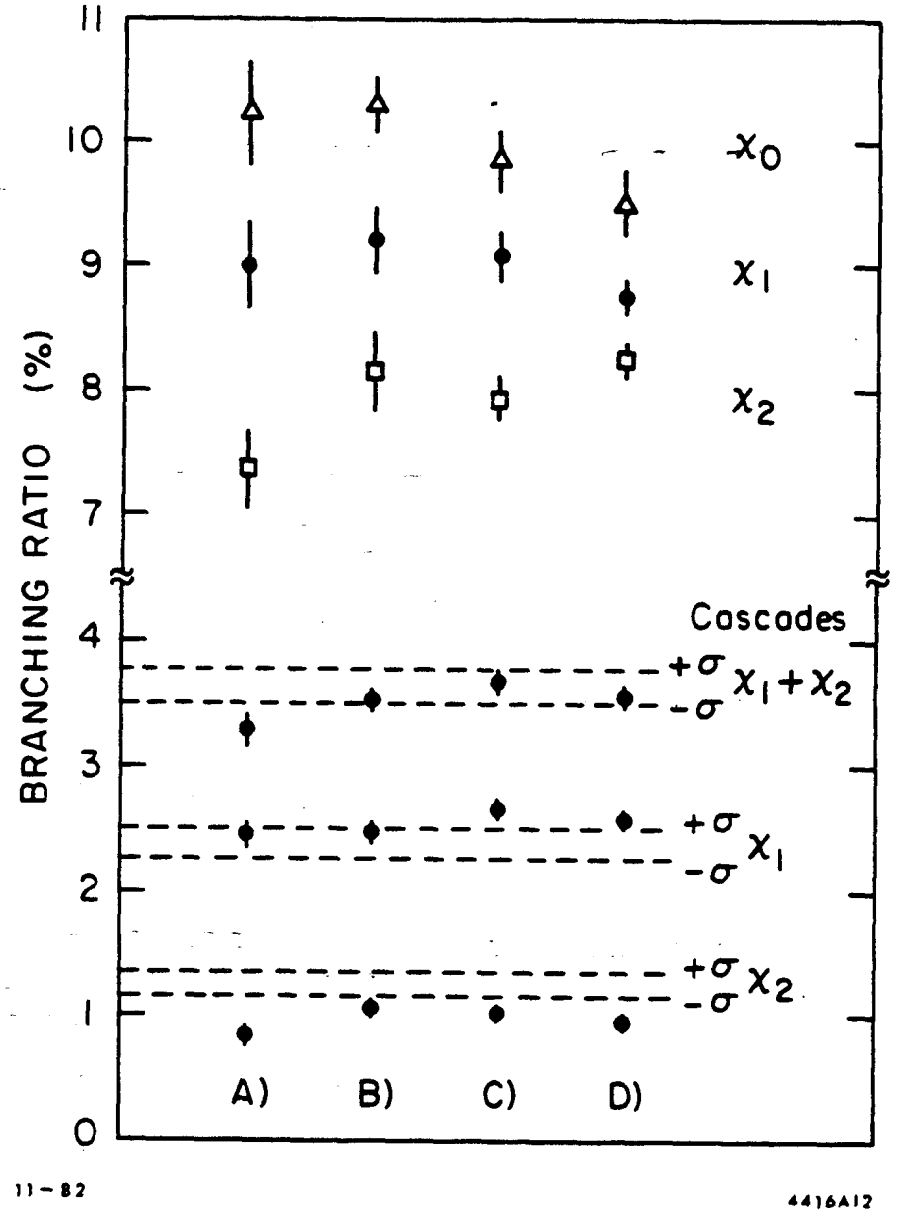
BRANCHING RATIO (%)
11
10
9
8
7
4
3
2
1
0
χ_0
χ_1
χ_2
Coscodes
$+\sigma$ $\chi_1+\chi_2$
$-\sigma$
$+\sigma$ χ_1
$-\sigma$
$+\sigma$ χ_2
$-\sigma$
A)
B)
C)
D)
11-82
4416A12

Figure 6

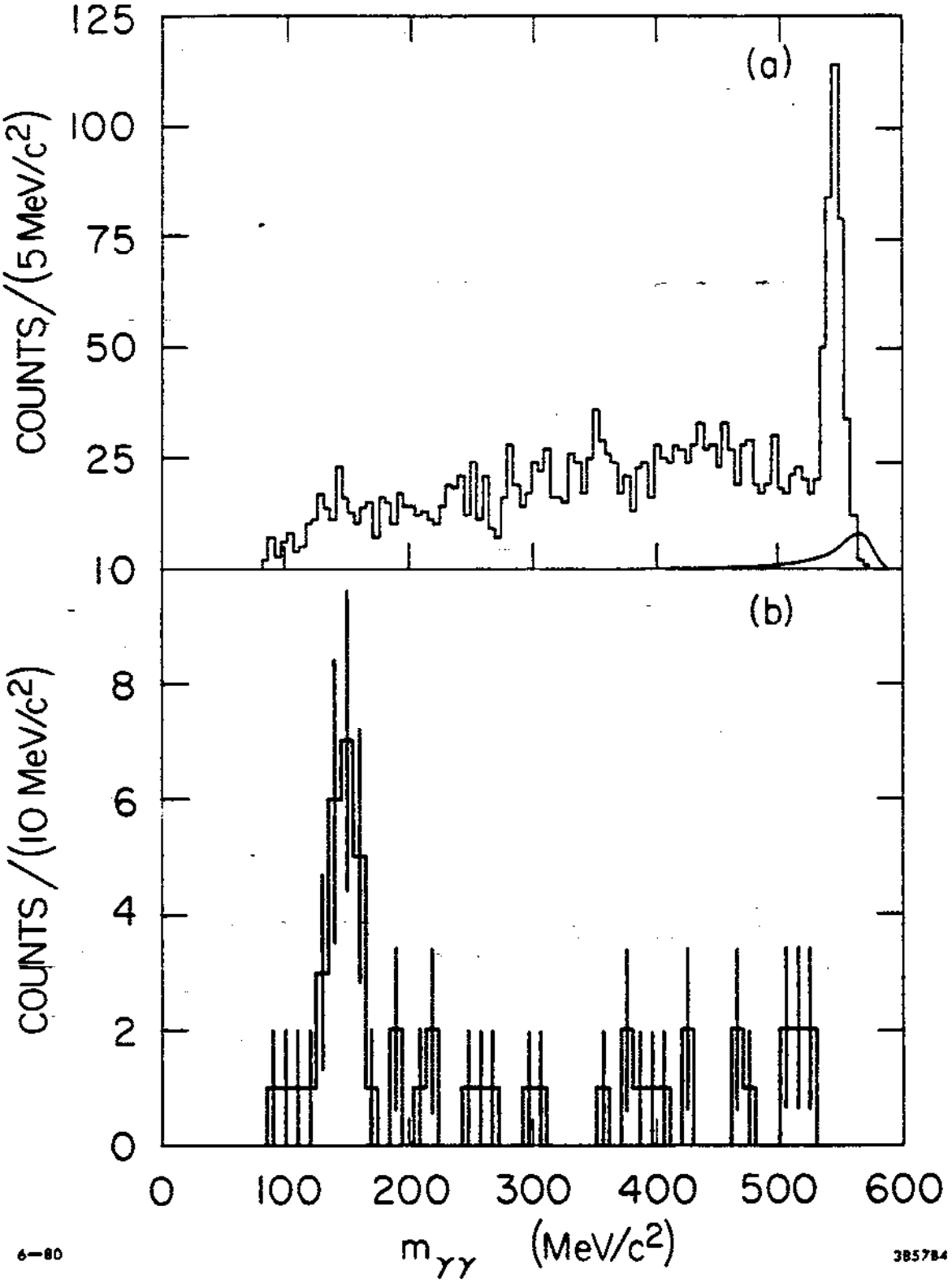
125
100
75
50
25
10
(a)
COUNTS/(5 MeV/c²)
8
6
4
2
0
(b)
COUNTS/(10 MeV/c²)
0
100
200
300
400
500
600
$m_{\gamma\gamma}$ (MeV/c²)
6-80
3857B4

Figure 7

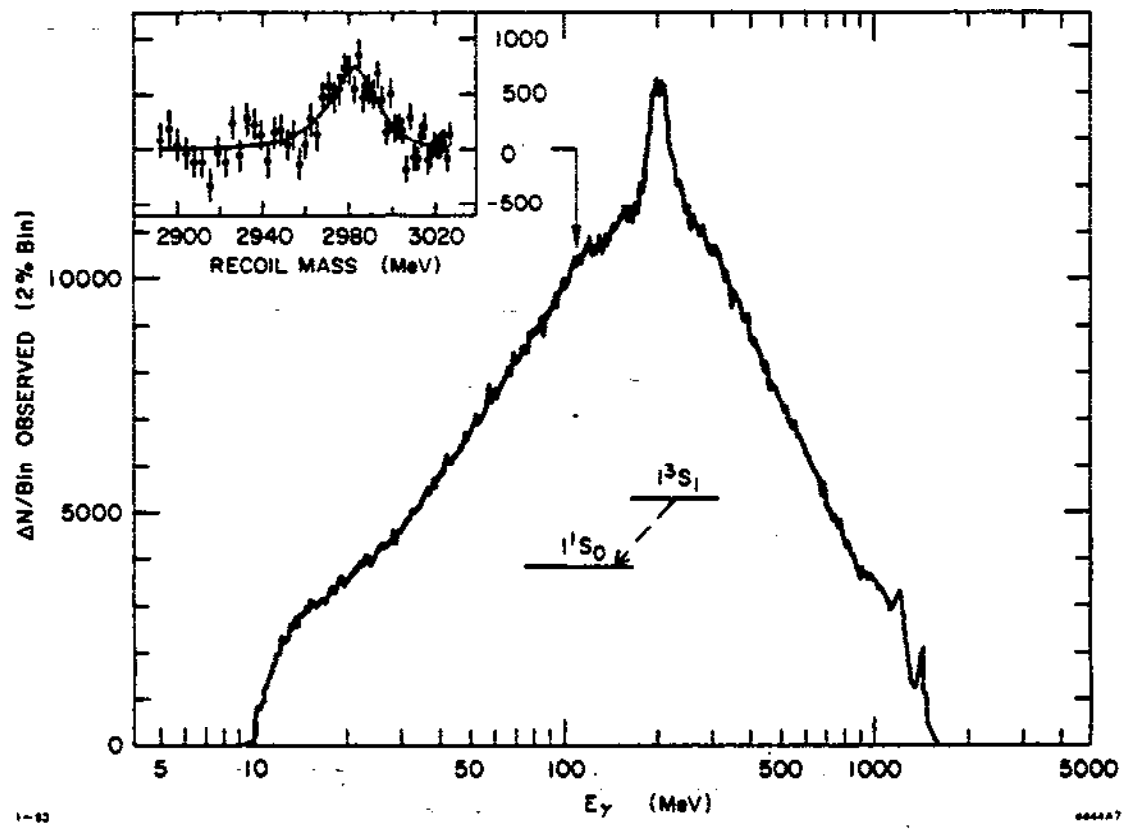
1000
500
0
-500
2900 2940 2980 3020
RECOIL MASS (MeV)
ΔN/Bin OBSERVED (2% Bin)
10000
5000
0
1^3S_1
1^1S_0
5
10
50
100
500
1000
5000
E_γ (MeV)

Figure 8

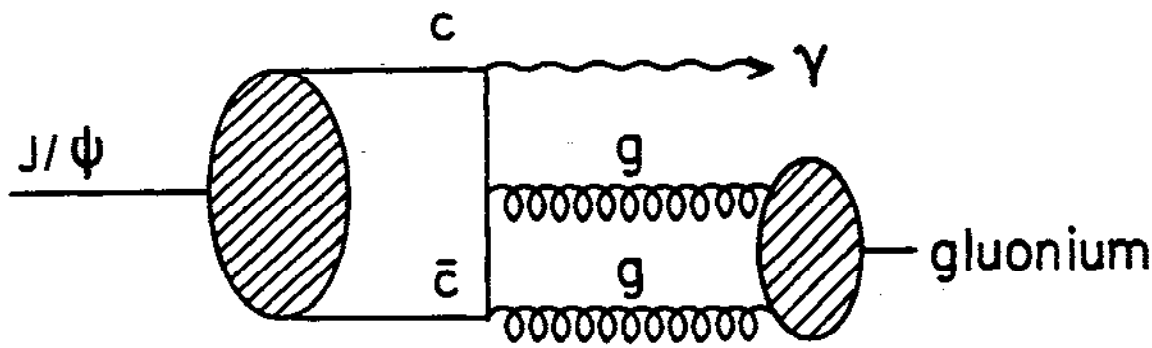

Figure 9

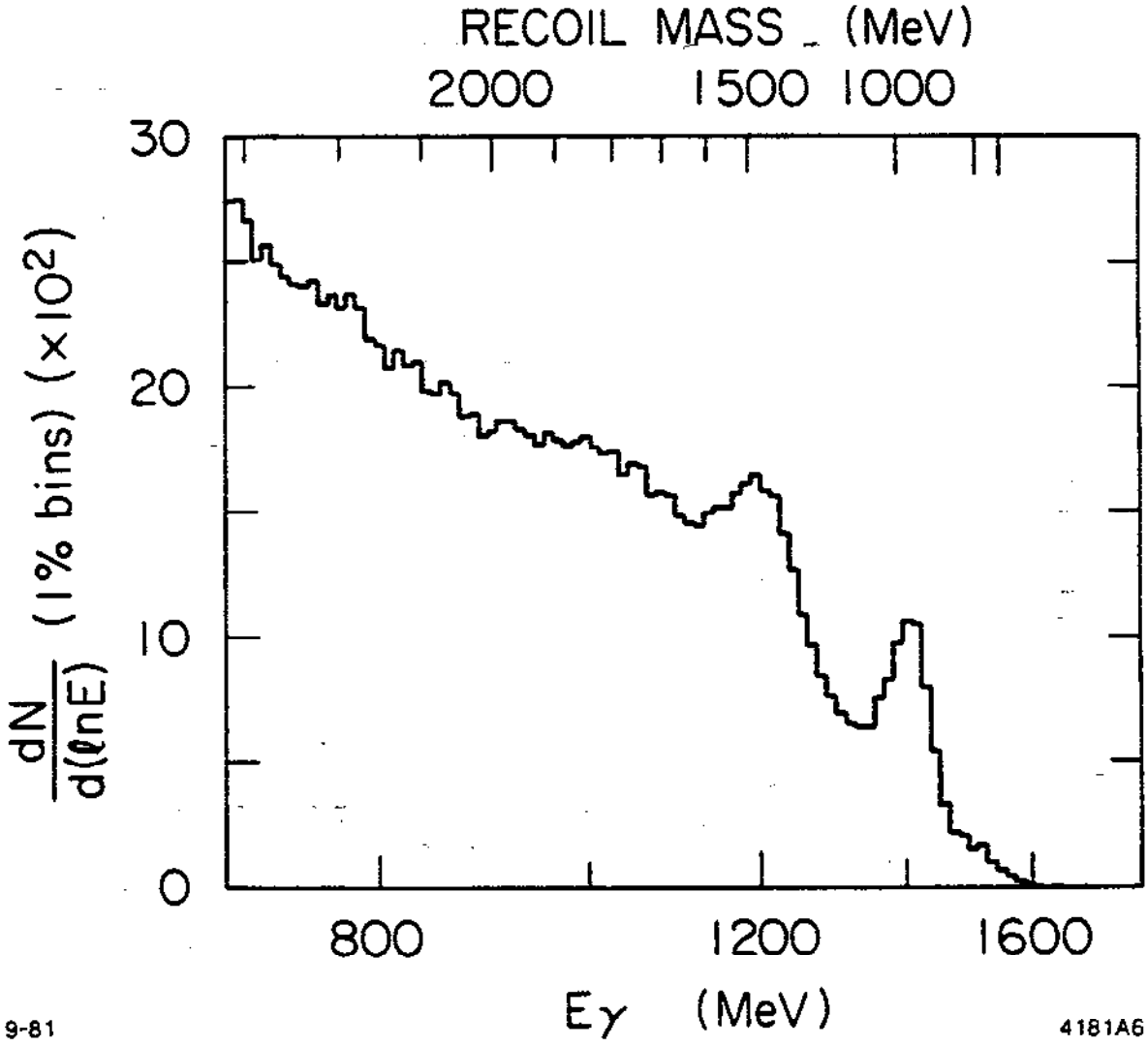
RECOIL MASS (MeV)
2000
1500
1000
30
20
10
0
$\frac{dN}{d(\ell nE)}$ (1% bins) ($\times 10^2$)
800
1200
1600
E_γ (MeV)
9-81
4181A6

Figure 10

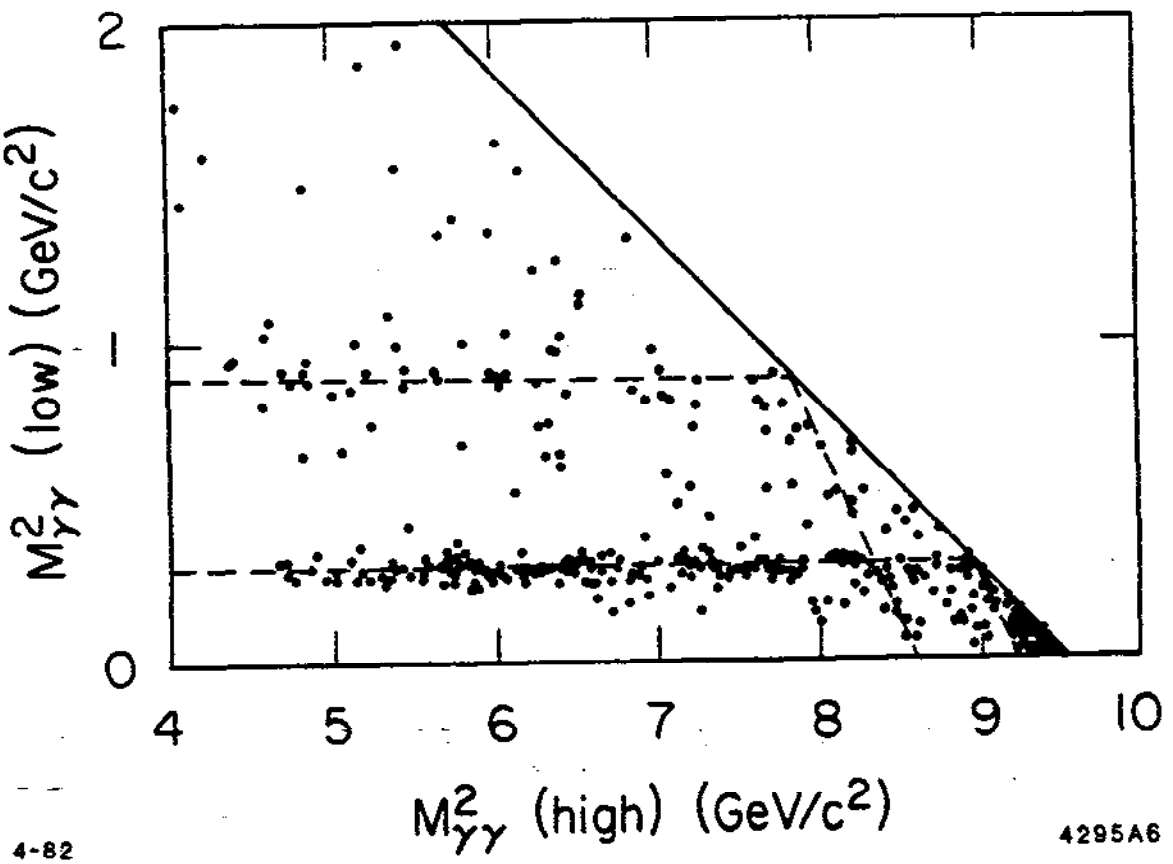
2
1
0
4
5
6
7
8
9
10
$M^2_{\gamma\gamma}$ (low) (GeV/c^2)
$M^2_{\gamma\gamma}$ (high) (GeV/c^2)
4-82
4295A6

Figure 11

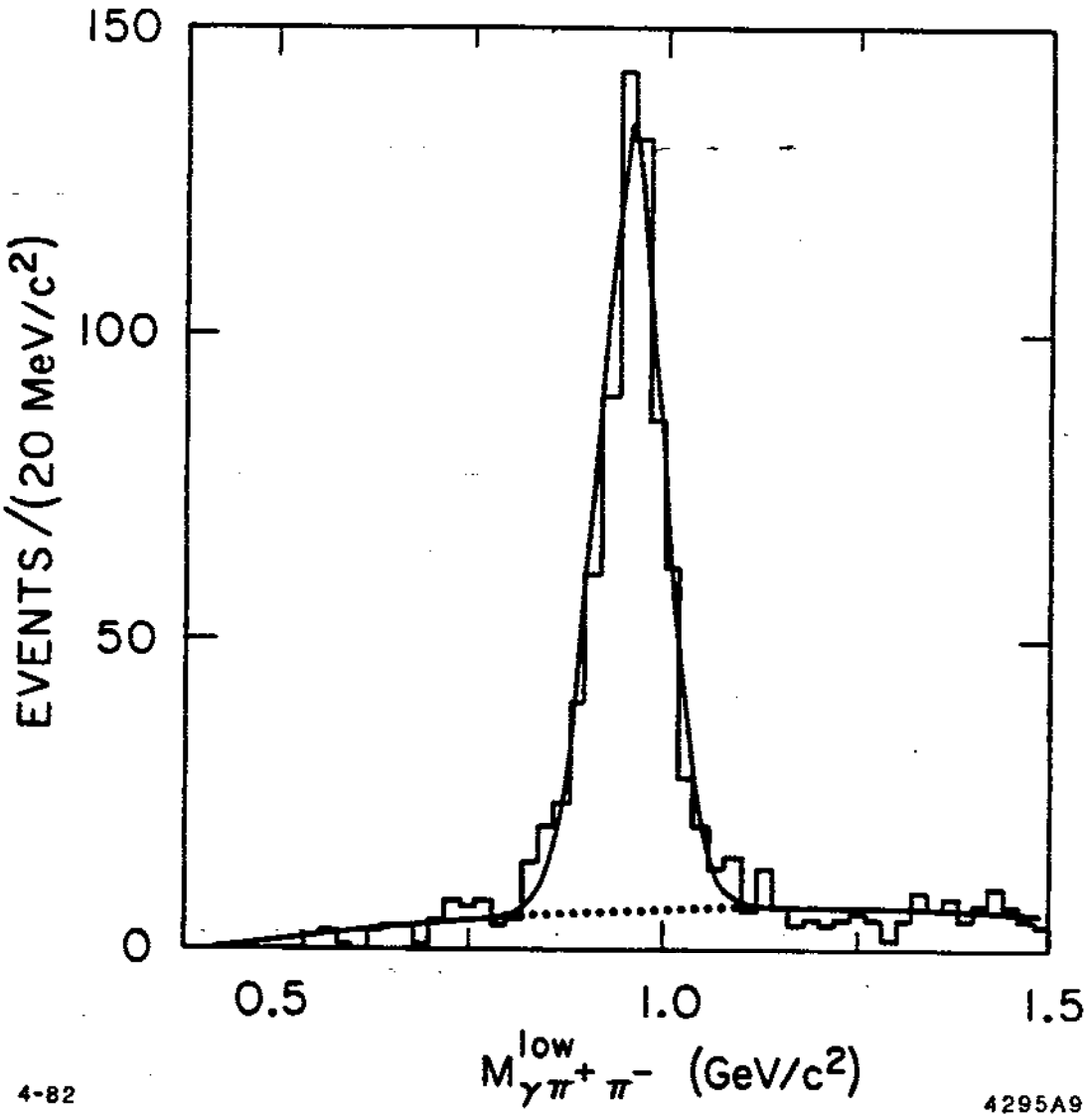
150
100
50
0
EVENTS/(20 MeV/c²)
0.5
1.0
1.5
$M^{low}_{\gamma\pi^+\pi^-}$ (GeV/c²)
4-82
4295A9

Figure 12

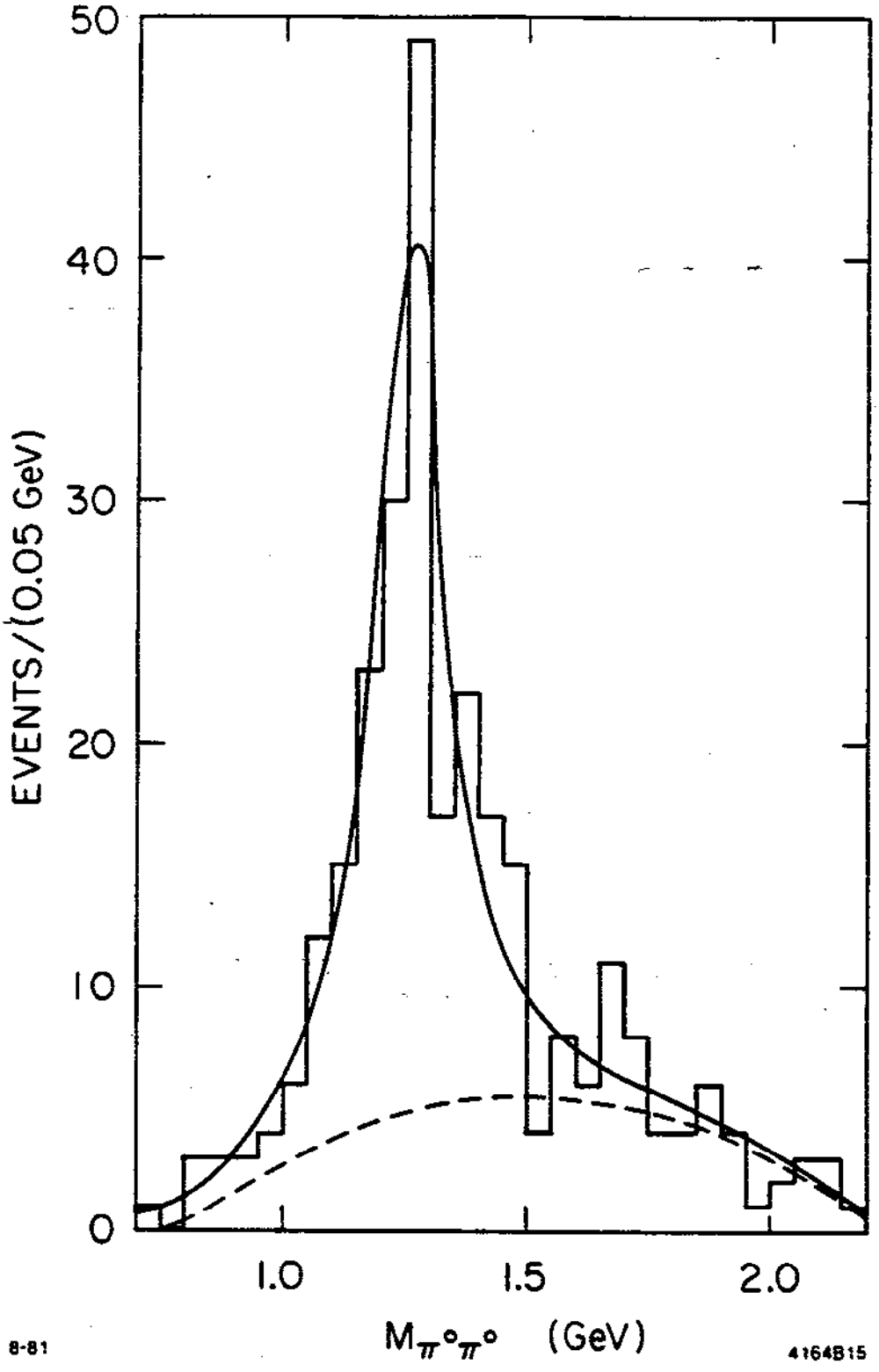

Figure 13

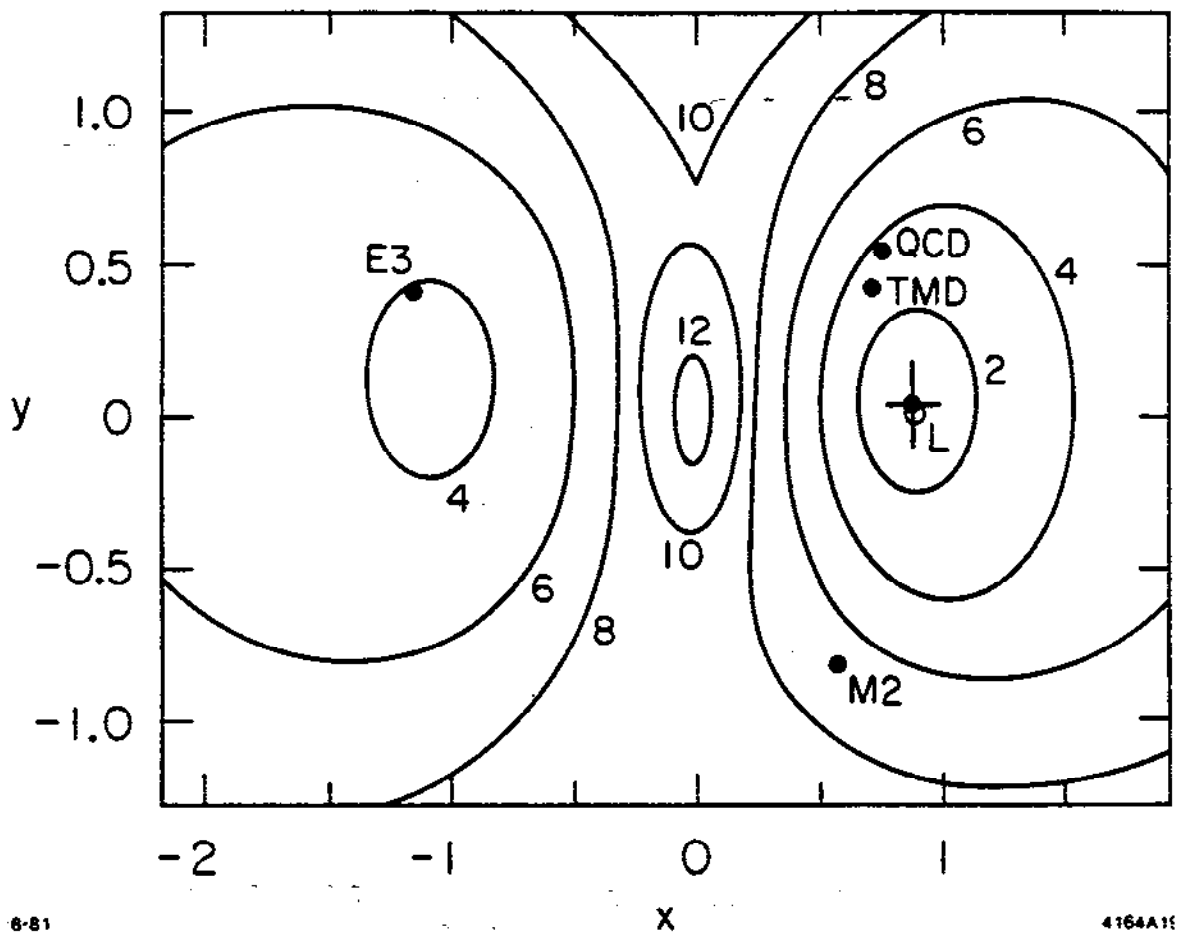

Figure 14

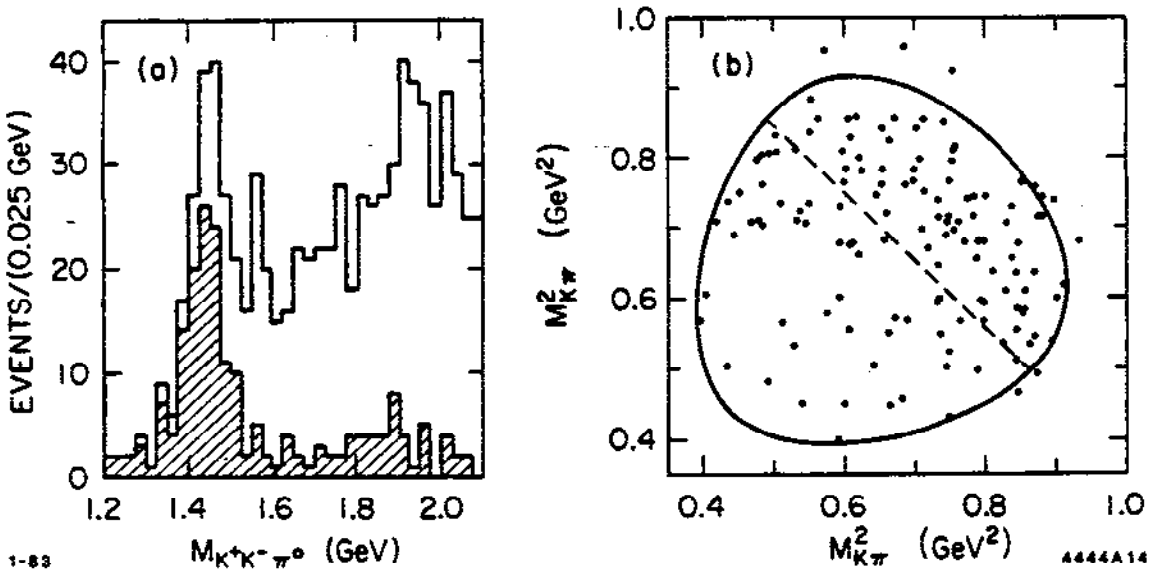
(a)
EVENTS/(0.025 GeV)
40
30
20
10
0
1.2
1.4
1.6
1.8
2.0
$M_{K^+K^-\pi^0}$ (GeV)
1-83
(b)
$M^2_{K\pi}$ (GeV^2)
1.0
0.8
0.6
0.4
0.4
0.6
0.8
1.0
$M^2_{K\pi}$ (GeV^2)
4444A14

Figure 15

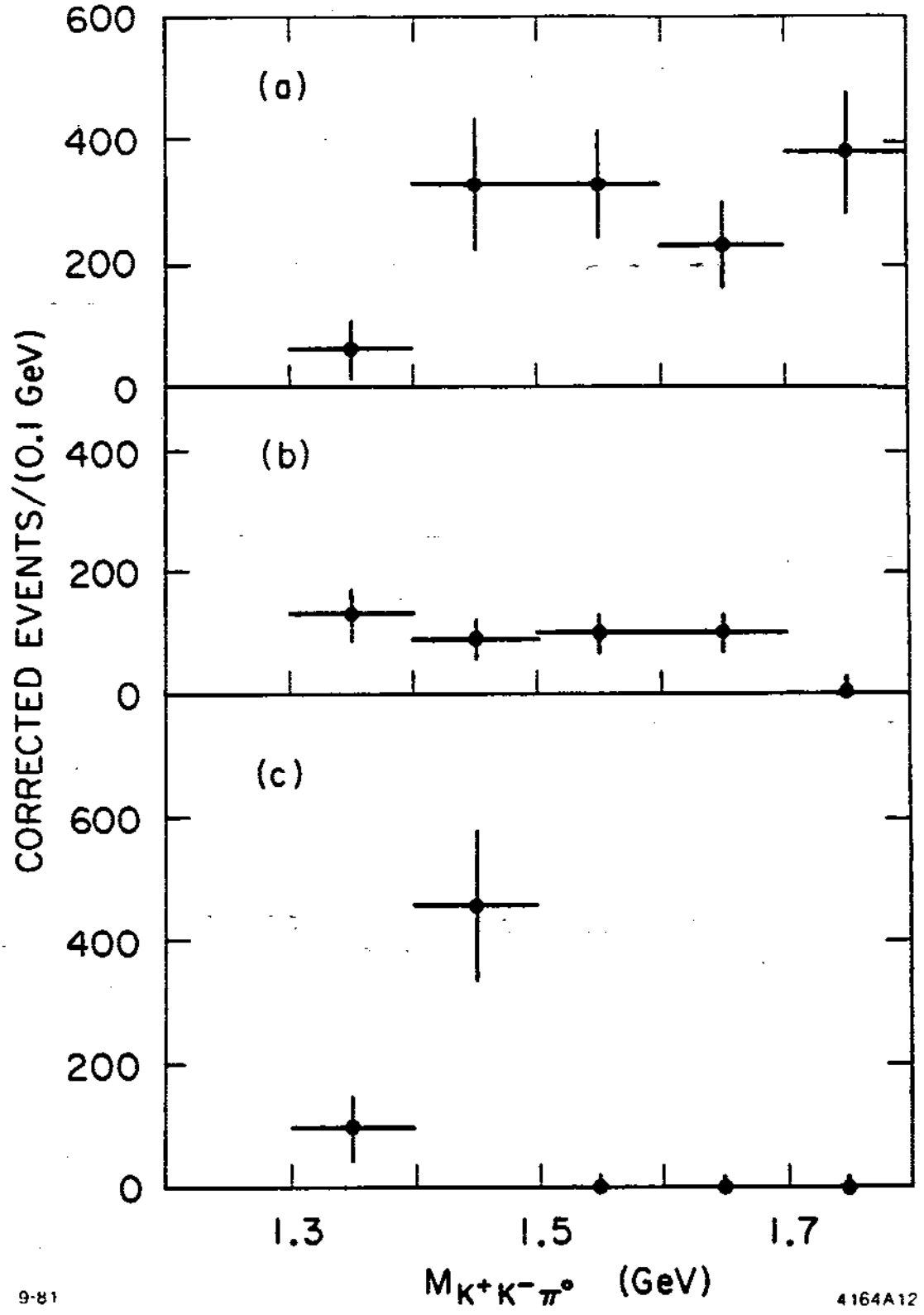
600
400
200
0
(a)
400
200
0
(b)
600
400
200
0
(c)
CORRECTED EVENTS/(0.1 GeV)
1.3
1.5
1.7
$M_{K^+K^-\pi^0}$ (GeV)
9-81
4164A12

Figure 16

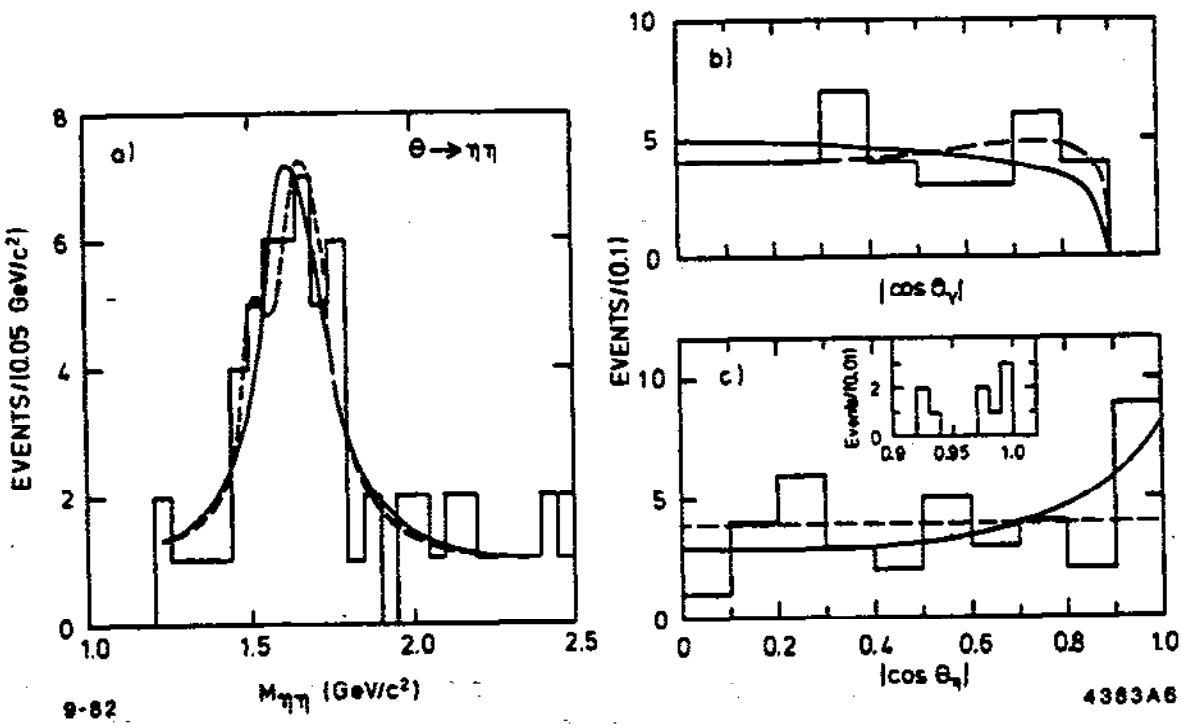
a)
θ→ηη
EVENTS/(0.05 GeV/c²)
$M_{\eta\eta}$ (GeV/c²)
9-82
b)
$|\cos\theta_{\gamma}|$
c)
EVENTS/(0.1)
$|\cos\theta_{\eta}|$
4383A6

Figure 17

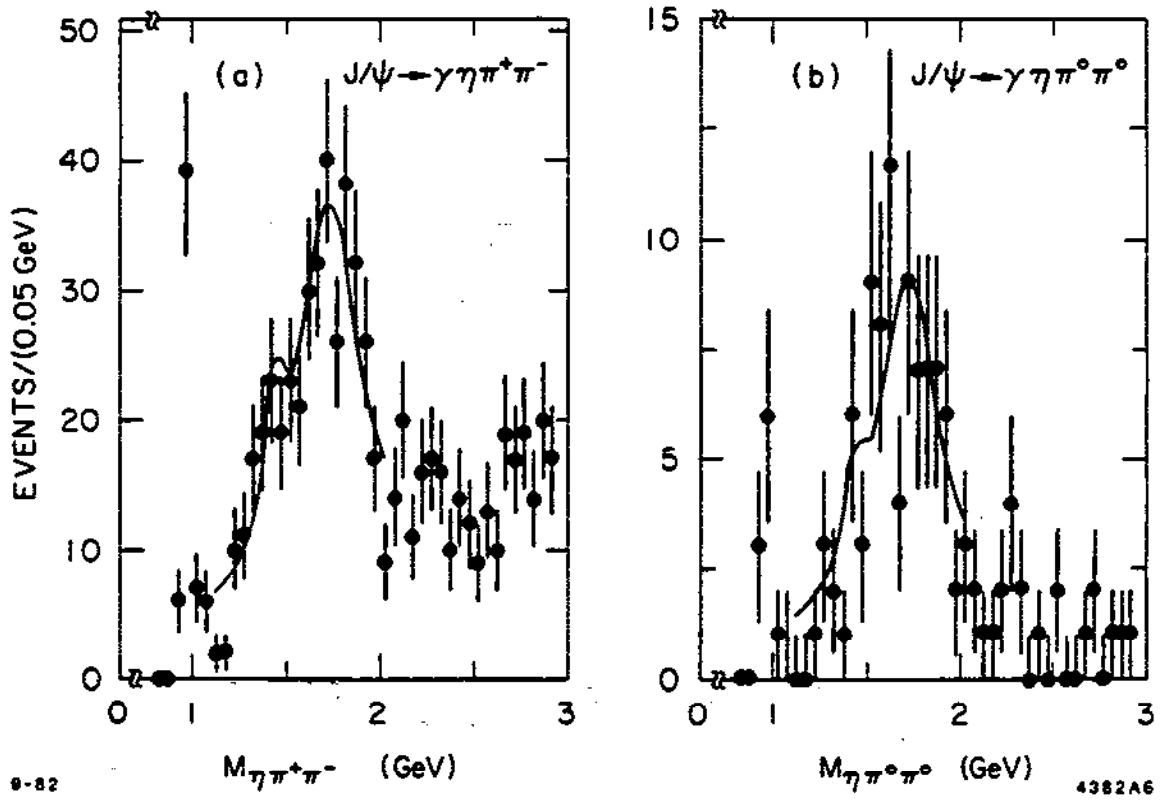
(a)
$J/\psi \to \gamma\eta\pi^+\pi^-$
EVENTS/(0.05 GeV)
$M_{\eta\pi^+\pi^-}$ (GeV)
9-82
(b)
$J/\psi \to \gamma\eta\pi^0\pi^0$
$M_{\eta\pi^0\pi^0}$ (GeV)
4382A6

Figure 18

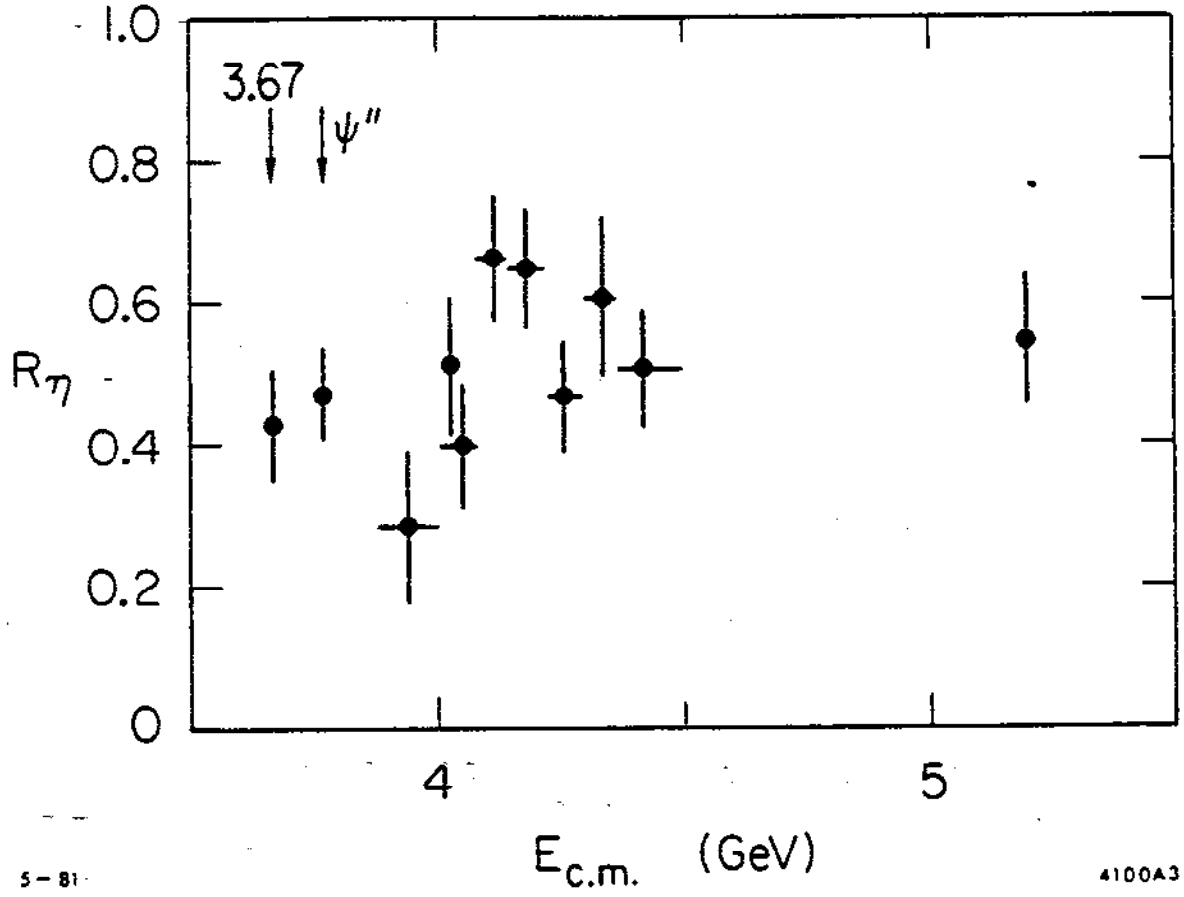

Figure 19

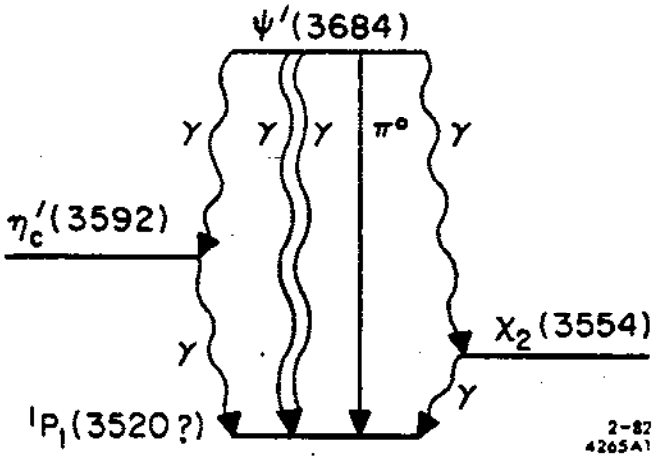

Figure 20

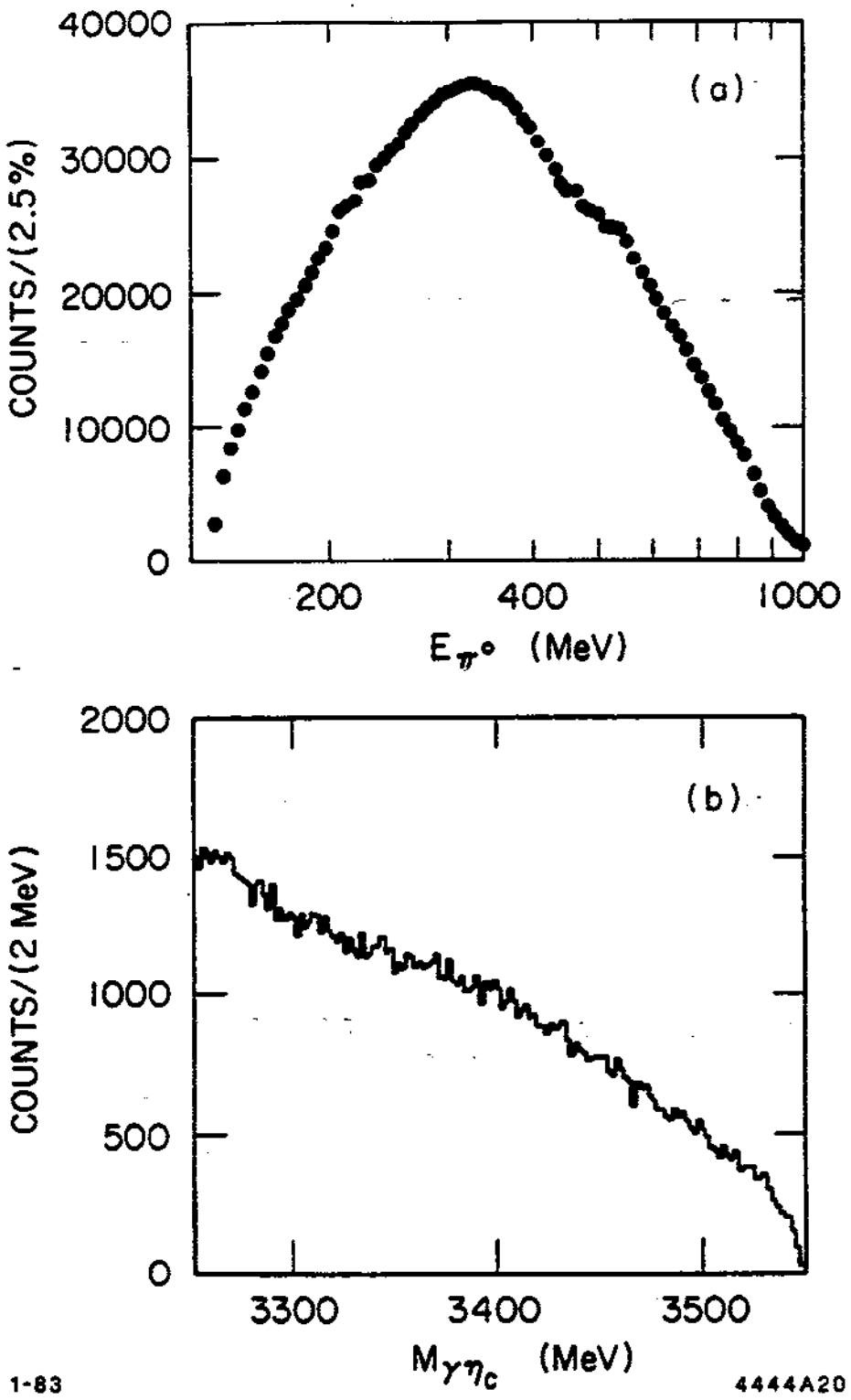
40000
30000
20000
10000
0
COUNTS/(2.5%)
(a)
200
400
1000
E_{π^0} (MeV)
2000
1500
1000
500
0
COUNTS/(2 MeV)
(b)
3300
3400
3500
$M_{\gamma\eta_c}$ (MeV)
1-83
4444A20

Figure 21

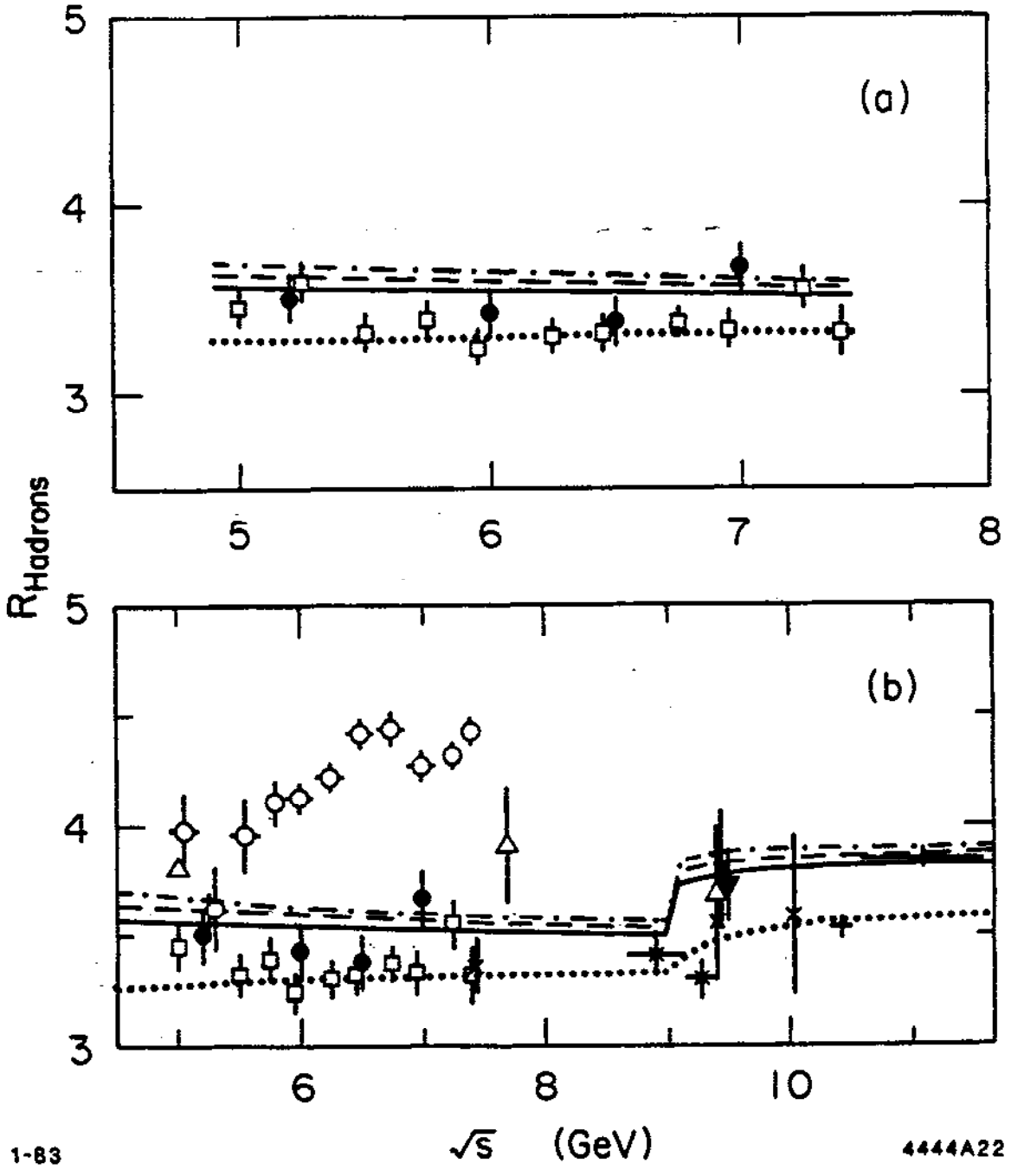

Figure 22

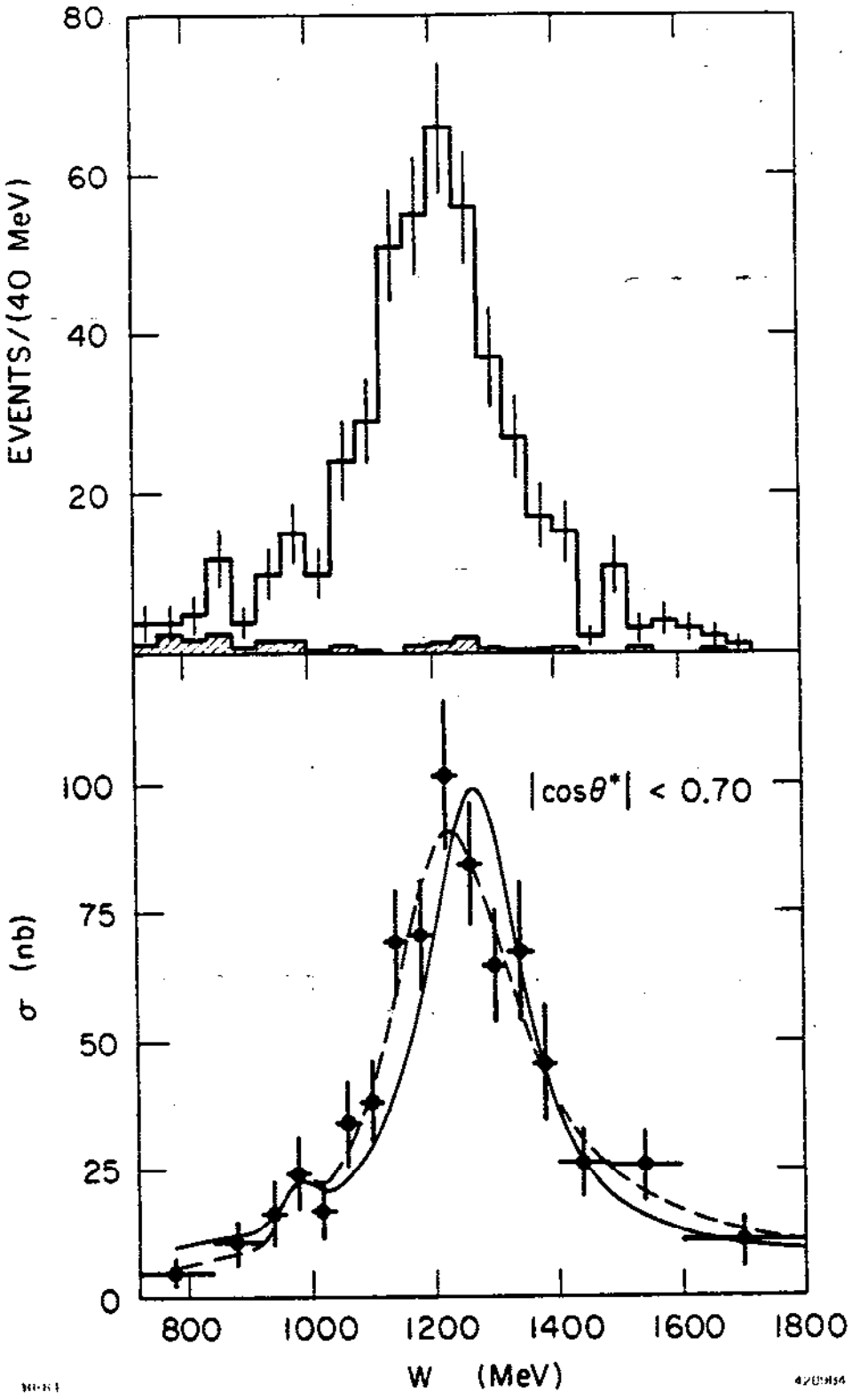
80
60
40
20
EVENTS/(40 MeV)
100
75
50
25
0
σ (nb)
|cosθ*| < 0.70
800
1000
1200
1400
1600
1800
W (MeV)

Figure 23

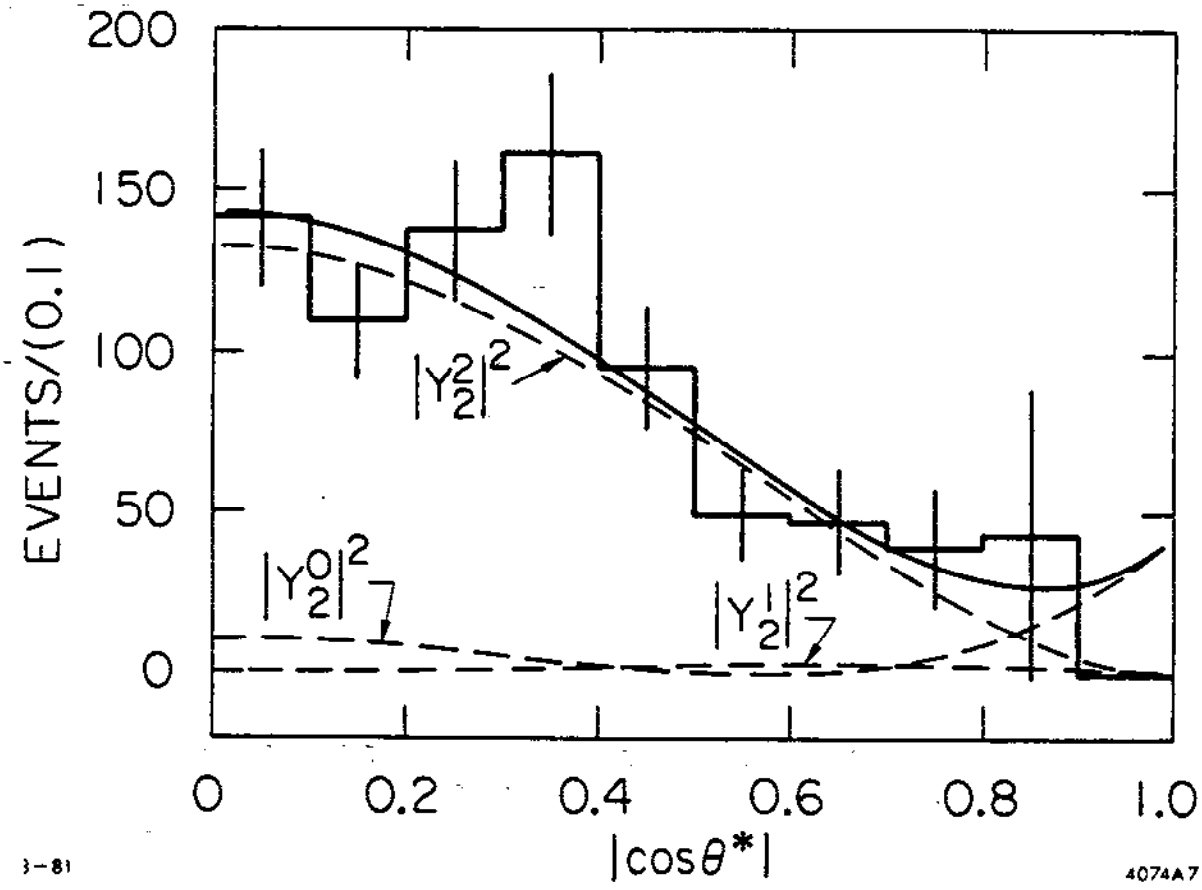
200
150
100
50
0
EVENTS/(0.1)
$|Y_2^2|^2$
$|Y_2^0|^2$
$|Y_2^1|^2$
0
0.2
0.4
0.6
0.8
1.0
$|\cos\theta^*|$
3-81
4074A7

Figure 24